Trends and Inferred Emissions of Atmospheric High Molecular Weight Perfluorocarbons

by

Diane Jean Ivy

B.S. in Civil Engineering, University of California - Berkeley (2004)
B.A. in Applied Math, University of California - Berkeley (2004)
M.S. in Civil Engineering, Georgia Institute of Technology (2007)

Submitted to the Department of Earth, Atmospheric and Planetary Sciences
in partial fulfillment of the requirements for the degree of

Doctor of Philosophy in Atmospheric Science

at the

MASSACHUSETTS INSTITUTE OF TECHNOLOGY

September 2012

Author .....
Department of Earth, Atmospheric and Planetary Sciences
September 2012

Certified by .....
Ronald G. Prinn
TEPCO Professor of Atmospheric Science
Thesis Supervisor

Accepted by .....
Robert D. van der Hilst
Schlumberger Professor of Earth Sciences
Head, Department of Earth, Atmospheric and Planetary Sciences

Trends and Inferred Emissions of Atmospheric High Molecular Weight Perfluorocarbons

by

Diane Jean Ivy

Submitted to the Department of Earth, Atmospheric and Planetary Sciences
on September 2012, in partial fulfillment of the
requirements for the degree of
Doctor of Philosophy in Atmospheric Science

Abstract

Atmospheric observations and atmospheric observation-based global emission estimates are presented for the five high molecular weight perfluorocarbons (PFCs): decafluorobutane (C_4F_{10}), dodecafluoropentane (C_5F_{12}), tetradecafluorohexane (C_6F_{14}), hexadecafluoroheptane (C_7F_{16}) and octadecafluorooctane (C_8F_{18}). Their atmospheric histories are based on measurements of 36 Northern Hemisphere and 46 Southern Hemisphere archived air samples, collected between 1973 and 2011, using two of the "Medusa" cryogenic preconcentration gas chromatography-mass spectrometry instruments, which are part of the Advanced Global Atmospheric Gases Experiment (AGAGE). A new calibration scale was prepared for each PFC, with estimated accuracies of 6.8 % for C_4F_{10}, 7.8 % for C_5F_{12}, 4.0 % for C_6F_{14}, 6.6 % for C_7F_{16} and 7.9 % for C_8F_{18}. Based on our observations, the 2011 globally averaged dry air mole fractions of these high molecular weight PFCs are: 0.17 parts-per-trillion (ppt, i.e., parts per 10^{12}) for C_4F_{10}, 0.12 ppt for C_5F_{12}, 0.27 ppt for C_6F_{14}, 0.12 ppt for C_7F_{16} and 0.09 ppt for C_8F_{18}.

Newly measured infrared absorption spectra are presented for C_7F_{16} and C_8F_{18}, and using these, their radiative efficiencies and global warming potentials (GWPs) are estimated. We find that the radiative efficiency of C_8F_{18} at $0.57\,W\,m^{-2}\,ppb^{-1}$ is similar to that of trifluoromethyl sulfur pentafluoride's (SF_5CF_3), which has the highest radiative efficiency of any known atmospheric species (*Forster et al.*, 2007). Using their radiative efficiencies, the 2011 observed globally averaged atmospheric mole fractions of the above five high molecular weight PFCs combine to contribute a global average radiative forcing of $0.35\,mW\,m^{-2}$, which is 6 % of the total anthropogenic PFC radiative forcing (*Montzka et al.*, 2011; *Oram et al.*, 2012).

Global emissions for C_4F_{10}, C_5F_{12}, C_6F_{14}, C_7F_{16} and C_8F_{18} were estimated from the observations using a 3-dimensional chemical transport model and a Bayseian inverse method that included a constraint on the annual growth rate of their emissions, consistent with the knowledge of the relevant industries emitting them (*Rigby et al.*, 2011). The derived so-called "top-down" emission estimates show that global emission rates were largest in the 1980s and 1990s for C_4F_{10} and C_5F_{12} and in the 1990s for

C_6F_{14}, C_7F_{16} and C_8F_{18}. After a subsequent decline, emission rates have remained relatively stable, within $\pm 20\,\%$ year-to-year variation, for the last 5 years. Using their calculated 100-year time horizon GWPs, the high molecular weight perfluorocarbons studied here contributed up to 15.4 % of the total PFC emissions expressed in carbon dioxide (CO_2)-equivalents in 1997 and 6 % of the total PFC emissions in 2009.

Furthermore, we compare our atmospheric observation-based global emissions to the available so-called "bottom-up" inventories, which are based on production information and end usage. Bottom-up emission estimates are available from the Emission Database for Global Atmospheric Research version 4.2 (EDGARv4.2) for C_4F_{10}, C_5F_{12}, C_6F_{14} and C_7F_{16}, and emission inventories of C_4F_{10}, C_5F_{12} and C_6F_{14} are also reported to the United Nations' Framework Convention on Climate Change (UNFCCC) by Annex 1 countries that have ratified the Kyoto Protocol (*European Commission, Joint Research Centre (JRC)/Netherlands Environmental Assessment Agency (PBL)*, 2009; *United National Framework Convention on Climate Change Secretariat*, 2011). The atmospheric observation-based emission estimates are 20 times larger than EDGARv4.2 for C_4F_{10} and over three orders of magnitude larger for C_5F_{12}. In contrast, the top-down emission estimates for C_6F_{14} largely agree with the bottom-up estimates from EDGARv4.2. Moreover, the top-down C_7F_{16} emission estimates are comparable to those of EDGARv4.2 at their peak in the 1990s, albeit with significant underestimation by EDGARv4.2 for the other time periods. There are no bottom-up emission estimates for C_8F_{18}, thus the emission rates reported here are the first for this gas. In general, the emission inventories for C_4F_{10}, C_5F_{12} and C_6F_{14} reported to the UNFCCC are five to ten times lower than those estimated in this study from observations. This underreporting to the UNFCCC may be due to only Annex 1 countries reporting inventories and also that some of these countries report a total PFC mixture in CO_2-equivalents, instead of individual PFC emissions rates.

Thesis Supervisor: Ronald G. Prinn
Title: TEPCO Professor of Atmospheric Science

Acknowledgments

First and foremost, I would like to thank my advisor Ron Prinn for all of his support and advice. It has been wonderful working with Ron, and he has offered me many amazing opportunities throughout my time at MIT. I would like to thank Ray Weiss and Paul Fraser for serving on my thesis committee and allowing me to work in their labs; I gained a tremendous amount of experience from both visits. I would like to thank Shuhei Ono for serving on my thesis committee and his support.

I am indebted to my fellow Prinn group members; in particular, Laura Meredith, Anita Ganesan and Matt Rigby. Not only have I learned a great deal from each of them, but they are some of my biggest supporters and great friends. I would also like to thank Robens Joseph for all his help over the past five years. I would like to thank my fellow fifth years: Daniela Domeisen, Malte Jansen and Neil Zimmerman for helping me with all the dynamics classes and making generals bearable.

I learned a great deal from my time at Scripps. I would like to thank my lab idol - Chris Harth - for all her advice, help and support. I would like to thank Tim Arnold for always helping me when I needed it and constantly making me laugh. Jens Mühle and Peter Salameh were a huge support and always willing to answer my questions; and I would like to thank Stephanie Mumma for her willingness to help when things went awry and her support.

My time at CSIRO was one of the most insightful experiences as an experimentalist. Paul Steele was a wonderful mentor and taught me a great deal. I would also like to thank Paul Krummel and Rebecca Gregory for their help and friendship. Michael Leist was helpful with the instrumentation at Aspendale.

I would like to thank my mom, Carrie Ivy, for all of her love and support. She has always given me every opportunity she could and helped me when I was too overwhelmed. I would like to thank my best friend, Ana Počivavsek, and her family for always being there and supportive for the past 22 years and pushing me to be a better person. I would lastly like to thank my good friends: Meg Bailey, Wendy Hung, Gretchen Adelson, Dana Gravem, Rachel Irving and Catherine Pautsch for

providing much needed fun and stress relief.

Contents

List of Figures

List of Tables

Chapter 1

Introduction

Perfluorocarbons (PFCs) are powerful greenhouse gases and included as one of the six classes of greenhouse gases regulated under the Kyoto Protocol to the United Nations Framework Convention on Climate Change (UNFCCC). Due to their long lifetimes and strong absorption in the infrared, PFCs are considered to have a nearly permanent effect on the Earth's radiative budget, when human timescales are considered. Thus, PFCs have global warming potentials (GWPs) three to four orders of magnitude higher than that of carbon dioxide (CO_2) on a 100-year time horizon (see Table 1.1) (*Forster et al.*, 2007).

Table 1.1: Lifetimes, Radiative Efficiencies and Global Warming Potentials of Perfluorocarbons

	Lifetime	Radiative Efficiency	Global Warming Potential (GWP)			
Species	[yr]	[W m^{-2} ppb^{-1}]	20-yr horizon	100-yr horizon	500-yr horizon	Reference
CF_4	50 000	0.10	5210	7390	11 200	*Forster et al.* (2007)
C_2F_6	10 000	0.26	8630	12 200	18 200	*Forster et al.* (2007)
C_3F_8	2600	0.26	6310	8830	12 500	*Forster et al.* (2007)
c-C_4F_8	3200	0.32	7310	10 300	14 700	*Forster et al.* (2007)
C_4F_{10}	2600	0.33	6330	8860	12 500	*Forster et al.* (2007)
C_5F_{12}	4100	0.41	6510	9160	13 300	*Forster et al.* (2007)
C_6F_{14}	3200	0.49	6600	9300	13 300	*Forster et al.* (2007)
C_7F_{16}	(3000)*	0.48	5630	7930	11 300	This study & *Ivy et al.* (2012)
	(3000)*	0.45	–	–	–	*Bravo et al.* (2010)
C_8F_{18}	(3000)*	0.57	5920	8340	11 880	This study & *Ivy et al.* (2012)
	(3000)*	0.50	5280	7390	10 500	*Bravo et al.* (2010)
$C_{10}F_{18}$	> 1000	0.56	> 5500	> 7500	> 9500	*Shine et al.* (2005)

*Lifetimes in parentheses have not been measured; a lifetime of 3000 years was chosen as it is similar to that of C_6F_{14}.

Atmospheric observations and atmospheric observation-based emission estimates are available for the lower molecular weight PFCs: carbon tetrafluoride (CF_4), hexafluoroethane (C_2F_6), octafluoropropane (C_3F_8) and octafluorocyclobutane (c-C_4F_8) (*Mühle et al.*, 2010; *Oram et al.*, 2012; *Saito et al.*, 2010). CF_4 is the most abundant PFC and has a significant natural abundance due to a lithospheric source (*Deeds et al.*, 2008; *Harnisch et al.*, 1996*b*,*a*; *Mühle et al.*, 2010). The predominant anthropogenic emissions of these lower molecular weight PFCs are from the production of aluminum and usage in the semiconductor industry and as refrigerants (*Mühle et al.*, 2010; *Oram et al.*, 2012). Both the aluminum and semiconductor industries have made efforts to reduce emissions of the lower molecular weight PFCs to the atmosphere (*International Aluminium Institute*, 2011; *Semiconductor Industry Association*, 2001; *World Semiconductor Council*, 2005). However, the global emission estimates by *Mühle et al.* (2010) and *Oram et al.* (2012) for the lower molecular weight PFCs concluded that so-called "bottom-up" emission estimates, which are based on production information and end usage, were underestimated when compared to estimates constrained by atmospheric observations, particularly for C_3F_8 and c-C_4F_8. These studies illustrate the valuable constraints that atmospheric observations provide for independently estimating emissions to verify or falsify the bottom-up emission estimates.

Currently, there is much less information available for the higher molecular weight PFCs: decafluorobutane (C_4F_{10}), dodecafluoropentane (C_5F_{12}), tetradecafluorohexane (C_6F_{14}), hexadecafluoroheptane (C_7F_{16}) and octadecafluorooctane (C_8F_{18}). Bottom-up emission estimates are provided by the Emission Database for Global Atmospheric Research version 4.2 (EDGARv4.2) for the high molecular weight PFCs, C_4F_{10}, C_5F_{12}, C_6F_{14} and C_7F_{16} from 1970 to 2008 (*European Commission, Joint Research Centre (JRC)/Netherlands Environmental Assessment Agency (PBL)*, 2009). Furthermore, C_4F_{10}, C_5F_{12} and C_6F_{14} emission inventories are reported from 1990 to 2009 to the UNFCCC by Annex 1 countries that have ratified the Kyoto Protocol (*United National Framework Convention on Climate Change Secretariat*, 2011). However, no emission data are available for octadecafluorooctane (C_8F_{18}).

Since the early 1990s, these higher molecular weight PFCs have had a relatively

minor role as replacements for ozone depleting substances (ODSs) that are regulated under the Montreal Protocol (*Harvey*, 2000). Of which, the most significant emission source of the high molecular weight PFCs comes from their usage as solvents in electronics and precision cleaning, which was approved under the Environmental Protection Agency's Significant New Alternatives Policy (SNAP) program (*Air and Radiation Global Programs Division*, 2006; *Tsai*, 2009). There are also small niche markets for C_4F_{10} and C_6F_{14} as fire suppressants (*Forte Jr. et al.*, 2000; *Kopylov*, 2002; *Tsai*, 2009) and C_4F_{10}, C_5F_{12} and C_6F_{14} as refrigerants (*European Commission, Joint Research Centre (JRC)/Netherlands Environmental Assessment Agency (PBL)*, 2009; *Schwaab et al.*, 2004; *Tsai*, 2009). Because of their large GWPs, emissions of these high molecular weight PFCs as ODSs replacements are expected to be decreasing as they are being replaced with lower GWP alternatives (*Harvey*, 2000; *UNEP Technology and Economic Assessment Panel*, 1999). The main sink for the PFCs is photolysis by Lyman-α radiation and a minor destruction pathway is reaction with $O(^1D)$ (*Ravishankara et al.*, 1993).

The PFCs C_5F_{12}-C_8F_{18}, which are liquid at room temperature, are additionally being used in the semiconductor manufacturing industry as heat transfer fluids and in vapor phase reflow soldering (*3M Electronics Markets Materials Division*, 2003; *Tsai*, 2009; *Tuma and Tousignant*, 2001). This emission source is a first-of-a-kind for fluorinated compounds, where previously deionized water and a mixture of deionized water and glyoxal were used (*Tuma and Tousignant*, 2001). While the semiconductor industry is making efforts to reduce PFC emissions, their efforts are focused on reducing emissions of the lower molecular weight PFCs. Therefore emission estimates based on atmospheric observations of the higher molecular weight PFCs are valuable for determining if these industries are indeed reducing all PFC emissions.

Laube et al. (2012) recently published atmospheric observations and global emission estimates using a 2-dimensional model for C_4F_{10}, C_5F_{12}, C_6F_{14} and C_7F_{16}. However, the emission estimates by *Laube et al.* (2012) were determined qualitatively and not estimated optimally by a Bayesian inverse method. Additionally, there are differences between the atmospheric mole fraction histories provided by *Laube et al.*

(2012) and those presented in this study, most likely due to calibration differences and instrumental nonlinearities.

1.1 Research Goal and Objectives

The main goal of this research is to provide atmospheric histories and atmospheric observation-based emission estimates for the high molecular weight PFCs: C_4F_{10}, C_5F_{12}, C_6F_{14}, C_7F_{16} and C_8F_{18}. Atmospheric observation-based emissions are beneficial in providing independent verification of bottom-up emission inventories, which often show large discrepancies when compared to top-down estimates; thus we hope to compare the emissions derived in this study to the available bottom-up inventories from EDGARv4.2 and the UNFCCC. Furthermore, we hope to update the total contribution of PFC emissions to the radiative forcing of the Earth's climate, by now including global emissions of the high molecular weight PFCs.

Approach To provide atmospheric observation-based emission estimates of the high molecular weight PFCs, atmospheric observations are needed to constrain the emission estimates. The atmospheric histories presented in this thesis were based on measurements of Northern Hemisphere (NH) and Southern Hemisphere (SH) archived air samples. These samples cover a 39-year period, from 1973 to 2011, and include 36 NH and 46 SH separate samples that were stored in high pressure cylinders. The composition of these samples were measured using so-called "Medusa" cryogenic preconcentration gas chromatography-mass spectrometry systems. To quantify the atmospheric samples, a new calibration scale was prepared for each species based on four gravimetric primary standards. Furthermore, the blanks and instrumental nonlinearities for each PFC were characterized on the Medusa systems and taken into account to provide the final dry air mole fractions for each archive sample.

Global annual emission estimates for the high molecular weight PFCs, C_4F_{10}, C_5F_{12}, C_6F_{14}, C_7F_{16} and C_8F_{18}, were estimated using a 3-dimensional chemical transport model (CTM), the Model of Ozone and Related chemical Tracers (MOZARTv4.5),

and a Bayesian inverse method, in which the atmospheric observations and an independent estimate of the annual emission growth rates are both used as constraints (*Emmons et al.*, 2010; *Rigby et al.*, 2011). The derived emissions based on the atmospheric measurements are compared to the available bottom-up emission data from EDGARv4.2 and the reported inventories to the UNFCCC. Furthermore, we compare our results to the recent work published by *Laube et al.* (2012) and offer potential reasons for differences between the two studies.

Lastly, to provide estimates of the radiative forcing for C_7F_{16} and C_8F_{18}, we measured their infrared (IR) absorption spectra. From the measured IR spectra, molecular radiative efficiencies and GWPs were determined for C_7F_{16} and C_8F_{18}. In this way, we are able to provide an updated estimate of the total radiative impact of global PFC emissions in CO_2-equivalents from 1978 to 2009, now including the high molecular weight PFCs.

Chapter 2

Experimental Methods

This chapter describes the experimental methods used to determine the atmospheric histories of the high molecular weight PFCs. Section 2.1 describes the instrumentation used to measure the dry air mole fractions in the archived air samples and the experiments to characterize the nonlinearities and blanks associated with the instrument. Section 2.2 outlines the preparation of primary gravimetric standards used to determine a new calibration scale, which allows for the quantification of the atmospheric samples. The last section, Section 2.3, describes the two sets of archived air samples measured in this study, consisting of samples filled in both the Northern and Southern Hemispheres, to construct the atmospheric histories of the high molecular weight PFCs.

2.1 Instrumentation

The cryogenic preconcentration gas chromatography-mass spectrometry (GC-MS: Agilent 6890-5973/5975) "Medusa" systems (*Miller et al.*, 2008) were used to measure the high molecular weight PFC dry air mole fractions in archived air samples at the Scripps Institution of Oceanography (SIO), University of California, San Diego (San Diego, California) and at the Commonwealth Scientific and Industrial Research Organisation (CSIRO), Division of Marine and Atmospheric Research (CMAR, Aspendale, Australia). These instruments are part of the Advanced Global Atmospheric

Gases Experiment (AGAGE) network (*Prinn et al.*, 2000).

For each measurement, the condensables in a 2-L air sample are preconcentrated onto a micro-trap and then cyrofocused onto a second micro-trap. The two micro-traps are made of 200 mg and 5.5 mg of 100/120 mesh HayeSep-D. Both microtraps are initially held at -160 °C and subsequently heated for desorption before the sample is injected onto a capillary column. Figure 2-1 shows a schematic diagram of the Medusa preconcentration system. Currently, the Medusa systems in AGAGE use a CP-PoraBOND Q fused silica PLOT column (25 m, 0.32 mm ID, 5 μm, Agilent Technologies) as the main column for separation of all analytes (except for CF_4 and NF_3) (see *Miller et al.* (2008) and *Arnold et al.* (2012) for details). However for the measurements at CSIRO, the Medusa was fitted with a GS-GasPro column (60 m, 0.32 mm ID, Agilent Technologies) as the main column, which had improved separation for these analytes.

The preconcentration system, gas chromatograph and mass spectrometer were all controlled with GCWerks© software. To maximize the measurement precisions, the quadrupole MS was operated in selective ion mode (SIM). Additionally, only a select number of species were measured in this experiment, as compared to the more than 50 species typically measured as part of the AGAGE network, to minimize the number of acquired ions and further improve sample precisions. Each sample measurement was bracketed by a reference gas analysis, allowing for correction of short-term instrumental drift (*Prinn et al.*, 2000). GCWerks© was also used for peak integration and calculating the final dry air mole fractions of each sample based on the bracketing reference gas analyses.

The detection limit for each species on both instruments was estimated as three times the baseline height of the noise of the target ion immediately preceding and following the elution of the species and is presented in Table 2.1. The differences in the detection limits between the two instruments are due to the improved separation of analytes on the GS-GasPro column used on the CSIRO Medusa and the newer model of MS (5975) used at SIO.

Blanks were checked almost daily with "zero-air". Repeated sampling of the zero-

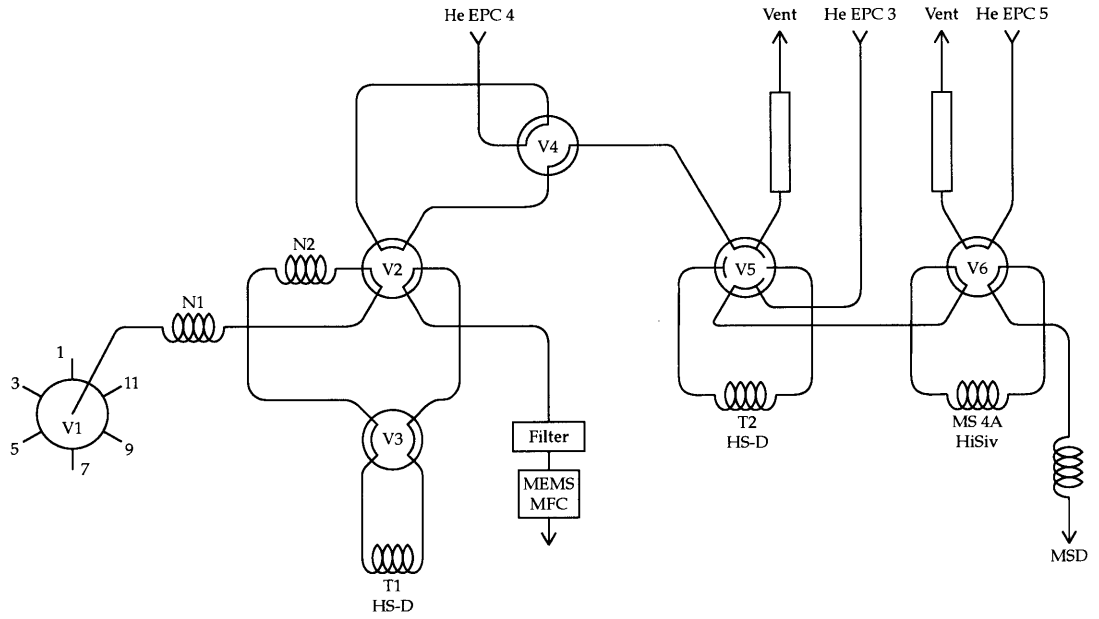

Figure 2-1: Schematic diagram of the preconcentration system Medusa. The multi-port valves (V1-V6) are used to control the sample flow. The Nafion membranes (N1 and N2) are used to dry the sample. The electron pressure controllers (EPC3-EPC5) control the carrier gas (Helium). The two micro-traps are shown as T1 and T2.

Table 2.1: Blanks, Standard Precisions and Detection Limits for C_4F_{10}, C_5F_{10}, C_6F_{14}, C_7F_{16} and C_8F_{18} on the SIO and CSIRO Medusa Systems*

Species	Main Column	MS	Blank [ppt**]	Standard Precision [ppt]	Detection Limit [ppt]
C_4F_{10}	PoraBOND	5975	0.0003	0.0042	0.0180
	GasPro	5973	0.0003	0.0067	0.0249
C_5F_{12}	PoraBOND	5975	0	0.0021	0.0120
	GasPro	5973	0.0022	0.0029	0.0096
C_6F_{14}	PoraBOND	5975	0.0001	0.0040	0.0057
	GasPro	5973	0.0001	0.0065	0.0117
C_7F_{16}	PoraBOND	5975	0.0060	0.0042	0.0048
	GasPro	5973	0.0030	0.0021	0.0129
C_8F_{18}	PoraBOND	5975	0.0054	0.0026	0.0102
	GasPro	5973	0.0053	0.0032	0.0153

*Standard precisions refer to the 1-σ standard deviation taken on the working standard used, which is a NH 2010 sample for the SIO Medusa and a 2010 sample filled at Cape Grim for the CSIRO Medusa.
**ppt = parts-per-trillion dry air mole fraction.

air, without analysis of the bracketing reference standard, confirmed that the zero-air was analyte-free for the PFCs measured in this study. A small blank was detected for the high molecular weight PFCs (see Table 2.1) and is most likely a memory effect due to the Nafion dryers used in the Medusa. The blanks were fairly consistent over the measurement period, and the observations were corrected with a mean value over the experimental time period.

2.1.1 Linearity Tests

In general, the instrument response, R, is related to the sample mole fraction, χ, by Equation (2.1), where ϵ is the nonlinearity parameter (*Prinn et al.*, 2000). Nonlinearities are important to characterize for low concentration atmospheric samples, which may vary significantly from the reference standard concentrations. Thus, characterizing any possible nonlinearities is particularly important for the early archived air samples, which have the lowest mole fractions. Two experiments were done to assess whether the instrument response of the Medusa systems were linear over the required range of mole fractions for each species.

$$R \propto \chi^{(1-\epsilon)} \tag{2.1}$$

Dilution Method

A whole-air sample from a 2010 Cape Grim Air Archive (CGAA) tank was decanted into a 35-L stainless steel tank (Essex Cryogenics), and spiked with a small volume of high-purity methane (CH_4) to increase the CH_4 mole fractions from ambient to ca. 8 parts-per-million (ppm, i.e., parts per 10^9) dry air mole fraction. From this spiked air sample, six subsamples were prepared in 6-L stainless steel SilcoCan flasks (Restek Inc.) using a vacuum manifold (see Figure 2-2). Each subsample was diluted by adding zero-air, which had previously been measured on the Medusa and found to be analyte-free for the PFCs studied here. The zero-air was added to the SilcoCan flasks using 1/16 inch stainless steel tubing in order to restrict the flow from the high pressure zero-air cylinder, hence avoiding the need for a regulator and any possibilities of contamination. The amount of zero-air added was varied to give a range of dilution factors (nominally from 6.25 % to 75 %). The actual dilution factors for each subsample were determined by precisely measuring the CH_4 dry air mole fractions (including that of the spiked parent sample) on a gas chromatography-flame ionization detector (GC-FID) system with a known linear response (*Francey et al.*, 2003). These subsamples were subsequently measured on the Medusa systems to determine the linearity of the Medusa measurements for each species. All but the lowest concentration subsample (dilution factor of 6.25 %) were above the detection limit for C_4F_{10}, C_5F_{12}, C_7F_{16} and C_8F_{18}. The lowest concentration subsample was slightly above the detection limit for C_6F_{14}. Thus, almost all possible mole fractions of the archived air samples were covered by this dilution method experiment. Figure 2-3 and Table 2.2 show the results of the nonlinearity experiments using the dilution method.

Volume Method

The second experiment to characterize the linearity of the instrument response involved sampling different volumes from a single whole-air sample (*Miller et al.*, 2008).

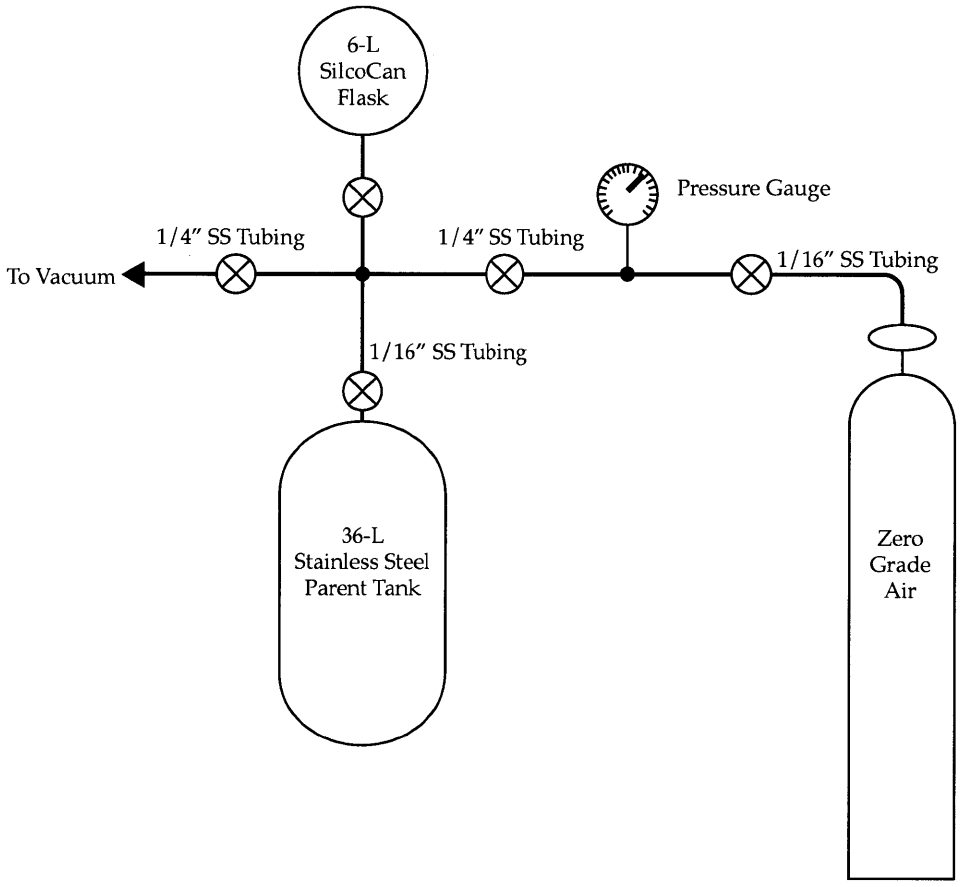

Figure 2-2: Schematic diagram of the vacuum manifold used for preparation of dilution samples for the dilution nonlinearity experiment.

Table 2.2: Dilution Method Nonlinear Experiment Normalized Measured Mole Fractions for C_4F_{10}, C_5F_{12}, C_6F_{14}, C_7F_{16} and C_8F_{18} on the CSIRO and SIO Medusa Systems*

		CSIRO Medusa		SIO Medusa	
Species	Dilution Factor	Mean [ppt/ppt**]	Stdev [ppt/ppt]	Mean [ppt/ppt]	Stdev [ppt/ppt]
C_4F_{10}	0.065	0.070	0.000	0.071	0.096
	0.125	0.161	0.021	0.132	0.096
	0.253	0.263	0.014	0.231	0.096
	0.500	0.549	0.035	0.472	0.096
	0.753	0.790	0.013	-	-
	1.000	1.103	0.038	1.000	0.096
C_5F_{12}	0.065	0.061	0.006	0.069	0.101
	0.125	0.121	0.017	0.141	0.101
	0.253	0.243	0.007	0.252	0.101
	0.500	0.483	0.003	0.526	0.101
	0.753	0.748	0.038	-	-
	1.000	1.008	0.021	1.000	0.101
C_6F_{14}	0.065	0.069	0.008	0.065	0.100
	0.125	0.125	0.002	0.135	0.100
	0.253	0.248	0.006	0.264	0.100
	0.500	0.498	0.013	0.505	0.100
	0.753	0.761	0.006	-	-
	1.000	1.034	0.040	1.000	0.100
C_7F_{16}	0.065	0.071	0.007	0.068	0.098
	0.125	0.126	0.013	0.127	0.098
	0.253	0.256	0.013	0.247	0.098
	0.500	0.495	0.009	0.496	0.098
	0.753	0.746	0.008	-	-
	1.000	0.995	0.013	1.000	0.098
C_8F_{18}	0.065	0.065	0.000	0.000	0.000
	0.125	0.128	0.039	0.138	0.096
	0.253	0.251	0.005	0.170	0.096
	0.500	0.509	0.019	0.502	0.096
	0.753	0.777	0.035	-	-
	1.000	1.000	0.024	1.000	0.096

*Only two measurements were made for the dilution samples on the SIO Medusa. Therefore, the reported standard deviations are the normalized standard precisions.
**ppt = parts-per-trillion dry air mole fraction.

The range of relative volumes sampled was from 6 % to 200 % of the standard 2-L sample. This volume method has the advantage of characterizing instrument responses at mole fractions above present day background levels, which could not be easily achieved through the dilution subsamples unless more concentrated samples were prepared. However, as the atmospheric samples measured in the air archives were all below current atmospheric background mole fractions, the volume method served only to complement the dilution method.

Linearity Parameter Estimation

Generally, the systems exhibited a linear response over much of the required range of mole fractions, with departures from linearity at mole fractions corresponding to those of the oldest archive samples, which have the lowest mole fractions. These nonlinearities are most likely due to a blank effect associated with the preconcentration system. After blank correction, the instrument exhibited a nearly linear response. Based on the dilution experiment measurements, a nonlinearity parameter, ϵ, was estimated for each PFC on each instrument.

By adding a proportionality constant to Equation (2.1), we have Equations (2.2) and (2.3), where we have assumed that ϵ is zero for the standard.

$$R_{std} = a\chi_{std} \tag{2.2}$$

$$R_{sam} = a\chi_{sam}^{(1-\epsilon)} \tag{2.3}$$

We define the normalized sensitivity, N_s, as the sample mole fraction if assuming perfect linearity divided by the actual "true" sample mole fraction (see Equation (2.4)). Substituting Equation (2.3) into Equation (2.4), shows that the normalized sensitivity is equal to $\chi_{sam}^{-\epsilon}$.

$$N_s = \frac{R_{sam}/a}{\chi_{sam}} = \frac{\chi_{sam}^{(1-\epsilon)}}{\chi_{sam}} = \chi_{sam}^{-\epsilon} \tag{2.4}$$

By rearranging Equation (2.3) to solve for χ_{sam} as a function of the instrument

response, R_{sam}, we get Equation (2.5).

$$\chi_{sam} = \left(\frac{R_{sam}}{a}\right)^{\frac{1}{(1-\epsilon)}} \tag{2.5}$$

Substituting the expression for χ_{sam}, as shown in Equation (2.5), into Equation (2.4) and simplifying the exponents gives Equation (2.6).

$$N_s = \left(\left(\frac{R_{sam}}{a}\right)^{\frac{1}{(1-\epsilon)}}\right)^{-\epsilon} = \left(\frac{R_{sam}}{a}\right)^{\frac{\epsilon}{(\epsilon-1)}} \tag{2.6}$$

Lastly by substituting an expression for a, from Equation (2.2), into Equation (2.6), we get a relationship of the normalized response, defined as $N_r = R_{sam}/R_{std}$, to the normalized sensitivity, N_s (see Equation (2.7)).

$$N_s = \left(\frac{R_{sam}\chi_{std}}{R_{std}}\right)^{\frac{\epsilon}{\epsilon-1}} = (N_r\chi_{std})^{\frac{\epsilon}{\epsilon-1}} \tag{2.7}$$

In order to estimate the nonlinearity parameter, ϵ, we used a Monte Carlo approach, where we solved for ϵ using a least-squares approach with the distributions of N_r varied based on the measurement uncertainties. This was necessary as some observations at the lower values of normalized response had relatively high uncertainties; not accounting for these larger relative uncertainties could potentially lead to large biases in the derived nonlinearity parameters. The nonlinearity parameters were relatively small and are presented in Table 2.3, with the largest nonlinearity for C_7F_{16}.

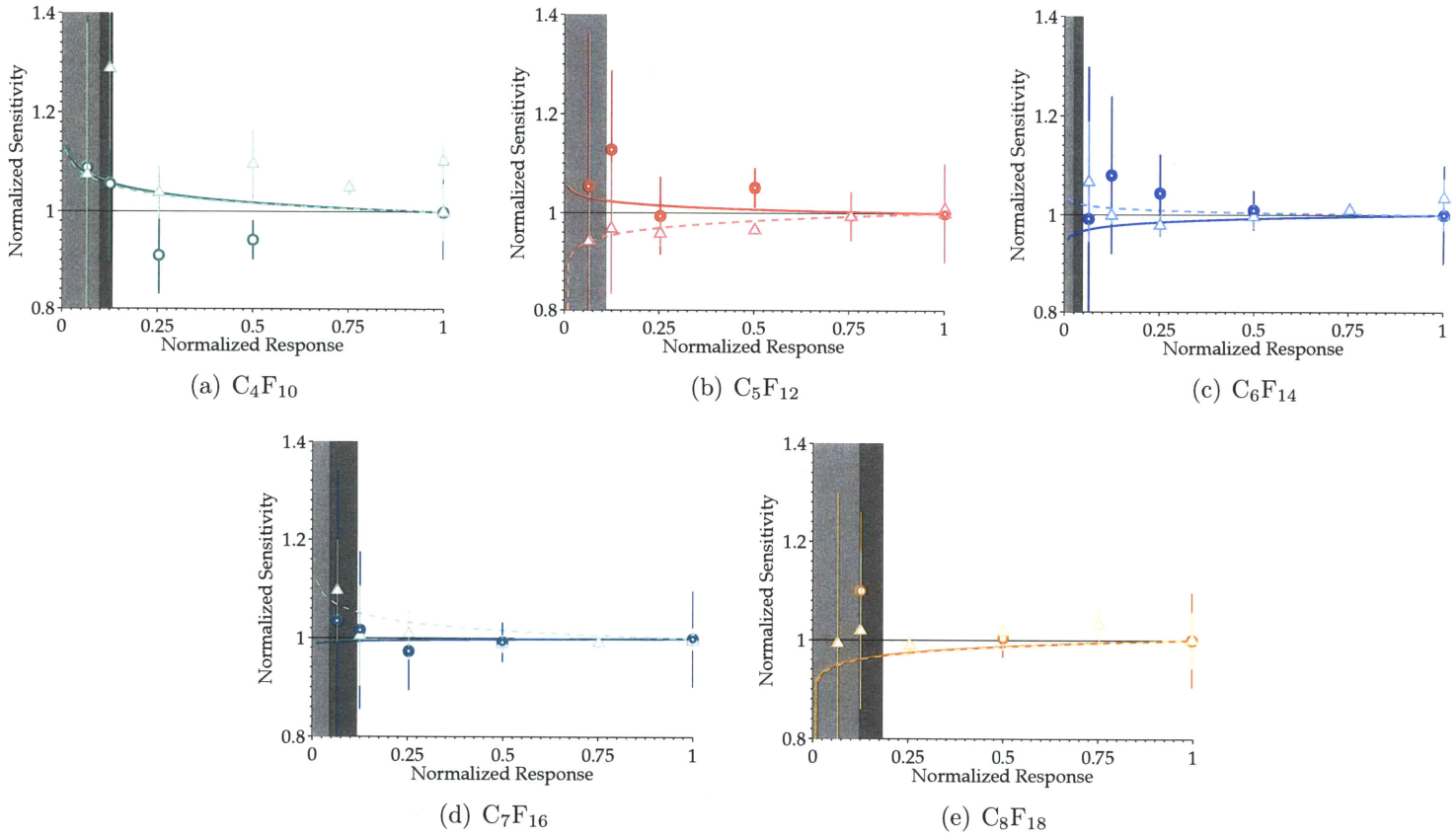

(a) C_4F_{10} (b) C_5F_{12} (c) C_6F_{14}

(d) C_7F_{16} (e) C_8F_{18}

Figure 2-3: The normalized sensitivity of the Medusa systems, N_s, as a function of the normalized response, N_r, for a) C_4F_{10}, b) C_5F_{12}, c) C_6F_{14}, d) C_7F_{16} and e) C_8F_{18}. The open circles are for the CSIRO Medusa and the open triangles are for the SIO Medusa; the associated vertical bars are the normalized measurement uncertainty. The normalized detection limits of the two instruments are shown as the grey shading - dark grey for CSIRO and light grey for SIO. The best fit lines to the data are also shown (see Equation (2.7)) for the CSIRO (solid lines) and SIO (dashed lines) Medusas. A line at one is plotted for reference, which indicates a perfectly linear response.

Table 2.3: Nonlinearity Parameters (ϵ) for C_4F_{10}, C_5F_{12}, C_6F_{14}, C_7F_{16} and C_8F_{18} on the CSIRO and SIO Medusa Systems

	CSIRO Medusa	SIO Medusa
C_4F_{10}	0.022	0.023
C_5F_{12}	-0.015	0.010
C_6F_{14}	0.007	-0.008
C_7F_{16}	0.024	0.001
C_8F_{18}	-0.020	-0.019

2.2 Calibration

In order to identify and quantify the high molecular weight PFCs, new gravimetric primary standards were prepared at SIO. Two approaches were used in preparing theses standards. The first was the method of external standards, which involves adding a known amount of PFC to a zero-air sample; the second was the method of internal additions that involves adding a known amount of PFC to a whole-air sample. One standard was prepared using the method of external standards with final dry air mole fractions of each PFC of ca. 10 parts-per-trillion (ppt, i.e., parts per 10^{12}). As no atmospheric observations were available prior to this work, the choice of 10 ppt as the target mole fractions in the standard was a first guess. Subsequently, the internal addition standards were prepared at lower target mole fractions, as the current ambient dry air mole fractions are much lower than the first primary standard.

The calibration gas preparation was done using stainless steel vacuum lines in the Weiss laboratory at SIO. The high-purity compounds for both sets of standards were purchased from Synquest Laboratories with purities of: C_4F_{10} (98 % min.), C_5F_{12} (99 % min.), C_6F_{14} (98.5 % min.), C_7F_{16} (98 % min.) and C_8F_{18} (99 % min.); the nitrous oxide (N_2O) was purchased from Scott Specialty Gases and had a purity of 99.9997 %, and the dichlorodifluoromethane (CCl_2F_2, CFC-12) had a purity of 99.99 %. Each high-purity compound was transferred to a stainless steel canister, which was made from a Vollrath Stainless Steel 125-mL beaker and a Swagelok 1/4 inch port connector at the SIO Machine shop. The stainless steel canisters were

Table 2.4: PFC/N_2O Mixture Target Concentrations, Ratios, Moles and Mass for the External Additions Standard

	N_2O	C_4F_{10}	C_5F_{12}	C_6F_{14}	C_7F_{16}	C_8F_{18}
Target Concentration [ppt]	320 000	10	10	10	10	10
Ratio to N_2O [ppt/ppt]	1	3.13E-05	3.13E-05	3.13E-05	3.13E-05	3.13E-05
Molecular Weight [g/mol]	44.01	238.027	288.035	338.04	388.049	438.057
Target Moles [mol]	0.5	1.56E-05	1.56E-05	1.56E-05	1.56E-05	1.56E-05
Target Mass [mg]	22 005	3.719	4.501	5.282	6.063	6.845

electropolished and subsequently rinsed twice with ethanol and dried. C_4F_{10} was transferred to the stainless steel canister using the vacuum line, as the high-purity compound from Synquest was in a gas cylinder. C_5F_{12}, C_6F_{14}, C_7F_{16} and C_8F_{18} are liquids at room temperature, and therefore they were transferred to the stainless steel canisters using a glass pipette. Once the high purity compounds were transferred to the stainless steel canisters, they were vacuum distilled for further purification by repeated cycles of freezing with liquid nitrogen, vacuum removal of non-condensable contaminants and then thawing.

2.2.1 External Additions

Only one standard was prepared using the external additions method. This standard was prepared following the bootstrap method by stepwise dilution with N_2O used as the bootstrap gas. First a PFC/N_2O mixture was prepared with a molar ratio of PFC to N_2O of 3.13E-05 (see Table 2.4). This mixture was prepared by cryo-transferring a known amount of high purity PFC to an evacuated glass capillary tube, which had been previously weighed, using a stainless steel vacuum line (see Figure 2-4). Once all of the high purity compound was transferred, the capillary tube was flame sealed using a micro-torch. The filled capillary tube was then re-weighed and a buoyancy correction was applied to provide the total mass/moles of PFC added to the mixture.

To transfer the PFC capillaries to the PFC/N_2O mixture, one capillary of each compound was loaded into a capillary breaker. The capillary breaker was connected to the vacuum line, evacuated and leak checked. The capillaries were then broken

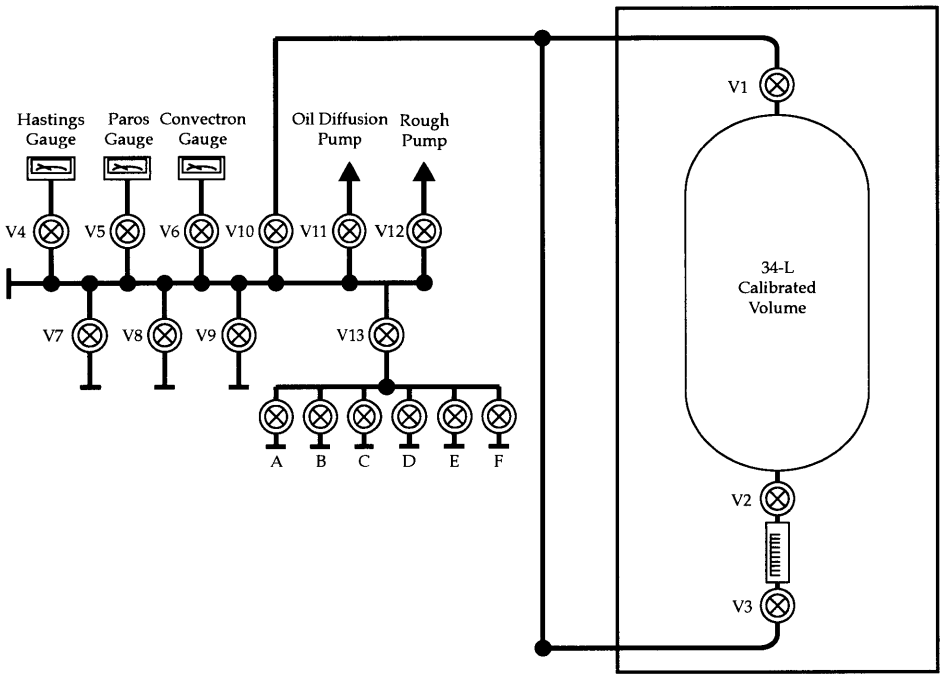

Figure 2-4: A schematic diagram of the SIO vacuum line used for transferring of high-purity compounds, vacuum distillation, capillary preparation and preparation of the PFC/N_2O and PFC/CFC-12/N_2O mixtures.

and the compounds were cryo-transferred to an evacuated 0.85-L stainless steel flask using liquid nitrogen. The capillary breaker was flushed ten times with N_2O in order to ensure that all of the compounds had transferred.

The amount of N_2O added to the PFC/N_2O mixture was measured in a temperature controlled, calibrated 34-L stainless steel volume (see Figure 2-4). The amount of N_2O added was estimated using Van der Waals equation (see Equation (2.8), where P is the pressure, n is the number of moles, V is the volume, R is the universal gas constant, T is the absolute temperature, a is the measure of the attraction between the molecules and b is the volume excluded by a mole of molecules). After measuring the N_2O, the N_2O was then cryo-transferred from the 34-L volume to the 0.85-L stainless steel flask, which already contained the PFCs, using liquid nitrogen. The 0.85-L flask was also weighed evacuated and filled, in order to provide a check to the total amount of N_2O added; the two measurements agreed within less than 1 %.

$$\left(P - \frac{n^2 a}{V^2}\right)(V - nb) = nRT \tag{2.8}$$

A primary standard was prepared by spiking a zero-air sample with the PFC/N_2O mixture in a 36-L electropolished stainless steel tank (Essex Cryogenics, Inc.). The zero-air was from Scott Marin and was further purified using a trap, containing glass beads, activated charcoal, Molecular Sieve 13X and Carboxen 1000, in a dry ice/ethanol bath at -79 °C. The zero-air was measured on the SIO Medusa prior to spiking to ensure it was analyte-free. Figure 2-5 shows the vacuum manifold used in preparing the primary standard. The amount of mixture added to the sample was determined using a 0.1792 cm^3 loop that was set to a specified pressure using a back pressure regulator. The precise amount of the PFC/N_2O mixture added to the tank was determined by precisely measuring the final N_2O dry air mole fraction on a gas chromatography/electron capture detector (GC-ECD) system.

This primary standard was measured on the SIO Medusa to identify and quantify the PFCs on the instrument. The current tropospheric background mole fractions are much lower than our prepared standard, causing possible nonlinearities in estimating

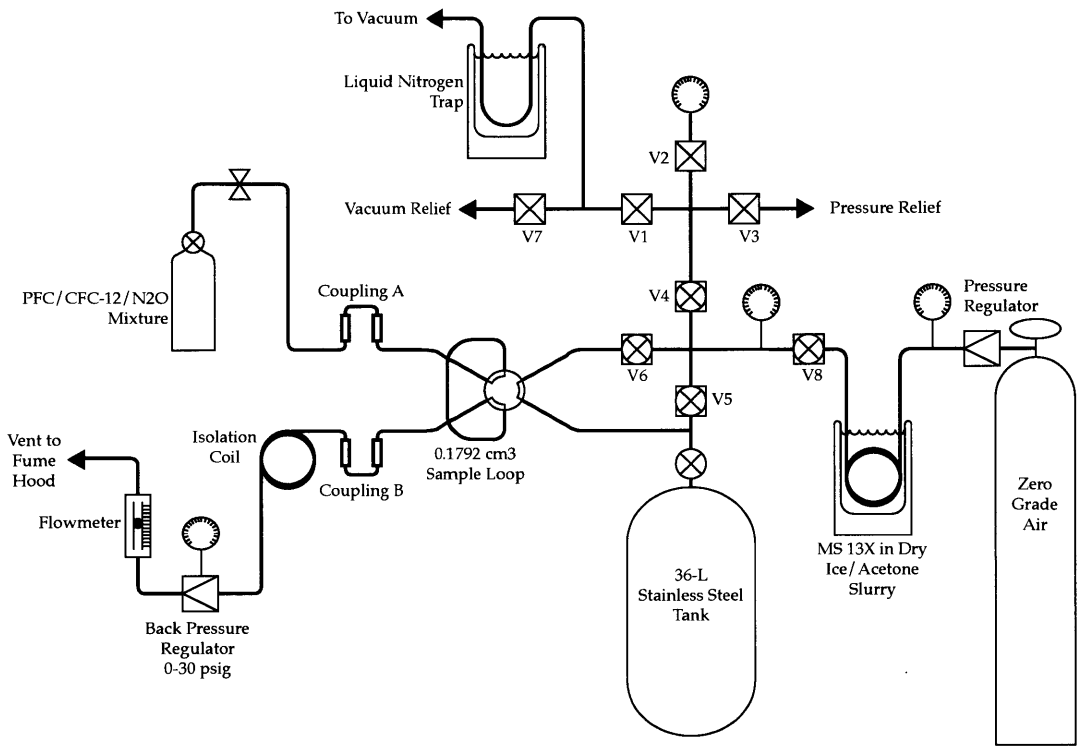

Figure 2-5: A schematic diagram of the spiking system used to prepare primary standards from the PFC/N_2O and PFC/CFC-12/N_2O mixtures.

our calibration scale. Therefore, we prepared an additional four standards using the internal additions method at lower target mole fractions. As only one standard was prepared by the external addition method, it is not included in our final scale estimation. However, this additional standard serves as a useful way to verify that the two methods agree, with a difference in the two estimated calibration scales (relative to a 2009 NH sample) of 7.0 % for C_4F_{10}, 11.3 % for C_5F_{12}, 8.9 % for C_6F_{14}, 5.9 % for C_7F_{16} and 2.3 % for C_8F_{18}.

2.2.2 Internal Additions

Four primary standards were prepared as internal additions with CFC-12 used as the bootstrap gas (*Prinn et al.*, 2000). Typically N_2O is used as the bootstrap gas,

Table 2.5: PFC/CFC-12/N_2O Mixture Target Concentrations, Ratios, Moles and Mass for the Internal Additions Standard

	N_2O	CFC-12	C_4F_{10}	C_5F_{12}	C_6F_{14}	C_7F_{16}	C_8F_{18}
Target Concentration [ppt]	320 000	540	1	1	2	1	1
Ratio to N_2O [ppt/ppt]	1	1.69E-3	3.12E-6	3.12E-6	3.12E-6	6.25E-6	3.12E-6
Ratio to CFC-12 [ppt/ppt]	592.6	1	1.85E-3	1.85E-3	3.71E-3	1.85e-3	1.85E-3
Molecular Weight [g/mol]	44.01	120.91	238.027	288.035	338.04	388.049	438.057
Target Moles [mol]	0.3	5.06E-4	9.38E-5	9.38E-5	1.88E-6	9.38E-5	9.38E-5
Target Mass [mg]	13 203	61.211	0.223	0.270	0.634	0.364	0.411

as in the case for the external additions; however these standards were prepared as internal additions, and the expected final N_2O dry air mole fractions would have been beyond the range of the currently available SIO calibration scale. Therefore, CFC-12 was used as the bootstrap gas, as the resulting final mole fractions of CFC-12 can be accurately measured on the Medusa.

Four gravimetric PFC/CFC-12/N_2O mixtures were prepared, with Chris Harth at SIO, with molar ratios of PFC to CFC-12 of (1.85 to 3.71)$\times 10^{-3}$ in 0.85-L stainless steel flasks, with CFC-12 as the bootstrap gas and N_2O as the balance gas (see Table 2.5). These mixtures were prepared similarly to the external additions, with the CFC-12 also being transferred using the capillary tubes.

Four primary standards were then prepared, by Chris Harth, by spiking decanted samples from a whole-air sample filled at La Jolla, CA (32.87 °N, 117.25 °W) with each of the PFC/CFC-12/N_2O mixtures. The decanted samples were spiked using the second vacuum manifold (see Figure 2-5), similarly as in the external additions method. The whole-air sample was measured on the Medusa to determine its initial CFC-12 dry air mole fraction and instrument response for each PFC. The additional dry air mole fractions added to the whole-air sample from the PFC/CFC-12/N_2O spike were ca. 2 ppt of C_6F_{14}, 1 ppt of the other PFCs and 540 ppt of CFC-12. The enhancement factor of the PFC/CFC-12/N_2O mixture added to the whole-air sample was determined by measuring the final CFC-12 dry air mole fractions on the Medusa. The final atmospheric mole fractions in the primary standard were

determined using Equation (2.9), where C_R is the concentration in the reference tank (taken as the decanted sample from La Jolla), C_S is the known concentration added to the primary standard, r_R is the instrument response of the reference tank and r_{R+S} is the instrument response to the spiked primary standard (*Ellison and Thompson*, 2008).

$$C_R = C_S \times \frac{r_R}{r_{R+S} - r_R} \tag{2.9}$$

As the spiked primary tank was measured against the reference tank, Equation (2.9) can be rewritten as Equation (2.10), where RL_{R+S} is the relative response of the instrument of the spiked primary standard to the unspiked decanted whole-air sample, or reference tank.

$$C_R = \frac{C_S}{RL_{R+S} - 1} \tag{2.10}$$

2.2.3 Summary

The primary standards were measured on the Medusa to determine the retention times and mass spectra of the high molecular weight PFCs, as well as to quantify the atmospheric observations. The mass spectra of the high molecular weight PFCs agree with published spectra from the National Institute of Standards and Technology (see Figure 2-6) and the retention times are consistent with what is expected based on their boiling points (*NIST Mass Spec Data Center, http://webbook.nist.gov*). Table 2.6 shows the target and qualifier mass-to-charge ratios, as well as the retention times, used on the SIO and CSIRO Medusa systems; the target mass-to-charge ratio is used for identification and quantitation, while the qualifiers are only used for ensuring the proper identification of the species.

The calibration scales were estimated by measuring each primary standard against a 2009 NH air archive sample, which is the reference tank for this scale. The calibration scales from both methods are presented in Table 2.7. We have used the mean of the four measurements of the 2009 NH archive air sample relative to each of the

primary standards prepared via the internal addition methods in determining the final calibration scale, also presented in Table 2.7, referred to as SIO-2012. This calibration scale has estimated accuracies of 6.8 % for C_4F_{10}, 7.8 % for C_5F_{12}, 4.0 % for C_6F_{14}, 6.6 % for C_7F_{16} and 7.9 % for C_8F_{18}, which takes into account the purity of the compound, the accuracy of the gravimetric balance, the precision of the boot-strap gas measurements and the precision of the standard measurements.

Table 2.6: Retention Times, Target and Qualifier Mass-to-Charge Ratios for C_4F_{10}, C_5F_{12}, C_6F_{14}, C_7F_{16} and C_8F_{18}*

Species	Main Column	MS	Retention Time [s]	Target [m/z]	Qualifier 1 [m/z]	Qualifier 2 [m/z]
C_3F_8	PoraBOND	5975	510			
	GasPro	5973	705			
$CHClF_2$ [HCFC-22]	PoraBOND	5975	539			
	GasPro	5973	757			
C_4F_{10}	**PoraBOND**	**5975**	**599**	119	219	131
	GasPro	**5973**	**794**	119	219	150
$CBrClF_2$ [H-1211]	PoraBOND	5975	669			
	GasPro	5973	823			
CH_3CCl_2F [HCFC-142b]	PoraBOND	5975	678			
	GasPro	5973	856			
C_5F_{12}	**PoraBOND**	**5975**	**676**	119	169	–
	GasPro	**5973**	**873**	119	169	181
$C_3H_2F_6$ [HFC-236fa]	PoraBOND	5975	617			
	GasPro	5973	876			
CH_2Cl_2	PoraBOND	5975	717			
	GasPro	5973	939			
C_6F_{14}	**PoraBOND**	**5975**	**742**	169	119	–
	GasPro	**5973**	**948**	119	169	219
$C_2H_3Cl_2F$ [HCFC-141b]	PoraBOND	5975	741			
	GasPro	5973	965			
CCl_4	PoraBOND	5975	849			
	GasPro	5973	1035			
C_7F_{16}	**PoraBOND**	**5975**	**800**	219	169	–
	GasPro	**5973**	**1040**	169	219	–
$C_4H_5F_5$ [HFC-365mfc]	PoraBOND	5975	672			
	GasPro	5973	1067			
CH_3CCl_3	PoraBOND	5975	841			
	GasPro	5973	1124			
C_8F_{18}	**PoraBOND**	**5975**	**855**	219	269	–
	GasPro	**5973**	**1168**	219	119	69
C_2Cl_4 [PCE]	PoraBOND	5975	959			
	GasPro	5973	1194			

*Additional compounds are shown for reference. Parameters for the oven are: ramping from 40 °C to 20 °C over 7 minutes for both the GasPro and PoraBOND with the ovens subsequently held at 200 °C. The pressure is ramping at the same time to maintain a constant flow from 6.1 to 15.1 psig for the PoraBOND column and from 9 to 18 psig for the GasPro column and subsequently held constant.

Table 2.7: Calibration Scale and Reference Sample Measurements for C_4F_{10}, C_5F_{12}, C_6F_{14}, C_7F_{16} and C_8F_{18} by External and Internal Additions Methods*

Species	External Additions [ppt***]	Internal Additions P-049** [ppt]	P-050 [ppt]	P-051 [ppt]	P-052 [ppt]	Mean [ppt]	Stdev [ppt]
C_4F_{10}	0.184	0.172±0.006	0.170±0.006	0.174±0.006	0.171±0.006	0.172	0.002
C_5F_{12}	0.110	0.124±0.005	0.124±0.005	0.123±0.005	0.124±0.006	0.124	0.001
C_6F_{14}	0.246	0.272±0.006	0.267±0.006	0.270±0.006	0.270±0.006	0.270	0.002
C_7F_{16}	0.111	0.118±0.005	0.120±0.006	0.114±0.005	0.120±0.006	0.118	0.003
C_8F_{18}	0.085	0.089±0.008	0.085±0.007	0.086±0.007	0.088±0.008	0.087	0.002

*These measurements are the concentration of a single reference tank T-008B, which is a 2009 Northern Hemisphere archive air sample, relative to each primary standard.
**P-049 through P-052 are the names of the primary standard samples prepared via the internal additions method.
***ppt = parts-per-trillion dry air mole fraction.

2.3 Archived Air Samples

2.3.1 Northern Hemisphere

The atmospheric histories of the high molecular weight PFCs are based on measurements made at SIO and CSIRO of NH and SH archived air samples, which cover a 39-year period. In total, 36 separate NH samples (33 measured at SIO and 3 measured at CSIRO) with fill dates from 1973 to 2011 were analyzed. These samples were filled during baseline conditions either at Cape Meares, Oregon (45.50 °N, 123.95 °W), La Jolla, California (32.87 °N, 117.25 °W) or Trinidad Head, California (41.05 °N, 124.05 °W) and one sample was filled at Harvard Forest, Massachusetts (42.53 °N, 72.19 °W) and are from the laboratories of R.F. Weiss, R.F. Keeling, and the late C.D. Keeling at SIO and R.A. Rasmussen at the Oregon Graduate Center (Beaverton, Oregon) (see Figure 2-7 for sample fill locations and Table 2.8 for number of samples per fill location). The fill techniques, tank materials, tank sizes and scientific purposes of the tanks varied. Two samples were identified as outliers with dry air mole fractions significantly higher than present day values. One 1978 sample was rejected for C_4F_{10} and C_5F_{12}, but a second sample with an identical fill date was also measured. Additionally a 1974 sample with an elevated dry air mole fraction was rejected for C_8F_{18}, as samples with similar fill dates were below the detection limit. From 2003 onward, a collection of tanks containing samples of NH air has been maintained as an air archive at the lab of R.F. Weiss at SIO. These samples were pumped into 35-L internally electropolished stainless steel cylinders (Essex Cryogenics) at Trinidad Head, California using a modified oil-free compressor (Rix Industries). Recent filled archive samples agree with in situ measurements made by the Medusa system at the time of the tank filling for the high molecular weight PFCs studied here, confirming that the modified Rix compressor does not compromise the integrity of these samples for the high molecular weight PFCs.

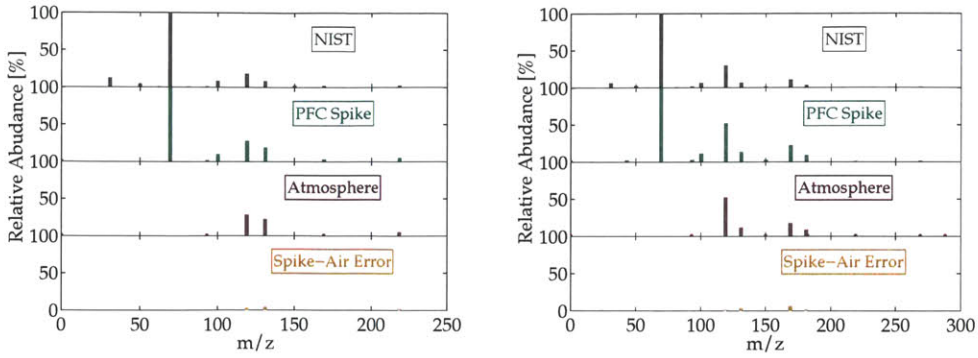

(a) C_4F_{10}

(b) C_5F_{12}

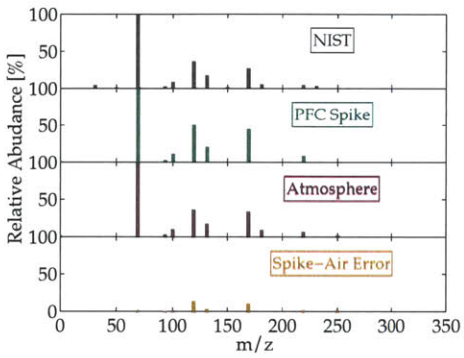

(c) C_6F_{14}

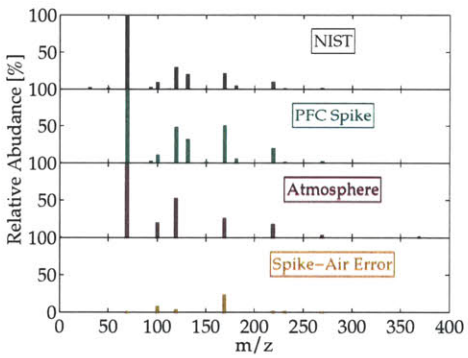

(d) C_7F_{16}

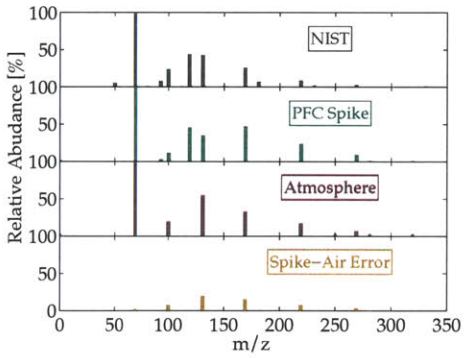

(e) C_8F_{18}

Figure 2-6: Relative mass spectra of a) C_4F_{10}, b) C_5F_{12}, c) C_6F_{14}, d) C_7F_{16} and e) C_8F_{18} provided from the NIST spectra library (top panel) (*NIST Mass Spec Data Center, http://webbook.nist.gov*), as well as those from the prepared standard via external additions (second panel) and a whole-air sample (third panel). The bottom panel shows the difference in relative abundance between the prepared standard and whole-air sample. Mass-to-charge ratios not shown in the whole-air sample had a coelution and could not be properly quantified.

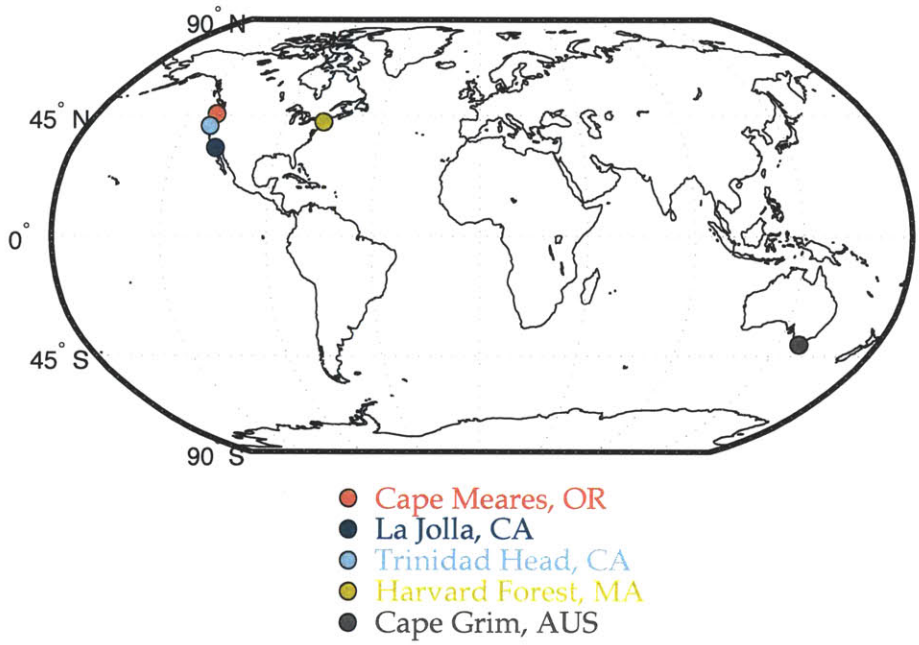

Figure 2-7: Map showing archived air sample fill locations.

Table 2.8: Number of Samples at Northern Hemisphere Locations

Location	No. Samples
La Jolla, CA	18
Trinidad Head, CA	15
Cape Meares, OR	1
Harvard Forest, MA	1

2.3.2 Southern Hemisphere

Forty-six separate SH samples, with fill dates between 1978 and 2010, were also measured (6 at SIO and 40 at CSIRO). All but three of these samples (which are from the M.A. Wahlen laboratory at SIO) are part of the CGAA collection (*Krummel et al.*, 2007; *Langenfelds et al.*, 1996). The CGAA samples analyzed as part of this study consist of whole-air samples cryogenically filled in 35-L internally electropolished stainless steel cylinders at the Cape Grim Baseline Air Pollution Station in Tasmania, Australia (40.68 °S, 144.69 °E), except for three that were cryogenically collected in 48-L aluminum cylinders; these latter three samples were rejected for C_8F_{18}, as their values were significantly higher than present-day background dry air mole fractions. Five archive samples, all collected in 2001 and 2002, had significantly higher than current baseline dry air mole fractions for C_7F_{16} and these values were consequently flagged as contaminated; these flagged samples included the three samples from the M.A. Wahlen laboratory and two CGAA samples. These five samples were all stored in stainless steel cylinders, and therefore a local source at the Cape Grim Station most likely influenced them. The Wahlen samples were also rejected for C_6F_{14}, as an unidentified analyte coeluted.

Three samples with fill dates of December 01, 2004, June 28, 2005 and February 10, 2006 were measured three separate times over the experimental time period (January 25, 2011, February 5, 2011 and February 14, 2011) at CSIRO. These "thread" samples served to ensure that the instrument was not drifting over the experiment period. Figure 2-8 shows the thread sample measurements by date on the CSIRO Medusa for the PFCs.

For both sets of archived samples, at least 3 replicate measurements were made of each sample; for younger samples, 5 to 6 replicate measurements were made since more air was available. The measurement errors on the samples are estimated as the 1-σ standard deviations of the repeat measurements, and samples below the detection limit of the Medusa were assigned a measurement error equal to that of the detection limit for the purpose of inverse modeling.

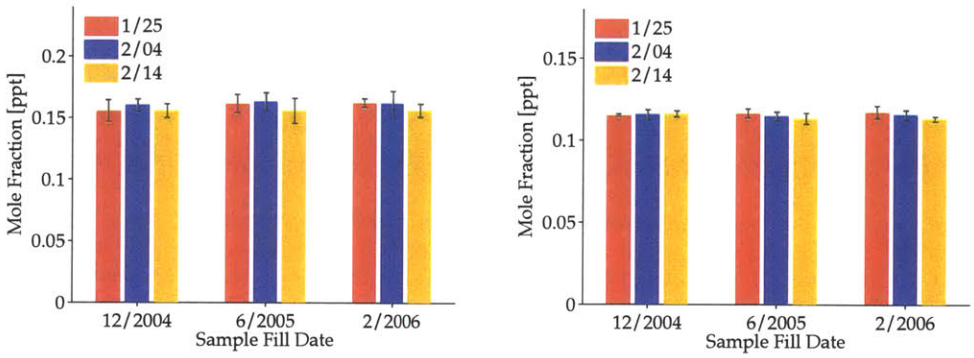

(a) C_4F_{10}

(b) C_5F_{12}

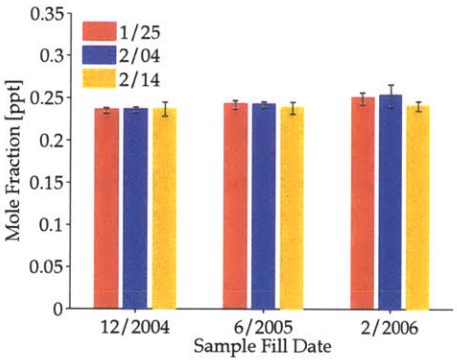

(c) C_6F_{14}

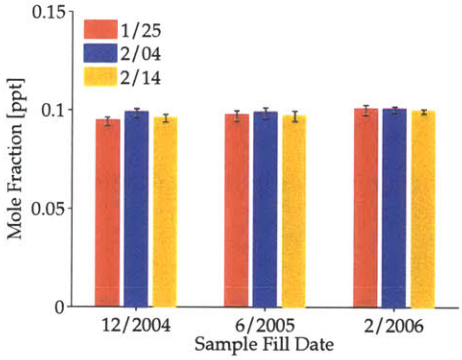

(d) C_7F_{16}

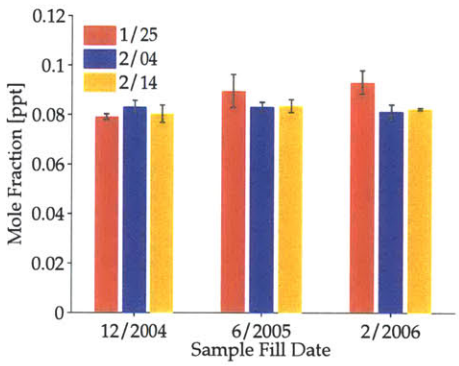

(e) C_8F_{18}

Figure 2-8: "Thread" sample measurements for a) C_4F_{10}, b) C_5F_{12}, c) C_6F_{14}, d) C_7F_{16} and e) C_8F_{18} measured on January 25, 2011, February 4, 2011 and February 14, 2011 showing reproducibility of the measurements at CSIRO over time. The associated error bars are the 1-σ standard deviations of the repeat measurements.

2.3.3 Subsamples

Seven subsamples of the CGAA, with fill dates covering the time period of 1986 to 2008, were decanted into 4.5-L internally electropolished stainless steel cylinders (Essex Cryogenics) using a vacuum manifold (see Figure 2-9) and subsequently measured on the SIO Medusa system; the parent samples were measured at CSIRO in Aspendale. These subsamples were used to verify whether the two instruments and the calibration scale propagation produced measurements that agreed within known uncertainties. As with the dilution samples, 1/16 inch stainless steel tubing was used in decanting the parent sample in order to restrict the flow rate and avoid the need for a pressure regulator, which could be a source of contamination. Figure 2-10 and Table 2.9 show the comparison of the subsamples to the parent samples measured on the two instruments. Generally, the measurements on the two systems agreed well within the measurement uncertainty. The most notable differences between the two instruments was for C_8F_{18}.

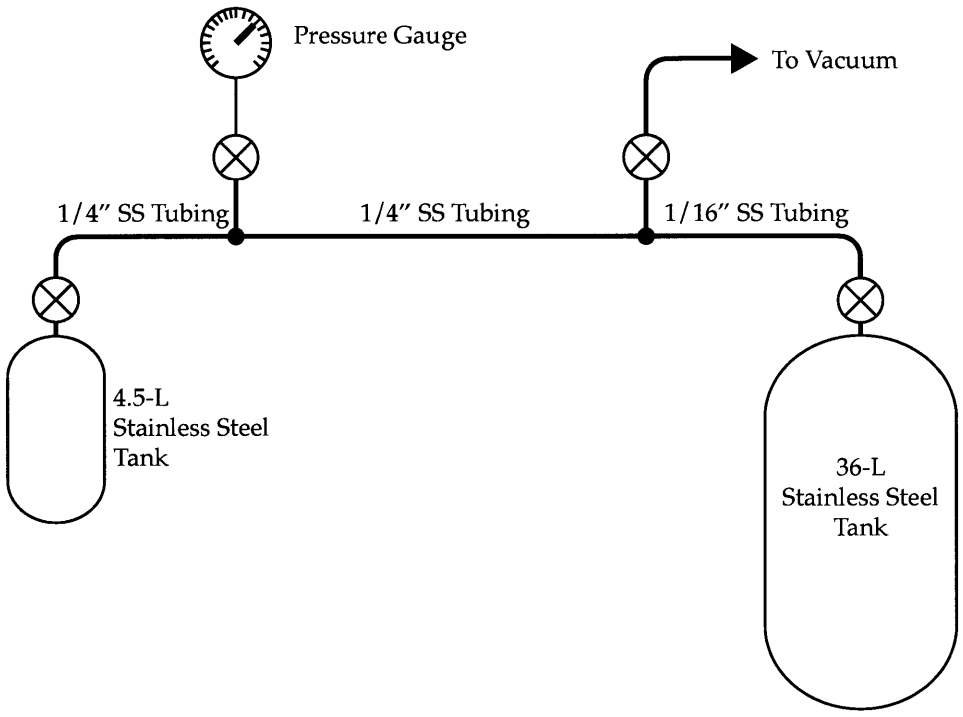

Figure 2-9: Schematic diagram of the vacuum manifold used for decanting Cape Grim Air Archive samples to evacuated 4.5-L stainless steel tanks, termed "subsamples", measured on the SIO Medusa.

Table 2.9: Atmospheric Measurements of Parent (CSIRO Medusa) and Subsample (SIO Medusa) Samples for C_4F_{10}, C_5F_{12}, C_6F_{14}, C_7F_{16} and C_8F_{18}

		Parent			Subsample		
Species	Sample Fill Date	Mean [ppt*]	Stdev [ppt]	n	Mean [ppt]	Stdev [ppt]	n
C_4F_{10}	6-Feb-1986	0.0483	0.0032	4	0.0469	0.0011	3
	26-Apr-1990	0.0785	0.0054	3	0.0717	0.0026	3
	4-Dec-1995	0.1052	0.0045	5	0.1102	0.0041	3
	25-Jun-1998	0.1270	0.0078	5	0.1222	0.0024	3
	15-Jan-2001	0.1357	0.0078	4	0.1396	0.0049	3
	10-Feb-2006	0.1607	0.0068	15	0.1555	0.0033	3
	12-Aug-2008	0.1624	0.0036	6	0.1679	0.0078	3
C_5F_{12}	6-Feb-1986	0.0368	0.0021	4	0.0345	0.0018	3
	26-Apr-1990	0.0573	0.003	3	0.0554	0.002	3
	4-Dec-1995	0.0857	0.0041	5	0.0830	0.0024	3
	25-Jun-1998	0.0947	0.0021	5	0.0945	0.0029	3
	15-Jan-2001	0.1062	0.0026	4	0.1067	0.0030	3
	10-Feb-2006	0.1155	0.0033	15	0.1225	0.0033	3
	12-Aug-2008	0.1186	0.0035	6	0.1279	0.0055	3
C_6F_{14}	6-Feb-1986	0.0354	0.0037	4	0.0389	0.0013	3
	26-Apr-1990	0.0565	0.0043	3	0.0561	0.0014	3
	4-Dec-1995	0.1020	0.0038	5	0.1064	0.0025	3
	25-Jun-1998	0.1618	0.0044	5	0.1683	0.0018	3
	15-Jan-2001	0.1997	0.0059	4	0.2026	0.0068	3
	10-Feb-2006	0.2481	0.0100	15	0.2482	0.0012	3
	12-Aug-2008	0.2554	0.0065	6	0.2635	0.0026	3
C_7F_{16}	6-Feb-1986	0.0254	0.0017	4	0.0234	0.0008	3
	26-Apr-1990	0.0452	0.003	3	0.0407	0.0005	3
	4-Dec-1995	0.0639	0.0016	5	0.0624	0.0026	3
	25-Jun-1998	0.0774	0.0013	5	0.0757	0.0015	3
	15-Jan-2001	0.0861	0.0023	4	0.0836	0.0018	3
	10-Feb-2006	0.1001	0.0018	15	0.0999	0.0021	3
	12-Aug-2008	0.1115	0.0008	6	0.1126	0.0012	3
C_8F_{18}	6-Feb-1986	0.0179	0.0046	4	0.0104	0.0022	3
	26-Apr-1990	0.0366	0.0023	2	0.024	0.0009	3
	4-Dec-1995	0.0477	0.0029	5	0.0431	0.0039	3
	25-Jun-1998	0.0625	0.0043	5	0.0577	0.0031	3
	15-Jan-2001	0.0734	0.0020	4	0.0703	0.0046	3
	10-Feb-2006	0.0863	0.0059	15	0.0787	0.0013	3
	12-Aug-2008	0.0903	0.0042	6	0.0830	0.0026	3

*ppt = parts-per-trillion dry air mole fraction.

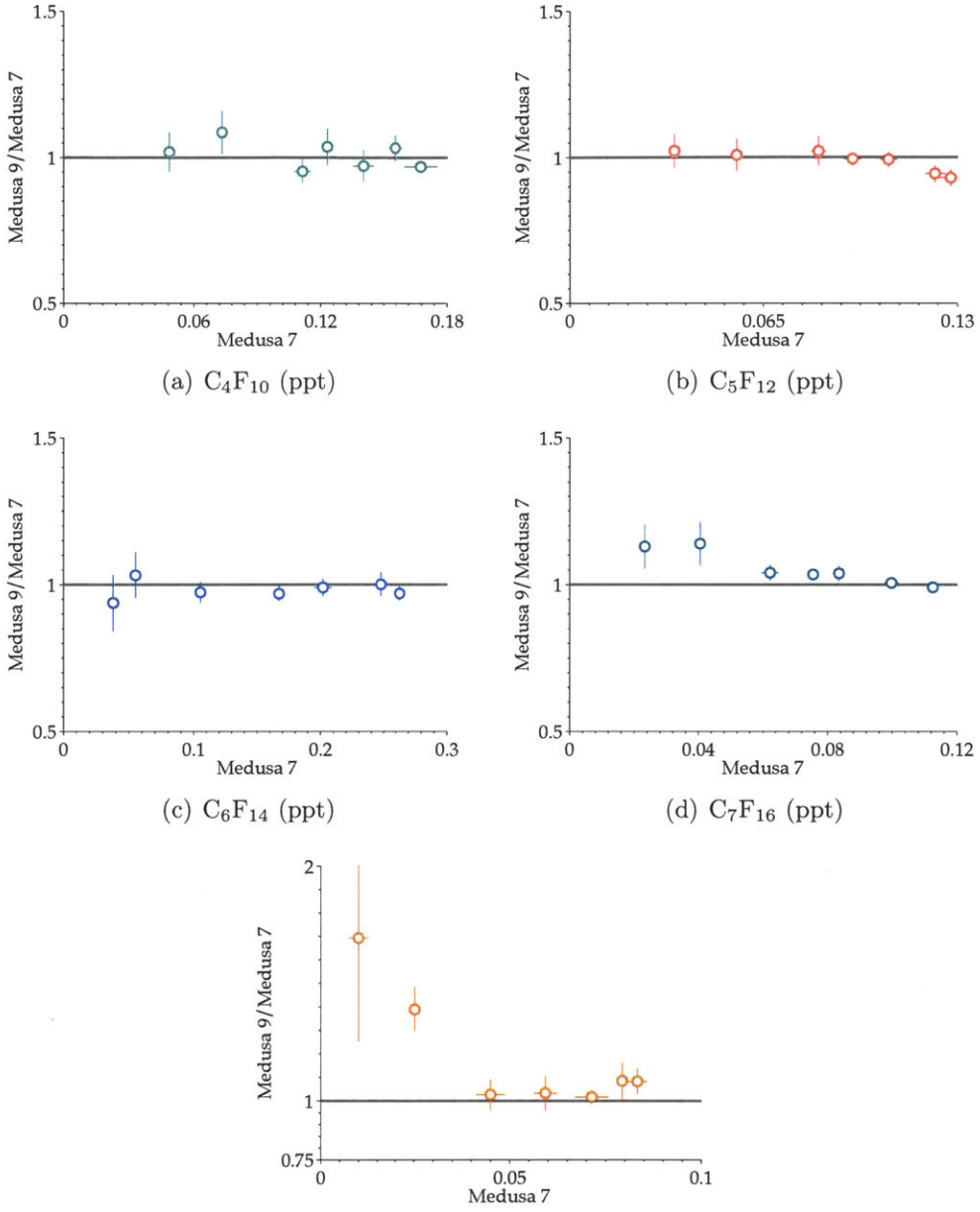

(a) C_4F_{10} (ppt)

(b) C_5F_{12} (ppt)

(c) C_6F_{14} (ppt)

(d) C_7F_{16} (ppt)

(e) C_8F_{18} (ppt)

Figure 2-10: Plots comparing the subsample measurements on the SIO Medusa (M7) to the relative measurements of the parent sample measurements on the CSIRO Medusa (M9) for a) C_4F_{10}, b) C_5F_{12}, c) C_6F_{14}, d) C_7F_{16} and e) C_8F_{18}. The associated horizontal and vertical lines are the measurement uncertainties. A line at one is plotted for reference.

Chapter 3

Inverse Modeling

This chapter outlines the methods used to estimate the global emissions for the high molecular weight PFCs based on the atmospheric observations. Section 3.1 describes the chemical transport model used to provide the forward reference model runs and the sensitivity estimates of the atmospheric mole fractions to changes in emission rates. The next section outlines the inverse method used to constrain the emission estimates, which takes into account the atmospheric observations and an independent estimate of the growth rate in emissions. Section 3.3 describes the two available bottom-up emission estimates from EDGARv4.2 and the UNFCCC.

3.1 Chemical Transport Model

The Model of Ozone and Related chemical Tracers (MOZARTv4.5) is a 3-dimensional chemical transport model (*Emmons et al.*, 2010). MOZARTv4.5 was developed jointly by the National Center for Atmospheric Research, the Geophysical Fluid Dynamics Laboratory and the Max Planck Institute for Meteorology. While MOZARTv4.5 was initially developed to simulate tropospheric ozone, it has subsequently also been used in several inverse modeling studies to constrain emission rates of long lived greenhouse gases (e.g. *Rigby et al.* (2011); *Saikawa et al.* (2011)).

In this study, MOZARTv4.5 was run offline to produce the reference run of modeled atmospheric mole fractions and to estimate the sensitivities of the atmospheric

mole fractions to perturbations in emission rates. Meteorological data were provided from the National Centers for Environmental Prediction/National Center for Atmospheric Research (NCEP/NCAR) reanalysis data (*Kalnay et al.*, 1996). The NCEP/NCAR reanalysis data for use in MOZARTv4.5 are available from 1990 to 2008 every 6 hours at a horizontal resolution of 1.8° longitude by 1.8° latitude and with 28 vertical levels in sigma coordinates, from the surface to 3 hPa. MOZARTv4.5 interpolated the meteorological data to a resolution of 2.8° longitude by 2.8° latitude, which was the chosen horizontal resolution of the model runs. For all years prior to 1990, NCEP/NCAR reanalysis data from 1990 were used; and for all years after 2008, the 2008 meteorological data were used. The PFCs were treated as tracers and no chemistry was input into MOZARTv4.5; this is a reasonable assumption given that the model run only spanned a few decades, while the PFCs' lifetimes are on the order of thousands of years (*Ravishankara et al.*, 1993). A zero initial condition field was assumed for all of the high molecular weight PFCs, with an initial year based on EDGARv4.2's first non-zero emissions of 1971 for C_4F_{10}, 1986 for C_5F_{12}, C_7F_{16} and C_8F_{18}, and 1980 for C_6F_{14}. Monthly means were output at the observation grid cell in the model runs, as the observations were assumed to be representative of the monthly averaged mole fractions. The upwind cells of the observation stations were chosen in MOZARTv4.5 as the representative grid cells, as the observations are assumed to be representative of background air.

3.2 Inverse Method

Often a minimum variance Bayesian approach is taken for atmospheric measurement-based emission estimates using atmospheric observations and an independent estimate of absolute emissions, also known as a prior, as a constraint. If the prior emission information is suspected to be largely biased, as it is for C_4F_{10} and C_5F_{12}, a large uncertainty is assumed for the prior. This results in the prior providing little influence on the derived emissions if numerous and precise observations are available at locations sensitive to the emission sources. Alternatively, if observations are not available

for a certain year, then the derived emissions can exhibit unphysical fluctuations due to the biased prior constraining the emissions.

Here, we use a growth constrained inverse method along with the atmospheric observations to derive global emissions. The growth based Bayesian inverse approach, which incorporates the growth rate of emissions as prior information in the inversion instead of absolute emission rates, overcomes some of these aforementioned biases (*Rigby et al.*, 2011). Firstly, in the inversion a linear model, matrix **E**, is used to relate the emissions, in vector **x**, to the observations, in vector **y** (see Equation (3.1) below). This model, matrix **E**, represents the integral of the net chemical production (emissions minus sinks) of the species along the Lagrangian back trajectory of the measured air mass (or its equivalent in an Eulerian framework). In order to estimate the sensitivities (matrix **E**) of the atmospheric mole fractions to changes in emission rates, MOZARTv4.5 was run with annual emissions increased by 10 % from a reference run for one year. In the subsequent year, the emissions were returned to those of the reference run. This provided an estimate of the sensitivities of mole fractions at the observation grid cells to changes in annual emission rates. Due to the computational expense of running MOZARTv4.5, these sensitivities were only tracked in the model for two years, and then the values were estimated to decay exponentially, due to mixing, to a globally well-mixed background value; one year was chosen as the time scale for the sensitivities to decay, which is appropriate in representing transport from the mid-latitudes in one hemisphere to the mid-latitudes in another.

$$\mathbf{y} = \mathbf{E}\mathbf{x} + residual \tag{3.1}$$

A finite differences approach was used to calculate the sensitivity estimates (see Equation (3.2) below, where e_{ijk} is the sensitivity of the observation, y_{ik}, to a change in emissions, x_j). Figure 3-1 shows an example of the sensitivity of the modeled mole fractions at the observation grid cells to changes in the global emission rates for each of the PFCs.

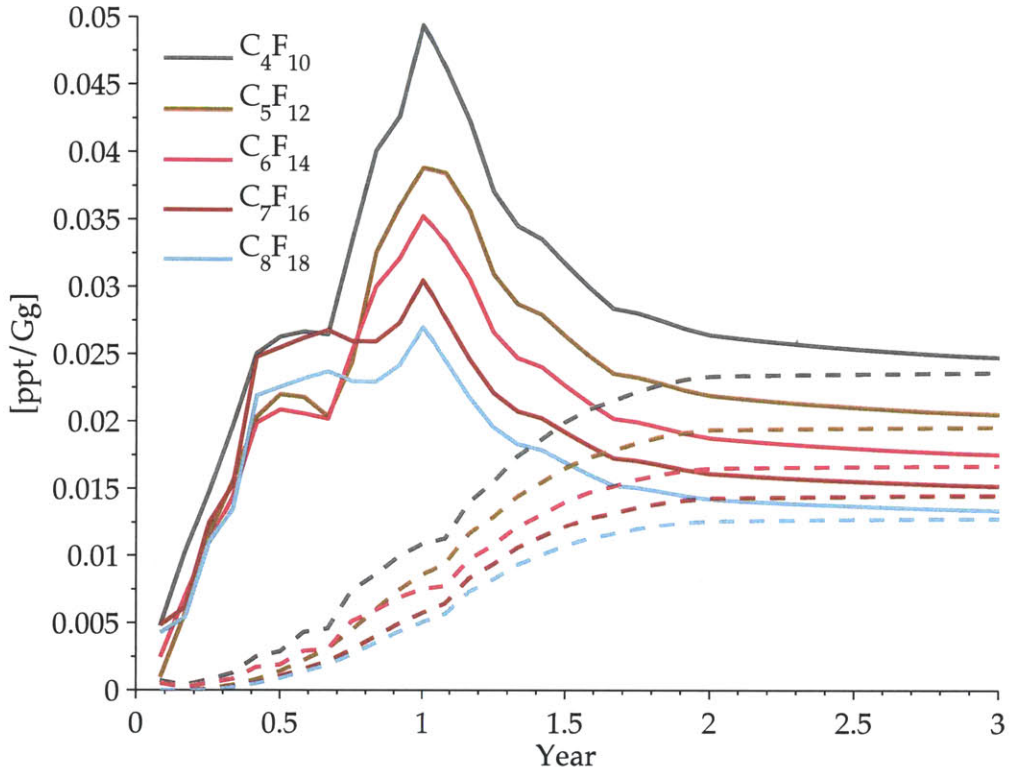

Figure 3-1: Sensitives at the Northern (solid lines) and Southern (dashed lines) Hemisphere grid cells to changes in emission rates for each of the high molecular weight PFCs.

$$e_{ijk} = \frac{\partial y_{ik}}{\partial x_j} \tag{3.2}$$

The growth constraint is introduced in the cost function (see Equation (3.3)), which aims to minimize the weighted differences between the observed mole fractions, $\mathbf{y}$, and modeled mole fractions, $\mathbf{Ex}$, and between the growth rate in the derived emissions, $\mathbf{Dx}$, and an independent estimate of the growth rate, $\mathbf{g}$. The matrix operator, $\mathbf{D}$, determines the growth rate of the derived emissions (see Equation (3.4)). Each of these constraints are inversely weighted by an estimate of their uncertainties (expressed as variances) in determining the optimal solution, where $\mathbf{R}$ is the covariance matrix containing the the observational uncertainties and $\mathbf{S}$ is the covariance

matrix containing the uncertainties in the independent growth rate of emissions.

$$J = (\mathbf{y} - \mathbf{Ex})^T \mathbf{R}^{-1} (\mathbf{y} - \mathbf{Ex}) + (\mathbf{Dx} - \mathbf{g})^T \mathbf{S}^{-1} (\mathbf{Dx} - \mathbf{g}) \tag{3.3}$$

$$\mathbf{D} = (1/\Delta T) \begin{pmatrix} -1 & 1 & 0 & \cdots & 0 \\ 0 & -1 & 1 & \cdots & 0 \\ \vdots & \vdots & \ddots & \ddots & \vdots \\ 0 & 0 & \cdots & -1 & 1 \\ 0 & 0 & \cdots & 0 & 0 \end{pmatrix} \tag{3.4}$$

The assumed independent growth rate, $\mathbf{g}$, was the annual average growth rate in emissions for each species from EDGARv4.2. EDGARv4.2 does not provide an uncertainty estimate and because of the underestimation in C_4F_{10} and C_5F_{12} in the EDGARv4.2 estimates, the error assumed on the growth rate for C_4F_{10} and C_5F_{12} was the mean annual growth rate in emissions of C_4F_{10}, C_5F_{12}, C_6F_{14} and C_7F_{16} from EDGARv4.2 and a minimum error equal to the temporal mean growth rate over the entire time period. For C_6F_{14}, the assumed error was the mean growth rate in emissions from 1980 to 2008 from EDGARv4.2 for C_6F_{14}, and likewise for C_7F_{16} and C_8F_{18}. These errors are squared for inclusion and expressed as variances in the covariance matrix, $\mathbf{S}$.

The solution that minimizes Equation (3.3) is shown in Equation (3.5), with the associated error covariance, matrix $\mathbf{P}$, for the solution shown in Equation (3.6). We express the errors associated with the derived solution as the square root of the diagonal elements of this error covariance matrix (matrix $\mathbf{P}$). Due to the low temporal frequency of the observations, only globally averaged emissions are able to be resolved.

$$\mathbf{x} = \mathbf{P} \left(\mathbf{E^T R^{-1} y} + \mathbf{D^T S^{-1} g} \right) \tag{3.5}$$

$$\mathbf{P} = \left(\mathbf{E^T R^{-1} E} + \mathbf{D^T S^{-1} D} \right)^{-1} \tag{3.6}$$

The year of onset of emissions in EDGARv4.2 appears to be later than the ob-

servations suggest, as observations are non-zero in earlier years. Therefore, an initial condition was also solved for in the inversion. The initial condition was applied globally; as the first SH observation is 5 years after the first NH observation, this should not have a large influence on the derived emissions.

3.2.1 Errors

Observational Errors The random error associated with a measurement can never be known. Nonetheless, its relative distribution can be inferred through the standard deviations of associated observational errors. This observational uncertainty includes an estimate of the uncertainties associated with the measurements, the sampling frequency, grid cell model mismatch and use of repeated dynamics when applicable (see Equation (3.7)) (*Rigby et al.*, 2010). These errors are added in quadrature, under the assumption that the individual errors are uncorrelated and normally distributed with a zero mean.

$$\sigma^2_{observational} = \sigma^2_{measurement} + \sigma^2_{samplingfrequency} + \sigma^2_{mismatch} + \sigma^2_{dynamics} \tag{3.7}$$

The measurement uncertainty, $\sigma_{measurement}$, can further be divided into errors associated with the instrument precision, flask error and intercalibration error (see Equation (3.8)) (*Chen and Prinn*, 2006). The instrument precision was taken from Table 2.1. The flask error was assumed to be the standard deviation of the individual flask measurements. No intercalibration error was used since only one calibration scale is available. Observations that were below the detection limit of the instruments were assigned a minimum uncertainty equal to that of the detection limit.

$$\sigma^2_{measurement} = \sigma^2_{instrumentprecision} + \sigma^2_{flaskerrors} + \sigma^2_{intercalibration} \tag{3.8}$$

The sampling frequency uncertainty, $\sigma_{samplingfrequency}$, provides a measure of the uncertainty in our assumption that a single flask is representative of the monthly mean

baseline variability. The sampling frequency error was estimated as the monthly mean variance, σ^2_{mon}, divided by the number of observations taken in that month, m (see Equation (3.9)). Since high frequency data are not available, the sampling frequency uncertainty was estimated as the standard deviation of the daily output mole fractions from MOZARTv4.5 over one month at the observation grid cell.

$$\sigma^2_{samplingfrequency} = \frac{\sigma^2_{mon}}{m} \tag{3.9}$$

The model mismatch error, $\sigma_{mismatch}$, is an estimate of the uncertainty in the assumption that the model grid cell average is representative of a single point measurement within the cell. We estimated the model mismatch error using MOZARTv4.5 as the 1-σ standard deviation of the surrounding eight grid cells and the grid cell that contains the observation location from the mean of all nine cells (see Equation (3.10)) (*Chen and Prinn*, 2006).

$$\sigma^2_{mismatch,k} = \frac{1}{9}\sum_{i=1}^{9}(y_{ik} - \bar{y}_k)^2 \tag{3.10}$$

Reanalysis meteorological data are not available for all required years for use in MOZARTv4.5; therefore to drive MOZARTv4.5, we used data from 1990 for 1971 to 1989 and from 2008 for 2009 to 2011. In order, to characterize the uncertainty in this use of repeated dynamics, $\sigma_{dynamics}$, a one year simulation was run multiple times with different meteorological data from other years, while the emissions and initial conditions were held constant (*Rigby et al.*, 2010). This introduced a mean uncertainty of 5 % at the observation grid cells and was also included in the observational uncertainty (see Equation (3.7)).

Model Errors Alternatively, we also estimated the uncertainty associated with the use of repeated dynamics in the derived emission estimates using a Monte Carlo approach, where the inversion was repeated 1000 times with randomly varied sensitivities of the modeled mole fractions to perturbations in emissions. The distribution of varied sensitivities was estimated by running the model multiple times with meteoro-

logical data from different years and calculating the mole fraction sensitivities, while the emissions and initial conditions were held constant (*Rigby et al.*, 2010). This error was found to be similar to that as estimated as the observational error, $\sigma_{dynamics}$, both of which were relatively small compared to the error propagated through the inversion.

3.3 Bottom-Up Emission Estimates

3.3.1 EDGARv4.2

In order to provide a reference run, the reference emissions were based on the bottom-up emission data available from EDGARv4.2 (*European Commission, Joint Research Centre (JRC)/Netherlands Environmental Assessment Agency (PBL)*, 2009). EDGARv4.2 has global annual emission estimates by source type for C_4F_{10}, C_5F_{12}, C_6F_{14} and C_7F_{16} from 1970 to 2008 (see Figure 3-2) and emissions disaggregated on to a 0.1° longitude by 0.1° latitude grid, with non-zero emissions starting in 1971 for C_4F_{10}, 1986 for C_5F_{12}, 1980 for C_6F_{14} and 1986 for C_7F_{16}. There are no EDGARv4.2 estimates available for C_8F_{18}, therefore C_7F_{16} estimates were used as a proxy. This approximation is based on the assumption that as C_7F_{16} and C_8F_{18} have similar properties, they will most likely have similar emission sources. Furthermore, as the archived samples are assumed to be representative of well-mixed background hemispheric air in the regions they were collected, the emission estimates should be relatively insensitive to the relative hemispheric spatial distributions of emissions. For 2009 to 2011, the emissions were linearly interpolated from the 2007 to 2008 data. The annual 0.1° longitude by 0.1° latitude emissions were regridded to a horizontal resolution of 2.8° longitude by 2.8° latitude for use in MOZARTv4.5. Figure 3-3 shows the temporal mean spatial distribution of emissions from 1970 to 2008 at the MOZARTv4.5 grid resolution for C_4F_{10}, C_5F_{12}, C_6F_{14} and C_7F_{16}.

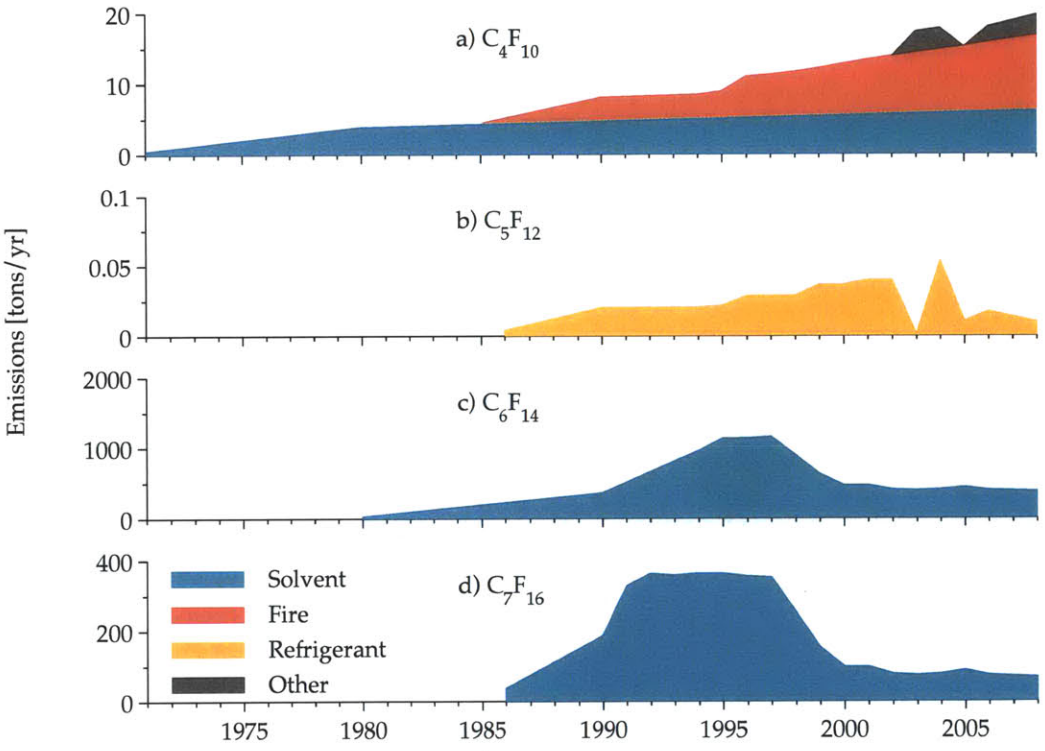

Figure 3-2: Global emission rates from 1971 to 2008 by source from EDGARv4.2 for a) C_4F_{10}, b) C_5F_{12}, c) C_6F_{14} and d) C_7F_{16}.

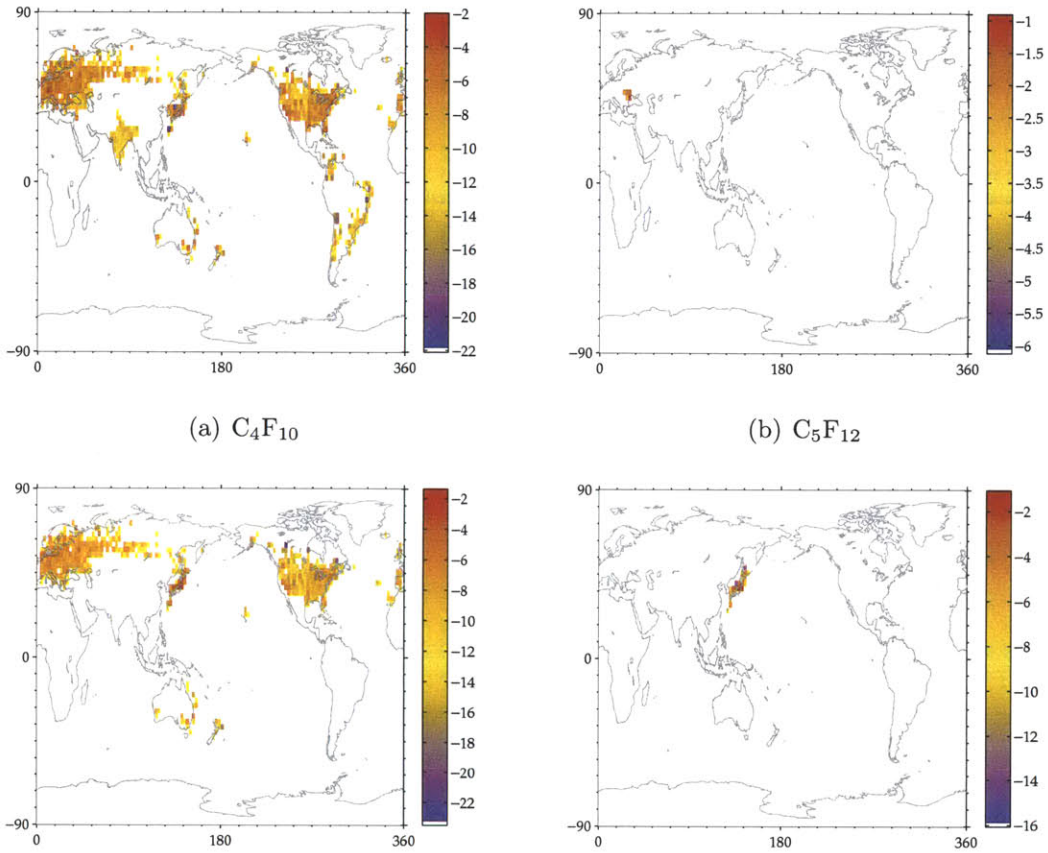

(a) C_4F_{10} (b) C_5F_{12}

(c) C_6F_{14} (d) C_7F_{16}

Figure 3-3: Temporal mean emission spatial distributions from 1970 to 2008 at a 2.8° latitude by 2.8° longitude resolution on a log scale for a) C_4F_{10}, b) C_5F_{12}, c) C_6F_{14} and d) C_7F_{16}.

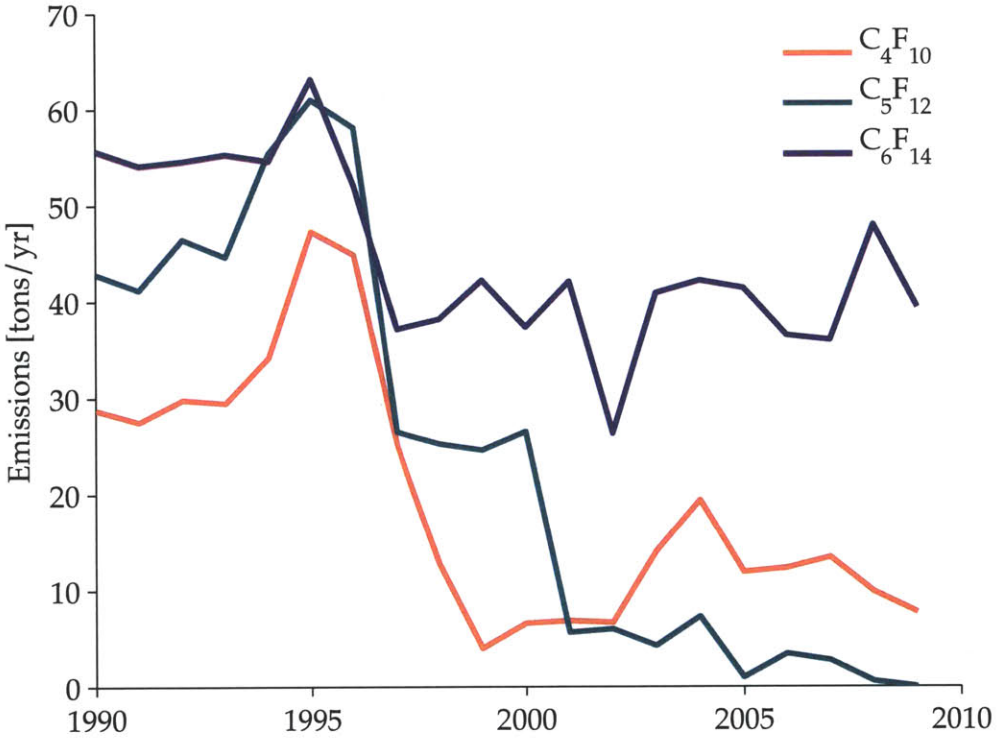

Figure 3-4: Reported emissions by Annex 1 countries that have ratified the Kyoto Protocol to the UNFCCC for C_4F_{10}, C_5F_{12} and C_6F_{14}.

3.3.2 UNFCCC Reported Inventories

Inventories for C_4F_{10}, C_5F_{12} and C_6F_{14} are also reported to the UNFCCC by Annex 1 countries that have ratified the Kyoto Protocol. Figure 3-4 shows the total reported inventories from 1990 to 2009. The country with the largest reported inventories to the UNFCCC is Belgium, with France, Spain, Switzerland and Romania following. Japan also reports inventories for C_6F_{14} to the UNFCCC, but only accounts for 2 % of the total C_6F_{14} inventory. In comparison, EDGARv4.2 suggests that 50 to 97 % of the emissions from C_6F_{14} are from Japan from usage as solvents. Figure 3-5 shows the total reported inventories to the UNFCCC by Annex 1 countries and the emissions from EDGARv4.2 for the same countries that have reported to the UNFCCC. Clearly, there are large discrepancies between the two bottom-up inventories.

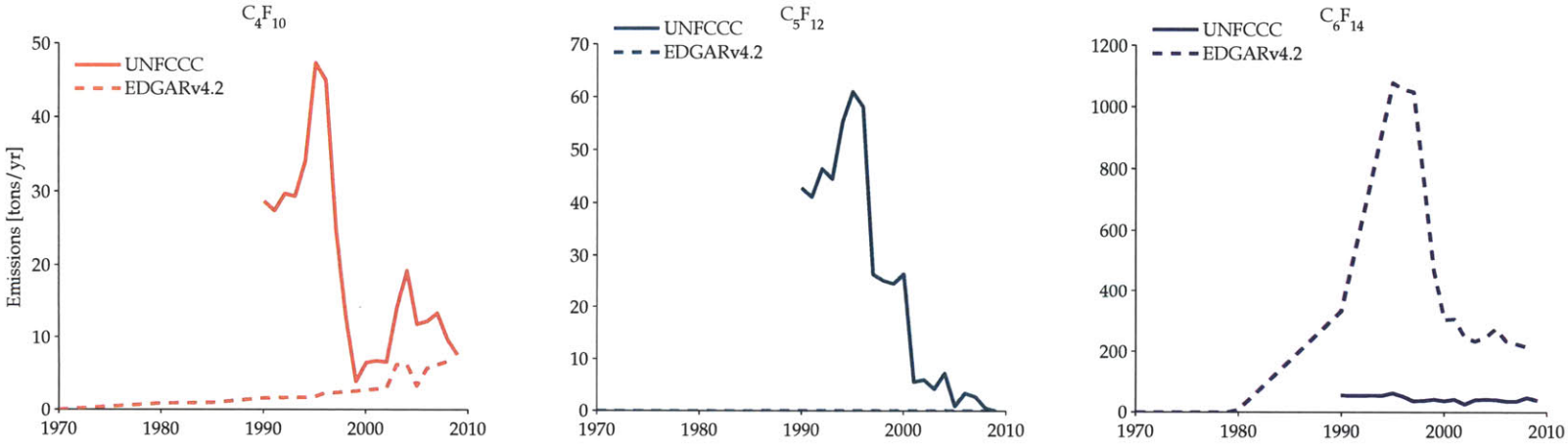

Figure 3-5: Reported emissions by Annex 1 countries that have ratified the Kyoto Protocol to the UNFCCC for C_4F_{10}, C_5F_{12} and C_6F_{14} and the estimated emissions in EDGARv4.2 for the UNFCCC reporting countries.

Interestingly the UNFCCC reported inventories for CF_4 and C_2F_6 appear more realistic, which include reported inventories from the United States and Japan (and for which Belgium is only a small fraction of the total European emissions). However, the C_3F_8 reported inventories to the UNFCCC show similar country emission profiles as the high molecular weight PFCs. This suggests that the UNFCCC reported inventories are reasonable for emissions from the aluminum industry, which primarily emits CF_4 and C_2F_6, and the discrepancy in the other PFC reported emissions is from the semiconductor industry. This may also be due to some countries reporting a mixture of total PFC emissions in CO_2-equivalents to the UNFCCC and may be part of the reason for the unrealistic emission profiles by country for C_3F_8 through C_6F_{14}. Lastly, as the reported inventories to the UNFCCC are not global, we used the EDGARv4.2 data in MOZARTv4.5 to produce the reference runs and to estimate the sensitivity of the modeled mole fractions to changes in emissions.

Chapter 4

Radiative Efficiencies of C_7F_{16} and C_8F_{18}

This chapter describes the estimation of the radiative efficiencies and global warming potentials of C_7F_{16} and C_8F_{18}. In the first section, we present the experimental methods and measurements of the infrared absorption cross-sections for C_7F_{16} and C_8F_{18}. Section 4.2 describes the radiative efficiency calculations using the measured infrared absorption cross-sections and an estimate of the radiative forcing per unit cross-section from *Pinnock et al.* (1995). The global warming potential estimates of C_7F_{16} and C_8F_{18} are presented in Section 4.3. This work was done in collaboration with Munkhbayar Baasandorj and Jim Burkholder at the National Oceanic and Atmospheric Administration (NOAA).

4.1 Infrared Absorption Cross-Sections

Roehl et al. (1995) reported infrared absorption cross-sections and GWPs for CF_4, C_2F_6, C_3F_8, C_4F_{10}, C_5F_{12} and C_6F_{14}, while more recently *Bravo et al.* (2010) reported these for C_8F_{18}. We expand on this work by presenting measured infrared absorption spectra of C_7F_{16} and C_8F_{18} using Fourier Transform Infrared (FTIR) spectroscopy at NOAA. We extended the spectral range measured for C_8F_{18}, and there are no previously published infrared absorption spectrum measurements for C_7F_{16} available.

The C_7F_{16} (98 % min. purity) and C_8F_{18} (99 % min. purity) samples were purchased from Synquest Laboratories. These samples were vacuum distilled for further purification by repeated cycles of freezing with liquid nitrogen, vacuum removal of non-condensable contaminants and then thawing. Various dilute gas mixtures of the samples were prepared manometrically in a Helium (He) bath gas in 12-L Pyrex bulbs for use in the infrared spectrum measurements. Absorption spectra were measured at a spectral resolution of $1\,cm^{-1}$ between 500 and $4000\,cm^{-1}$. Spectra were obtained using two different pathlength absorption cells: a single-pass 16 cm long cell and a low-volume multi-pass cell ($750\,cm^3$, 485 cm optical pathlength). Infrared absorption band strengths (absorption cross-sections) were obtained using Beer's law with spectra recorded over a range of sample concentrations at various bath gas pressures (see Equation (4.1), where A is the measured absorbance, I is the measured light intensity, σ_λ is the absorption cross section, L is the optical path length and c is the concentration of gas) (*Bravo et al.*, 2010). The infrared spectra of C_7F_{16} and C_8F_{18} were found to be independent of bath gas pressure for pressures between 20 and 600 Torr (He bath gas). The sample concentrations in the infrared absorption cell were varied over the range of (0.10 to 8.28) $\times\, 10^{15}$ molecule cm^{-3} for C_7F_{16} and (0.05 to 7.08) $\times\, 10^{15}$ molecule cm^{-3} for C_8F_{18}, where the sample concentrations were determined using absolute pressure measurements and the known mole fraction.

$$A = -ln\left(\frac{I(\lambda)}{I_0(\lambda)}\right) = \sigma_\lambda L c \tag{4.1}$$

Figure 4-1 shows the infrared absorption spectra of C_7F_{16} and C_8F_{18}. The C_7F_{16} and C_8F_{18} spectra show weak absorption between 500 and $1000\,cm^{-1}$, but strong absorption bands between 1000 and $1400\,cm^{-1}$. The integrated absorption band strengths were determined to be $(3.61\pm0.21) \times 10^{-16}\,cm^2$ molecule^{-1} cm^{-1} for C_7F_{16} ($1075–1375\,cm^{-1}$) and $(4.02\pm0.24) \times 10^{-16}\,cm^2$ molecule^{-1} cm^{-1} for C_8F_{18} ($1100–1400\,cm^{-1}$) (see Equation (4.2), where $S(T)$ is the integrated absorption band strength between two wavenumbers, $\bar{\nu}_1$ and $\bar{\nu}_2$). The quoted uncertainties are at the 2-σ (95 % confidence) level and include estimated systematic uncertainties.

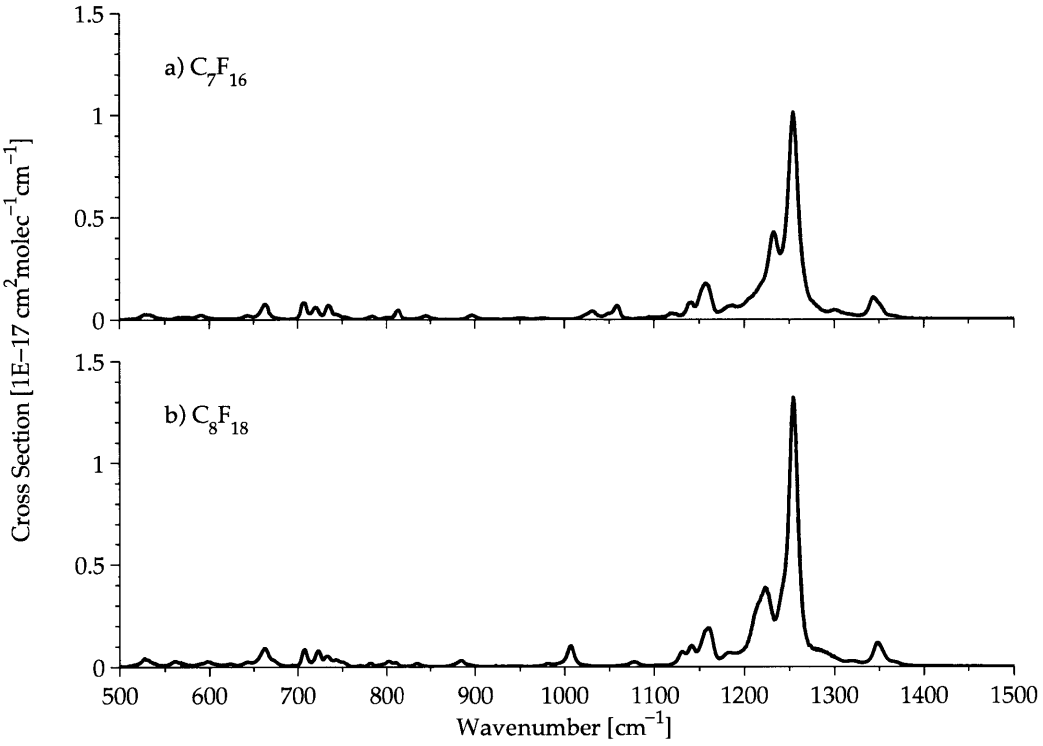

Figure 4-1: Average absorption cross-sections for a) C_7F_{16} and b) C_8F_{18} measured at $1\,cm^{-1}$ resolution and 296 K. The spectra were measured over a range of 500–$4000\,cm^{-1}$, although only the main spectral features are presented.

$$S(T) = \int_{\bar{\nu}_1}^{\bar{\nu}_2} \sigma(\bar{\nu}, T) d\bar{\nu} \tag{4.2}$$

4.2 Radiative Efficiencies

In order to estimate the relative change in radiative forcing per unit change in atmospheric abundance, the radiative efficiencies were estimated for C_7F_{16} and C_8F_{18} using the measured spectra and the method given by *Pinnock et al.* (1995). *Pinnock et al.* (1995) provided a simplified method for estimating the radiative efficiency of a molecule without the need for a detailed radiative transfer model. The *Pinnock et al.* (1995) method provides an estimate of the instantaneous radiative forcing per

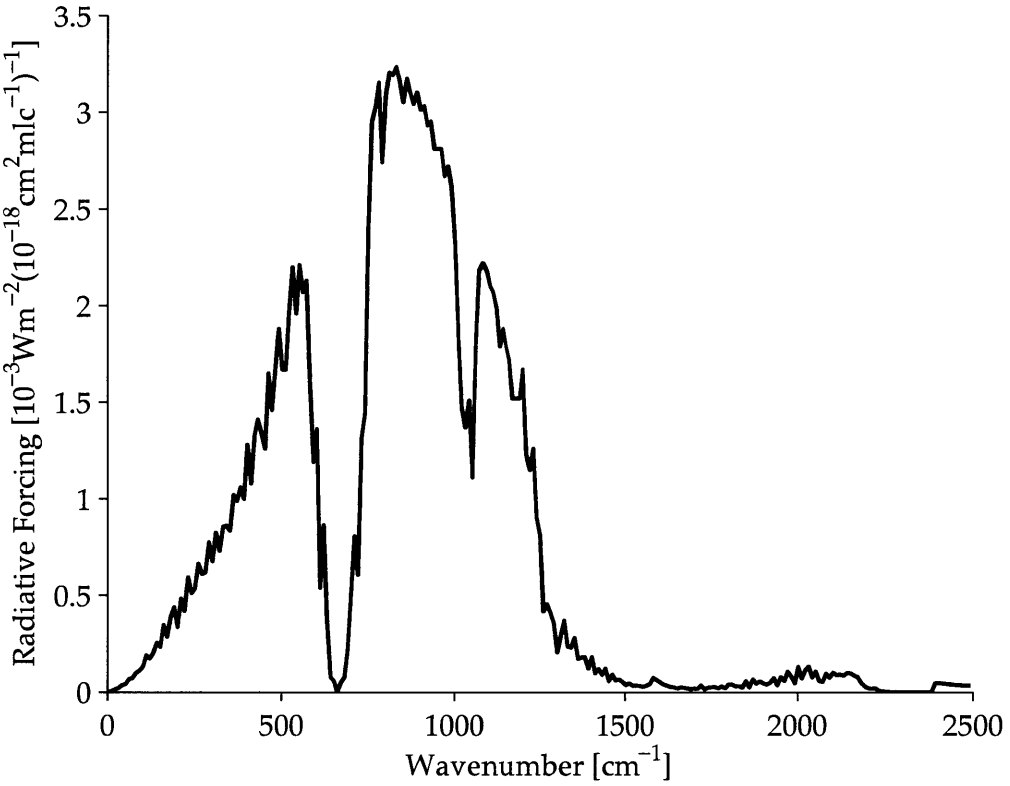

Figure 4-2: Radiative forcing per unit cross section per unit wavenumber, F_i, from *Pinnock et al.* (1995).

unit cross section (see Figure 4-2). Using Equation (4.3), the radiative efficiencies for C_7F_{16} and C_8F_{18} can be calculated, where $\bar{\sigma}_i$ is the average absorption cross section over a 10 cm^{-1} band and F_i is the radiative forcing per unit cross section per unit wavenumber for a 1 ppb increase in the species, as shown in Figure 4-2. The radiative efficiencies for C_7F_{16} and C_8F_{18} are 0.48 and 0.57 $W\,m^{-2}\,ppb^{-1}$, respectively (see Table 1.1). The radiative efficiency for C_8F_{18} is approximately equal to that of trifluoromethyl sulfur pentafluoride (SF_5CF_3), which is the highest of any measured atmospheric species (*Forster et al.*, 2007).

$$RE = \sum_{i=1}^{250} 10\bar{\sigma}_i(\bar{\nu}_i)F_i(\bar{\nu}_i) \tag{4.3}$$

The radiative efficiencies reported here are in reasonably good agreement, within

7 %, with those estimated by *Bravo et al.* (2010). The infrared measurements by *Bravo et al.* (2010) for C_8F_{18} were limited to the spectral range of 700-1400 cm^{-1}. A radiative efficiency value, based on our measurements, of 0.53 $W\,m^{-2}\,ppb^{-1}$ for C_8F_{18} can be obtained if a spectral range of 700–1400 cm^{-1} is used. Therefore, we attribute the difference between the values reported by *Bravo et al.* (2010) and those estimated here for C_8F_{18} to the different spectral ranges of the measurements. The radiative efficiencies estimated by *Bravo et al.* (2010), based on theoretical calculations and including a larger spectral range of 0-2500 cm^{-1}, are closer to our results for C_8F_{18}, with a difference of only 3.6 %. *Bravo et al.* (2010) did not measure the infrared spectra of C_7F_{16} and instead provided a theoretical calculation of the radiative efficiency of C_7F_{16} at 0.45 $W\,m^{-2}\,ppb^{-1}$, which is in good agreement with the results from the work presented here.

4.3 Global Warming Potential

Global warming potentials (GWPs) provide a measure of the climatic impact of emissions of a trace gas relative to a reference gas, usually chosen as carbon dioxide (CO_2) (*Forster et al.*, 2007; *UNEP Technology and Economic Assessment Panel*, 1999). The radiative efficiencies, along with an estimate of the atmospheric lifetime of the species, allow GWPs to be estimated. Following the standard method outlined by *Forster et al.* (2007), the GWPs were calculated for C_7F_{16} and C_8F_{18} using Equation (4.4), where TH is the chosen time horizon and ΔF is the change in radiative forcing from a pulse of emissions of the gas x or the reference gas r (CO_2). The change in radiative forcing due to a gas can be estimated using Equation (4.5), where a_x is the radiative efficiency of gas x, ΔB_x is the atmospheric emission pulse and τ_x is the atmospheric lifetime of the species x (*Forster et al.*, 2007; *UNEP Technology and Economic Assessment Panel*, 1999).

$$GWP(TH) = \frac{\int_0^{TH} \Delta F_x \cdot dt}{\int_0^{TH} \Delta F_r \cdot dt} \tag{4.4}$$

$$\int_0^{TH} \Delta F_x \cdot dt \cong a_x \int_0^{TH} \Delta B_x(t) \cdot dt \cong a_x \Delta B_x(0) \tau_x (1 - exp^{(-TH/\tau_x)}) \qquad (4.5)$$

No lifetimes have been reported for C_7F_{16} and C_8F_{18}. *Ravishankara et al.* (1993) determined that the major atmospheric removal pathway for the perfluoroalkanes, CF_4 through C_6F_{14}, was via photolysis by hydrogen Lyman-α radiation (121.6 nm) with a possible minor pathway due to reaction with $O(^1D)$. Based on the work by *Ravishankara et al.* (1993), we assume that C_7F_{16} and C_8F_{18} will have similar lifetimes, on the order of thousands of years, and have chosen a lifetime of 3000 years for the GWP calculations, which is close to the lifetime of C_6F_{14}. The GWPs for C_7F_{16} and C_8F_{18} are estimated to be 7930 and 8340 for a 100-year time horizon with CO_2 as the reference gas (see Table 1.1). As the expected lifetimes of C_7F_{16} and C_8F_{18} are much longer than the chosen time horizons, these GWP calculations are relatively insensitive to the assumed lifetime. To confirm this, a sensitivity analysis to the assumed lifetime in the GWP estimate was done following *Shine et al.* (2005). A difference of 7.9 % and 1.1 % was found in the calculated 100-yr time horizon GWPs when using assumed lifetimes of 500 instead of 3000 years or 10 000 instead of 3000 years, respectively.

Chapter 5

Results and Discussion

5.1 Atmospheric Observations

5.1.1 Atmospheric Histories

The atmospheric histories from 1973 to 2011 for the high molecular weight PFCs, C_4F_{10}, C_5F_{12}, C_6F_{14}, C_7F_{16} and C_8F_{18}, are shown in Figures 5-1 through 5-5. C_4F_{10} and C_5F_{12} are present in the earliest archived samples at 0.015 ppt and 0.011 ppt respectively, but these measurements are considered below the estimated detection limits of the instruments (see Figure 5-1 and Figure 5-2). Analysis of firn air samples from Greenland confirm that there is no detectable natural abundance for these PFCs. C_4F_{10} and C_5F_{12} exhibit quasi-exponential growth in the 1980s and then grow nearly linearly to present day globally averaged background dry air mole fractions of 0.17 ppt and 0.12 ppt, respectively (taken as the average between the NH and SH spline fit data, see Section 5.1.2 for discussion of the spline fits). The slowdown in growth for C_4F_{10} and C_5F_{12} in the 2000s suggest that emissions are decreasing, as is supported by the decline in the inter-hemispheric gradients seen in the observations.

C_6F_{14} and C_7F_{16} are not detectable in the archived samples until 1984-1985 and grow quasi-exponentially until 1999 and 1992, respectively (see Figures 5-3 and 5-4). C_8F_{18} follows a similar trend to that of C_6F_{14}, although it is not detectable until the mid 1990s (see Figure 5-5), which is most likely due to lower emission rates for

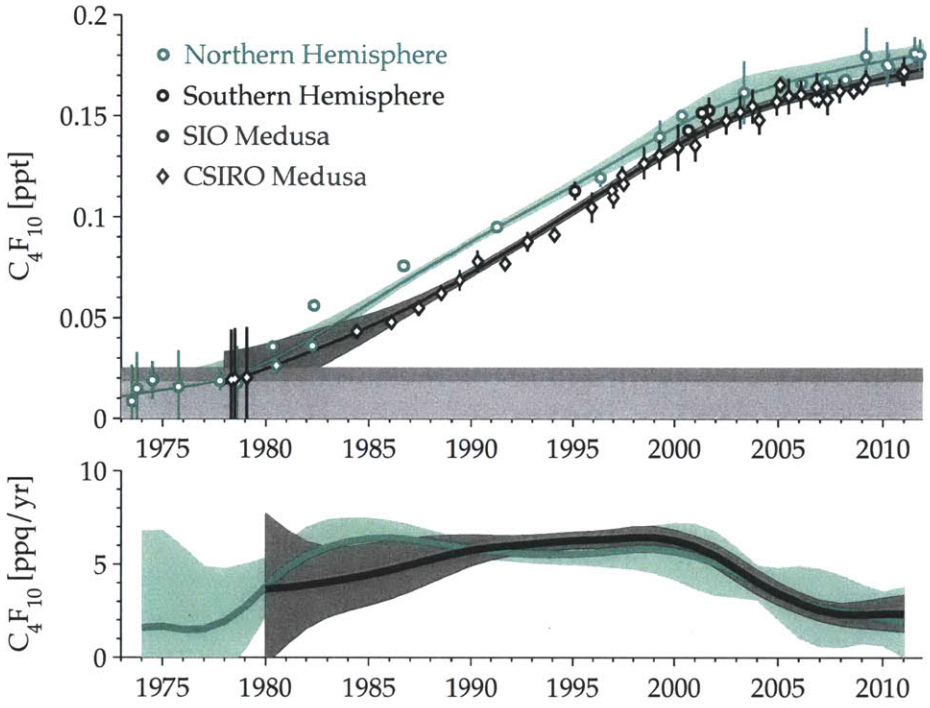

Figure 5-1: The top panel shows the dry air mole fractions of C_4F_{10} based on Northern Hemisphere (color circles and diamonds) and Southern Hemisphere (black circles and diamonds) archived air sample measurements. The circles are for the samples measured on the SIO Medusa and the diamonds are for the samples measured on the CSIRO Medusa. The vertical bars on the observations denote the 1-σ standard deviations of the sample measurements (often the measurement uncertainty is too small to be seen on the figure). The color and black lines are the cubic smoothing spline fits to the Northern Hemisphere and Southern Hemisphere observations, respectively, and the shading is the estimated uncertainty. The grey shading shows the detection limits for the two Medusa systems, with light grey for the SIO Medusa and dark grey for the CSIRO Medusa. The bottom panel shows the average annual growth rates of mole fractions in parts-per-quadrillion (ppq, i.e., parts per 10^{15}) per year for the Northern (color) and Southern (black) Hemispheres, calculated from the smoothing spline fits, and the growth rate in mole fractions estimated uncertainties, shown as the shading.

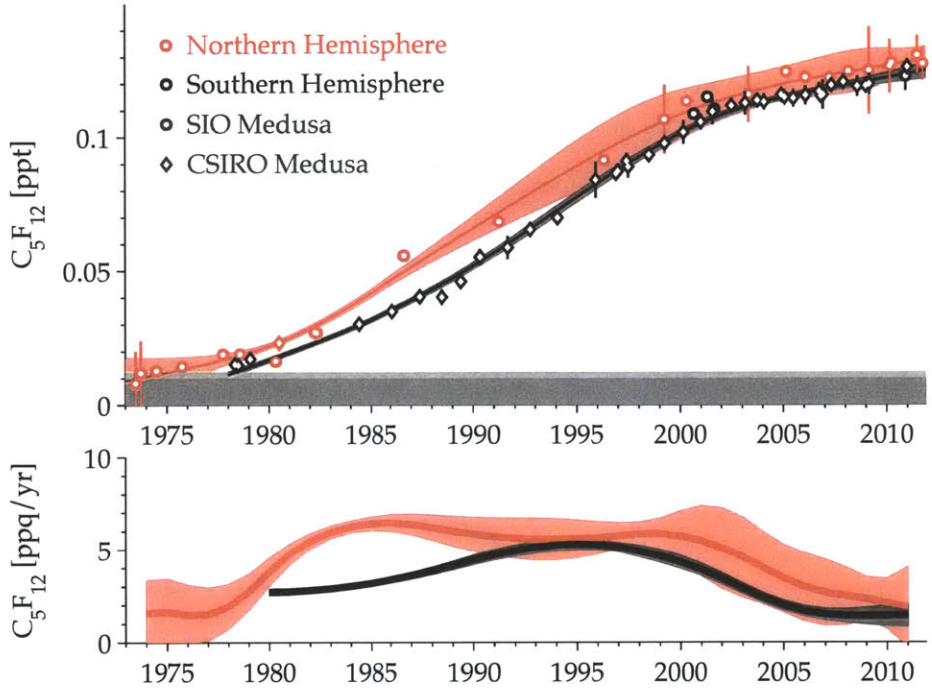

Figure 5-2: Same as Figure 5-1 but for C_5F_{12}.

C_8F_{18}. C_6F_{14} is the most abundant of the PFCs studied here at a globally averaged background tropospheric dry air mole fraction of 0.27 ppt in 2011. The globally averaged dry air mole fraction in 2011 is 0.12 ppt for C_7F_{16} and 0.09 ppt for C_8F_{18} (which is the least abundant of all of the PFCs).

Emissions of these high molecular weight PFCs based on EDGARv4.2 are of anthropogenic origin and primarily released in the NH (*European Commission, Joint Research Centre (JRC)/Netherlands Environmental Assessment Agency (PBL)*, 2009). Therefore as expected, we see higher atmospheric mole fractions in the NH than the SH for C_4F_{10} through C_8F_{18}, due to the 1–2 year mixing time between the two tropospheric hemispheres. Higher variability in the NH samples can be seen in the early years for C_4F_{10} and C_5F_{12}, as compared to the SH samples. This is attributed to sampling of less well-mixed air due to emissions originating primarily in the NH, although efforts were made to fill these samples during baseline conditions. There is one NH sample with a fill date in 1986 with anomalously low values for C_6F_{14}, C_7F_{16}

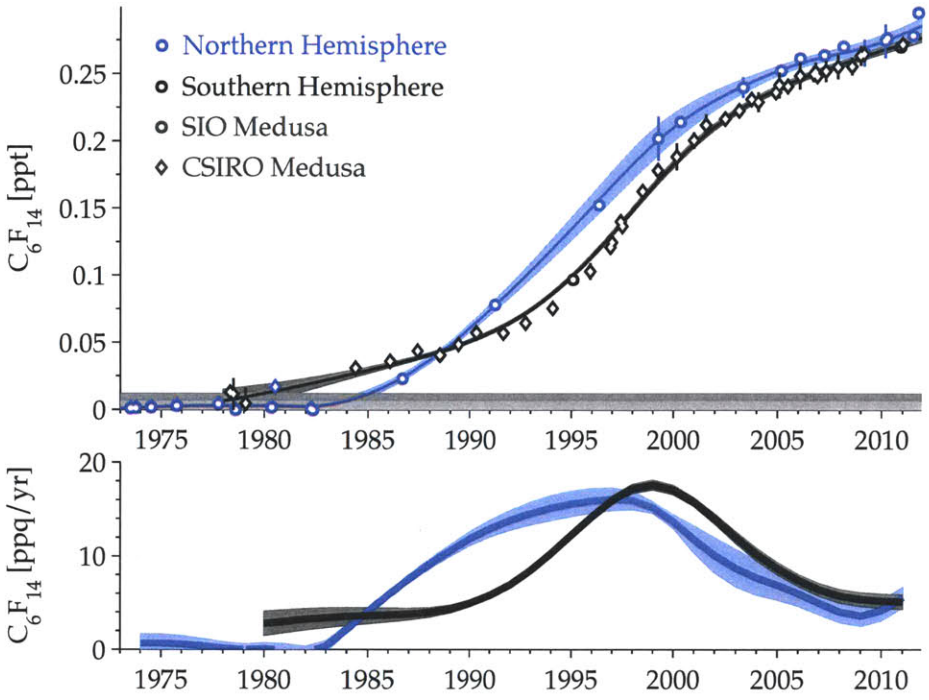

Figure 5-3: Same as Figure 5-1 but for C_6F_{14}.

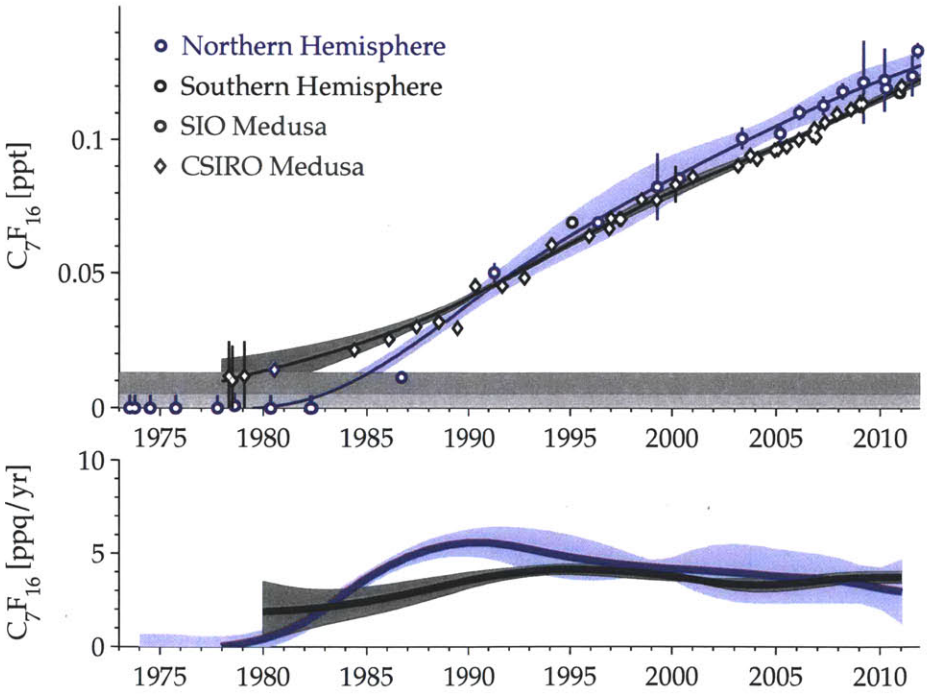

Figure 5-4: Same as Figure 5-1 but for C_7F_{16}.

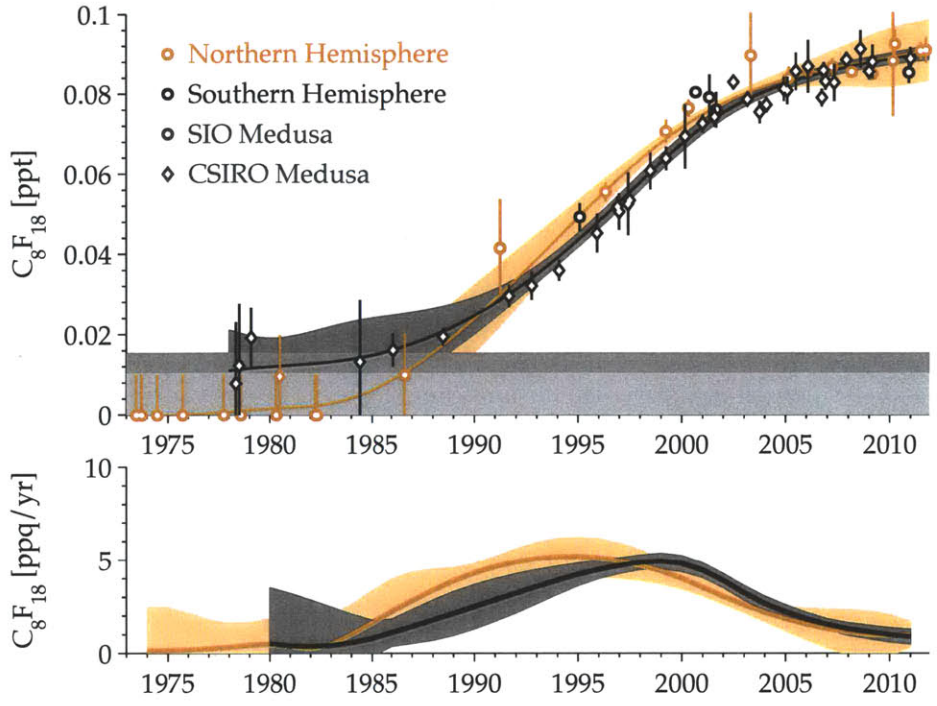

Figure 5-5: Same as Figure 5-1 but for C_8F_{18}.

and C_8F_{18} (lower even than the atmospheric mole fractions found in the SH samples with similar fill dates). However, this 1986 NH air sample is close to the detection limit of the SIO instrument. Furthermore, this sample was not filled for the purpose of an air archive and has been shown to have anomalously low mole fractions for C_2F_6, C_3F_8 and sulfur hexafluoride (SF_6), most likely due to the fill technique (*Jens Mühle, SIO, personal communication, 2012*).

5.1.2 Cubic Smoothing Spline Fits

Due to the sparseness of the available observational data set, the annual mean mole fractions and growth rates presented here are based on cubic smoothed spline fits to the observations. The observations were weighted by the inverse of their measurement uncertainty and a 50 % attenuation period of 4 years was used, which is slightly larger than the mean data-spacing, in estimating the smoothing splines (*Enting et al.*, 2006). The uncertainties associated with the spline fits were estimated using a Monte Carlo

approach, where the spline fitting was repeated 1000 times with randomly varied observations that had distributions based on their measurement uncertainty. The uncertainty on each spline fit was taken as the 1-σ standard deviation of these runs. The annual hemispheric growth rate was also calculated for each of the 1000 runs and the uncertainty associated with the annual growth rate was estimated as the 1-σ standard deviation of these 1000 calculated growth rates. The smoothed spline fits are shown along with the observations in Figures 5-1 through 5-5. The bottom panels of Figures 5-1 through 5-5 show the annual hemispheric growth rates estimated from the cubic smoothed spline fits for each PFC. Based on the cubic smoothing spline fits to the observations, the NH, SH and globally averaged mole fractions and growth rates, and their 1-σ uncertainties for each PFC are presented in Tables 5.1 through 5.5.

5.1.3 Atmospheric Growth Trends

The atmospheric growth rates for C_4F_{10} are relatively constant at 5 to 6 parts-per-quadrillion (ppq, i.e., parts per 10^{15}) per year from 1985 to 2000 and then decline to $2.2\,\mathrm{ppq\,yr^{-1}}$ in 2011 (see Figure 5-1). The C_5F_{12} growth rates follow a similar trend to those of C_4F_{10}; namely remaining relatively constant between 4 to $5\,\mathrm{ppq\,yr^{-1}}$ from 1980 to 2000, and then declining to $1.4\,\mathrm{ppq\,yr^{-1}}$ in 2011 (see Figure 5-2).

The growth rate of C_6F_{14} is almost negligible until 1983, then rapidly increases peaking in 1999 at $16.6\,\mathrm{ppq\,yr^{-1}}$, and then decreases to a 2011 annual global average rate of $5.0\,\mathrm{ppq\,yr^{-1}}$. Trends in the C_7F_{16} and C_8F_{18} growth rates are similar to those of C_6F_{14}; although the trend in the growth rate of atmospheric mole fractions for C_7F_{16} deviates from the other PFCs in more recent years, in that its growth rate has been relatively constant at 3 to $4\,\mathrm{ppq\,yr^{-1}}$ for the last 15 years. The atmospheric mole fraction trends and growth rates of C_8F_{18} follow a similar pattern to those of C_6F_{14}, although with lower absolute values, with a 2011 mean growth rate of $0.9\,\mathrm{ppq\,yr^{-1}}$.

As mentioned earlier, the primary sources of emissions from the bottom-up estimates from EDGARv4.2 are in the NH; this is confirmed by the lag in the observed SH growth rates as compared to those in the NH. One thing to note is that the abso-

lute maximum growth rate is higher in the SH than in the NH for C_6F_{14} and C_8F_{18}. This is most likely a result of the lack of NH data in the 1990s to constrain the cubic smoothed spline fit and not a result of SH emissions dominating over NH emissions.

Table 5.1: Northern and Southern Hemisphere and Global Average Annual Mean Mole Fractions and Growth Rates and Associated Uncertainties 1980-2011 for C_4F_{10}*

	Northern Hemisphere		Southern Hemisphere		Global Average	
	Mole Fraction	Growth Rate	Mole Fraction	Growth Rate	Mole Fraction	Growth Rate
Year	[ppt**]	[ppq yr^{-1}***]	[ppt]	[ppq yr^{-1}]	[ppt]	[ppq yr^{-1}]
1980	0.021 ± 0.009	3.3 ± 1.5	0.019 ± 0.015	3.6 ± 4.0	0.020 ± 0.012	3.5 ± 2.8
1981	0.025 ± 0.009	4.4 ± 1.5	0.023 ± 0.013	3.7 ± 3.0	0.024 ± 0.011	4.0 ± 2.3
1982	0.030 ± 0.007	5.2 ± 1.5	0.026 ± 0.012	3.8 ± 2.3	0.028 ± 0.010	4.5 ± 1.9
1983	0.035 ± 0.006	5.7 ± 1.4	0.030 ± 0.011	4.0 ± 1.9	0.033 ± 0.009	4.9 ± 1.7
1984	0.041 ± 0.005	6.1 ± 1.2	0.034 ± 0.010	4.1 ± 1.8	0.038 ± 0.007	5.1 ± 1.5
1985	0.047 ± 0.004	6.3 ± 1.0	0.039 ± 0.008	4.3 ± 1.7	0.043 ± 0.006	5.3 ± 1.4
1986	0.054 ± 0.003	6.4 ± 0.9	0.043 ± 0.007	4.6 ± 1.6	0.048 ± 0.005	5.5 ± 1.3
1987	0.060 ± 0.003	6.4 ± 0.7	0.048 ± 0.006	4.8 ± 1.5	0.054 ± 0.004	5.6 ± 1.1
1988	0.067 ± 0.002	6.3 ± 0.6	0.053 ± 0.004	5.1 ± 1.3	0.060 ± 0.003	5.7 ± 1.0
1989	0.073 ± 0.002	6.1 ± 0.5	0.058 ± 0.003	5.4 ± 1.1	0.065 ± 0.003	5.7 ± 0.8
1990	0.079 ± 0.002	5.9 ± 0.5	0.063 ± 0.003	5.7 ± 0.9	0.071 ± 0.002	5.8 ± 0.7
1991	0.085 ± 0.002	5.7 ± 0.4	0.069 ± 0.002	5.8 ± 0.7	0.077 ± 0.002	5.8 ± 0.5
1992	0.090 ± 0.002	5.6 ± 0.4	0.075 ± 0.002	6.0 ± 0.5	0.083 ± 0.002	5.8 ± 0.5
1993	0.096 ± 0.002	5.6 ± 0.5	0.081 ± 0.002	6.1 ± 0.5	0.088 ± 0.002	5.8 ± 0.5
1994	0.101 ± 0.003	5.5 ± 0.5	0.087 ± 0.002	6.2 ± 0.4	0.094 ± 0.002	5.8 ± 0.5
1995	0.107 ± 0.003	5.5 ± 0.6	0.093 ± 0.002	6.2 ± 0.4	0.100 ± 0.002	5.9 ± 0.5
1996	0.112 ± 0.003	5.6 ± 0.7	0.100 ± 0.002	6.3 ± 0.4	0.106 ± 0.002	5.9 ± 0.6
1997	0.118 ± 0.003	5.7 ± 0.8	0.106 ± 0.002	6.3 ± 0.5	0.112 ± 0.003	6.0 ± 0.7
1998	0.124 ± 0.004	5.8 ± 1.1	0.112 ± 0.002	6.4 ± 0.6	0.118 ± 0.003	6.1 ± 0.8
1999	0.130 ± 0.004	5.8 ± 1.3	0.119 ± 0.002	6.5 ± 0.6	0.124 ± 0.003	6.2 ± 1.0
2000	0.135 ± 0.005	5.8 ± 1.5	0.125 ± 0.002	6.4 ± 0.6	0.130 ± 0.004	6.1 ± 1.1
2001	0.141 ± 0.006	5.6 ± 1.8	0.132 ± 0.003	6.1 ± 0.5	0.136 ± 0.004	5.9 ± 1.2
2002	0.147 ± 0.007	5.2 ± 1.8	0.138 ± 0.003	5.7 ± 0.6	0.142 ± 0.005	5.5 ± 1.2
2003	0.152 ± 0.008	4.8 ± 1.4	0.143 ± 0.002	5.1 ± 0.7	0.147 ± 0.005	5.0 ± 1.0
2004	0.156 ± 0.009	4.3 ± 0.9	0.148 ± 0.002	4.4 ± 0.7	0.152 ± 0.006	4.3 ± 0.8
2005	0.160 ± 0.009	3.7 ± 1.3	0.152 ± 0.002	3.7 ± 0.6	0.156 ± 0.006	3.7 ± 1.0
2006	0.164 ± 0.008	3.2 ± 1.8	0.155 ± 0.002	3.2 ± 0.6	0.159 ± 0.005	3.2 ± 1.2
2007	0.167 ± 0.007	2.8 ± 2.0	0.158 ± 0.002	2.7 ± 0.6	0.162 ± 0.004	2.7 ± 1.3
2008	0.169 ± 0.006	2.6 ± 1.9	0.161 ± 0.002	2.4 ± 0.6	0.165 ± 0.004	2.5 ± 1.2
2009	0.172 ± 0.006	2.4 ± 1.6	0.163 ± 0.002	2.3 ± 0.7	0.167 ± 0.004	2.3 ± 1.1
2010	0.174 ± 0.005	2.2 ± 1.5	0.165 ± 0.002	2.3 ± 0.9	0.170 ± 0.004	2.3 ± 1.2
2011	0.176 ± 0.005	2.0 ± 1.8	0.168 ± 0.002	2.4 ± 1.0	0.172 ± 0.004	2.2 ± 1.4

*Annual hemispheric mean mole fractions and growth rates are estimated from the smoothing cubic spline fits.
**ppt = parts-per-trillion dry air mole fraction.
***ppq = parts-per-quadrillion dry air mole fraction.

Table 5.2: Northern and Southern Hemisphere and Global Average Annual Mean Mole Fractions and Growth Rates and Associated Uncertainties 1980-2011 for C_5F_{12}*

	Northern Hemisphere		Southern Hemisphere		Global Average	
	Mole Fraction	Growth Rate	Mole Fraction	Growth Rate	Mole Fraction	Growth Rate
Year	[ppt**]	[ppq yr^{-1}***]	[ppt]	[ppq yr^{-1}]	[ppt]	[ppq yr^{-1}]
1980	0.018 ± 0.002	2.2 ± 0.7	0.012 ± 0.001	2.7 ± 0.2	0.015 ± 0.001	2.4 ± 0.4
1981	0.020 ± 0.001	2.5 ± 0.5	0.015 ± 0.001	2.7 ± 0.2	0.018 ± 0.001	2.6 ± 0.4
1982	0.023 ± 0.001	3.0 ± 0.4	0.018 ± 0.001	2.8 ± 0.2	0.020 ± 0.001	2.9 ± 0.3
1983	0.026 ± 0.001	3.5 ± 0.3	0.021 ± 0.001	2.8 ± 0.1	0.023 ± 0.001	3.2 ± 0.2
1984	0.030 ± 0.001	4.0 ± 0.3	0.024 ± 0.001	3.0 ± 0.1	0.027 ± 0.001	3.5 ± 0.2
1985	0.034 ± 0.001	4.4 ± 0.3	0.027 ± 0.001	3.1 ± 0.1	0.030 ± 0.001	3.8 ± 0.2
1986	0.039 ± 0.001	4.7 ± 0.4	0.030 ± 0.001	3.3 ± 0.2	0.034 ± 0.001	4.0 ± 0.3
1987	0.043 ± 0.002	4.9 ± 0.5	0.033 ± 0.001	3.5 ± 0.2	0.038 ± 0.001	4.2 ± 0.4
1988	0.048 ± 0.002	4.9 ± 0.7	0.037 ± 0.001	3.7 ± 0.2	0.043 ± 0.001	4.3 ± 0.4
1989	0.053 ± 0.002	4.9 ± 0.8	0.041 ± 0.001	4.0 ± 0.2	0.047 ± 0.002	4.5 ± 0.5
1990	0.058 ± 0.003	4.9 ± 0.9	0.045 ± 0.001	4.3 ± 0.2	0.051 ± 0.002	4.6 ± 0.6
1991	0.063 ± 0.004	4.9 ± 1.0	0.049 ± 0.001	4.6 ± 0.3	0.056 ± 0.003	4.7 ± 0.6
1992	0.068 ± 0.005	4.8 ± 1.1	0.054 ± 0.001	4.9 ± 0.3	0.061 ± 0.003	4.8 ± 0.7
1993	0.073 ± 0.006	4.8 ± 1.1	0.059 ± 0.001	5.1 ± 0.3	0.066 ± 0.004	4.9 ± 0.7
1994	0.077 ± 0.007	4.7 ± 1.1	0.064 ± 0.002	5.2 ± 0.3	0.071 ± 0.004	5.0 ± 0.7
1995	0.082 ± 0.008	4.6 ± 1.0	0.069 ± 0.002	5.3 ± 0.3	0.076 ± 0.005	5.0 ± 0.6
1996	0.087 ± 0.009	4.5 ± 0.9	0.075 ± 0.002	5.3 ± 0.2	0.081 ± 0.005	4.9 ± 0.5
1997	0.091 ± 0.010	4.3 ± 0.7	0.080 ± 0.002	5.2 ± 0.2	0.085 ± 0.006	4.8 ± 0.5
1998	0.095 ± 0.010	4.1 ± 0.6	0.085 ± 0.002	5.0 ± 0.3	0.090 ± 0.006	4.6 ± 0.5
1999	0.099 ± 0.011	3.9 ± 0.8	0.090 ± 0.002	4.8 ± 0.3	0.095 ± 0.006	4.3 ± 0.6
2000	0.103 ± 0.010	3.6 ± 1.3	0.094 ± 0.001	4.5 ± 0.3	0.099 ± 0.006	4.0 ± 0.8
2001	0.107 ± 0.010	3.2 ± 1.9	0.099 ± 0.001	4.1 ± 0.3	0.103 ± 0.005	3.6 ± 1.1
2002	0.110 ± 0.009	2.8 ± 2.1	0.103 ± 0.001	3.7 ± 0.3	0.106 ± 0.005	3.2 ± 1.2
2003	0.112 ± 0.008	2.5 ± 2.1	0.106 ± 0.001	3.1 ± 0.3	0.109 ± 0.004	2.8 ± 1.2
2004	0.115 ± 0.007	2.2 ± 1.9	0.109 ± 0.001	2.6 ± 0.2	0.112 ± 0.004	2.4 ± 1.1
2005	0.117 ± 0.006	2.0 ± 1.8	0.111 ± 0.001	2.2 ± 0.3	0.114 ± 0.004	2.1 ± 1.0
2006	0.119 ± 0.006	1.8 ± 1.8	0.113 ± 0.001	1.8 ± 0.3	0.116 ± 0.004	1.8 ± 1.0
2007	0.120 ± 0.006	1.6 ± 1.7	0.115 ± 0.001	1.6 ± 0.3	0.118 ± 0.004	1.6 ± 1.0
2008	0.122 ± 0.007	1.4 ± 1.5	0.117 ± 0.001	1.4 ± 0.3	0.119 ± 0.004	1.4 ± 0.9
2009	0.123 ± 0.007	1.3 ± 1.2	0.118 ± 0.001	1.4 ± 0.4	0.121 ± 0.004	1.4 ± 0.8
2010	0.124 ± 0.008	1.3 ± 1.3	0.119 ± 0.001	1.4 ± 0.5	0.122 ± 0.004	1.3 ± 0.9
2011	0.126 ± 0.007	1.3 ± 2.1	0.121 ± 0.002	1.4 ± 0.6	0.123 ± 0.004	1.4 ± 1.4

*Annual hemispheric mean mole fractions and growth rates are estimated from the smoothing cubic spline fits.
**ppt = parts-per-trillion dry air mole fraction.
***ppq = parts-per-quadrillion dry air mole fraction.

Table 5.3: Northern and Southern Hemisphere and Global Average Annual Mean Mole Fractions and Growth Rates and Associated Uncertainties 1980-2011 for C_6F_{14}*

	Northern Hemisphere		Southern Hemisphere		Global Average	
	Mole Fraction	Growth Rate	Mole Fraction	Growth Rate	Mole Fraction	Growth Rate
Year	[ppt**]	[ppq yr^{-1}***]	[ppt]	[ppq yr^{-1}]	[ppt]	[ppq yr^{-1}]
1980	0.003 ± 0.002	0.0 ± 0.6	0.008 ± 0.008	2.7 ± 1.3	0.005 ± 0.005	1.4 ± 0.9
1981	0.003 ± 0.002	0.0 ± 0.6	0.010 ± 0.007	2.9 ± 1.2	0.007 ± 0.004	1.5 ± 0.9
1982	0.003 ± 0.002	-0.3 ± 0.6	0.013 ± 0.006	3.1 ± 1.1	0.008 ± 0.004	1.4 ± 0.9
1983	0.002 ± 0.002	-0.2 ± 0.6	0.017 ± 0.005	3.3 ± 1.0	0.010 ± 0.004	1.6 ± 0.8
1984	0.003 ± 0.003	1.3 ± 0.4	0.020 ± 0.004	3.5 ± 0.9	0.011 ± 0.003	2.4 ± 0.7
1985	0.005 ± 0.003	3.2 ± 0.3	0.024 ± 0.003	3.6 ± 0.8	0.014 ± 0.003	3.4 ± 0.6
1986	0.009 ± 0.003	5.0 ± 0.3	0.027 ± 0.002	3.6 ± 0.7	0.018 ± 0.003	4.3 ± 0.5
1987	0.015 ± 0.003	6.8 ± 0.4	0.031 ± 0.002	3.7 ± 0.6	0.023 ± 0.002	5.3 ± 0.5
1988	0.022 ± 0.002	8.4 ± 0.5	0.035 ± 0.002	3.9 ± 0.5	0.029 ± 0.002	6.2 ± 0.5
1989	0.032 ± 0.002	10.0 ± 0.6	0.039 ± 0.001	4.1 ± 0.4	0.035 ± 0.002	7.0 ± 0.5
1990	0.042 ± 0.002	11.3 ± 0.7	0.043 ± 0.001	4.6 ± 0.3	0.043 ± 0.002	8.0 ± 0.5
1991	0.054 ± 0.003	12.4 ± 0.8	0.048 ± 0.001	5.4 ± 0.3	0.051 ± 0.002	8.9 ± 0.6
1992	0.067 ± 0.003	13.4 ± 1.0	0.054 ± 0.001	6.4 ± 0.3	0.060 ± 0.002	9.9 ± 0.6
1993	0.081 ± 0.004	14.2 ± 1.2	0.061 ± 0.001	7.7 ± 0.3	0.071 ± 0.003	11.0 ± 0.7
1994	0.095 ± 0.005	14.9 ± 1.3	0.069 ± 0.001	9.4 ± 0.3	0.082 ± 0.003	12.1 ± 0.8
1995	0.110 ± 0.006	15.4 ± 1.3	0.079 ± 0.001	11.3 ± 0.3	0.095 ± 0.004	13.3 ± 0.8
1996	0.126 ± 0.007	15.8 ± 1.3	0.092 ± 0.002	13.3 ± 0.4	0.109 ± 0.004	14.5 ± 0.8
1997	0.142 ± 0.009	16.0 ± 1.2	0.106 ± 0.002	15.2 ± 0.4	0.124 ± 0.005	15.6 ± 0.8
1998	0.158 ± 0.010	16.1 ± 1.0	0.122 ± 0.002	16.7 ± 0.5	0.140 ± 0.006	16.4 ± 0.7
1999	0.174 ± 0.011	15.6 ± 0.6	0.139 ± 0.002	17.6 ± 0.5	0.156 ± 0.006	16.6 ± 0.5
2000	0.189 ± 0.011	14.5 ± 0.7	0.156 ± 0.002	17.5 ± 0.5	0.173 ± 0.007	16.0 ± 0.6
2001	0.203 ± 0.010	12.6 ± 1.4	0.174 ± 0.002	16.5 ± 0.4	0.188 ± 0.006	14.6 ± 0.9
2002	0.214 ± 0.009	10.8 ± 1.9	0.189 ± 0.003	14.9 ± 0.5	0.202 ± 0.006	12.8 ± 1.2
2003	0.224 ± 0.008	9.3 ± 2.0	0.203 ± 0.002	12.9 ± 0.6	0.214 ± 0.005	11.1 ± 1.3
2004	0.233 ± 0.006	8.1 ± 1.8	0.215 ± 0.002	11.0 ± 0.7	0.224 ± 0.004	9.5 ± 1.2
2005	0.241 ± 0.005	7.2 ± 1.5	0.226 ± 0.002	9.3 ± 0.7	0.233 ± 0.003	8.3 ± 1.1
2006	0.248 ± 0.004	6.4 ± 1.3	0.234 ± 0.002	8.0 ± 0.6	0.241 ± 0.003	7.2 ± 1.0
2007	0.254 ± 0.003	5.5 ± 1.2	0.242 ± 0.002	6.9 ± 0.6	0.248 ± 0.003	6.2 ± 0.9
2008	0.259 ± 0.003	4.4 ± 1.1	0.248 ± 0.002	6.0 ± 0.7	0.253 ± 0.003	5.2 ± 0.9
2009	0.263 ± 0.003	3.7 ± 1.1	0.254 ± 0.002	5.5 ± 0.7	0.258 ± 0.003	4.6 ± 0.9
2010	0.266 ± 0.004	3.7 ± 1.1	0.259 ± 0.002	5.3 ± 0.7	0.263 ± 0.003	4.5 ± 0.9
2011	0.270 ± 0.005	4.9 ± 1.0	0.264 ± 0.002	5.1 ± 0.7	0.267 ± 0.003	5.0 ± 0.9

*Annual hemispheric mean mole fractions and growth rates are estimated from the smoothing cubic spline fits.
**ppt = parts-per-trillion dry air mole fraction.
***ppq = parts-per-quadrillion dry air mole fraction.

Table 5.4: Northern and Southern Hemisphere and Global Average Annual Mean Mole Fractions and Growth Rates and Associated Uncertainties 1980-2011 for C_7F_{16}*

	Northern Hemisphere		Southern Hemisphere		Global Average	
	Mole Fraction	Growth Rate	Mole Fraction	Growth Rate	Mole Fraction	Growth Rate
Year	[ppt**]	[ppq yr^{-1}***]	[ppt]	[ppq yr^{-1}]	[ppt]	[ppq yr^{-1}]
1980	0.000 ± 0.002	0.3 ± 0.5	0.011 ± 0.008	1.9 ± 1.6	0.005 ± 0.005	1.1 ± 1.0
1981	0.000 ± 0.002	0.6 ± 0.5	0.013 ± 0.007	1.9 ± 1.3	0.006 ± 0.004	1.2 ± 0.9
1982	0.001 ± 0.002	1.0 ± 0.5	0.015 ± 0.006	2.0 ± 1.1	0.008 ± 0.004	1.5 ± 0.8
1983	0.002 ± 0.002	1.7 ± 0.5	0.017 ± 0.005	2.1 ± 0.9	0.009 ± 0.004	1.9 ± 0.7
1984	0.004 ± 0.002	2.5 ± 0.4	0.019 ± 0.005	2.2 ± 0.8	0.011 ± 0.004	2.3 ± 0.6
1985	0.007 ± 0.003	3.3 ± 0.3	0.021 ± 0.004	2.3 ± 0.8	0.014 ± 0.003	2.8 ± 0.6
1986	0.011 ± 0.003	4.0 ± 0.4	0.023 ± 0.003	2.5 ± 0.7	0.017 ± 0.003	3.3 ± 0.5
1987	0.015 ± 0.003	4.6 ± 0.4	0.026 ± 0.003	2.7 ± 0.6	0.020 ± 0.003	3.7 ± 0.5
1988	0.020 ± 0.003	5.0 ± 0.5	0.029 ± 0.002	3.0 ± 0.6	0.024 ± 0.002	4.0 ± 0.5
1989	0.025 ± 0.003	5.4 ± 0.6	0.032 ± 0.002	3.2 ± 0.5	0.028 ± 0.002	4.3 ± 0.5
1990	0.030 ± 0.003	5.6 ± 0.7	0.035 ± 0.001	3.5 ± 0.4	0.033 ± 0.002	4.5 ± 0.6
1991	0.036 ± 0.003	5.6 ± 0.8	0.039 ± 0.001	3.7 ± 0.3	0.037 ± 0.002	4.6 ± 0.6
1992	0.042 ± 0.004	5.5 ± 1.0	0.043 ± 0.001	3.9 ± 0.3	0.042 ± 0.002	4.7 ± 0.6
1993	0.047 ± 0.004	5.3 ± 1.2	0.046 ± 0.001	4.0 ± 0.2	0.047 ± 0.003	4.6 ± 0.7
1994	0.052 ± 0.005	5.1 ± 1.2	0.051 ± 0.001	4.1 ± 0.2	0.051 ± 0.003	4.6 ± 0.7
1995	0.057 ± 0.006	4.9 ± 1.2	0.055 ± 0.001	4.1 ± 0.3	0.056 ± 0.004	4.5 ± 0.7
1996	0.062 ± 0.007	4.7 ± 1.1	0.059 ± 0.001	4.1 ± 0.3	0.060 ± 0.004	4.4 ± 0.7
1997	0.067 ± 0.008	4.5 ± 0.9	0.063 ± 0.001	4.1 ± 0.3	0.065 ± 0.005	4.3 ± 0.6
1998	0.071 ± 0.009	4.4 ± 0.6	0.067 ± 0.001	4.0 ± 0.3	0.069 ± 0.005	4.2 ± 0.5
1999	0.075 ± 0.009	4.3 ± 0.3	0.071 ± 0.002	4.0 ± 0.3	0.073 ± 0.006	4.1 ± 0.3
2000	0.080 ± 0.010	4.2 ± 0.6	0.075 ± 0.002	3.8 ± 0.2	0.077 ± 0.006	4.0 ± 0.4
2001	0.084 ± 0.009	4.1 ± 1.1	0.079 ± 0.002	3.7 ± 0.1	0.081 ± 0.006	3.9 ± 0.6
2002	0.088 ± 0.008	4.1 ± 1.4	0.082 ± 0.002	3.5 ± 0.2	0.085 ± 0.005	3.8 ± 0.8
2003	0.092 ± 0.007	4.0 ± 1.6	0.086 ± 0.002	3.4 ± 0.3	0.089 ± 0.004	3.7 ± 0.9
2004	0.096 ± 0.005	3.9 ± 1.6	0.089 ± 0.002	3.3 ± 0.4	0.092 ± 0.004	3.6 ± 1.0
2005	0.100 ± 0.004	3.8 ± 1.5	0.092 ± 0.001	3.3 ± 0.4	0.096 ± 0.003	3.6 ± 0.9
2006	0.103 ± 0.004	3.7 ± 1.4	0.096 ± 0.001	3.4 ± 0.3	0.100 ± 0.002	3.5 ± 0.8
2007	0.107 ± 0.004	3.7 ± 1.3	0.099 ± 0.001	3.5 ± 0.3	0.103 ± 0.002	3.6 ± 0.8
2008	0.111 ± 0.005	3.6 ± 1.1	0.103 ± 0.001	3.6 ± 0.3	0.107 ± 0.003	3.6 ± 0.7
2009	0.114 ± 0.005	3.4 ± 1.0	0.106 ± 0.001	3.7 ± 0.3	0.110 ± 0.003	3.6 ± 0.6
2010	0.118 ± 0.006	3.2 ± 1.1	0.110 ± 0.001	3.7 ± 0.3	0.114 ± 0.003	3.5 ± 0.7
2011	0.121 ± 0.006	3.0 ± 1.6	0.114 ± 0.001	3.7 ± 0.3	0.117 ± 0.004	3.4 ± 1.0

*Annual hemispheric mean mole fractions and growth rates are estimated from the smoothing cubic spline fits.
**ppt = parts-per-trillion dry air mole fraction.
***ppq = parts-per-quadrillion dry air mole fraction.

5.1.4 Atmospheric Radiative Forcing

Based on the globally averaged dry air mole fractions (Tables 5.1 through 5.5), the global radiative forcing of each PFC can be estimated using the radiative efficiencies presented in Table 1.1. For C_4F_{10}, C_5F_{12} and C_6F_{14} we use the radiative efficiencies given by *Forster et al.* (2007), and for C_7F_{16} and C_8F_{18}, we use the radiative efficiencies estimated in Section 4.2. Figure 5-6 shows the anthropogenic radiative forcing for each PFC, including the lower molecular weight PFCs from 1973 to 2010. CF_4, C_2F_6 and c-C_4F_8 contribute the most to the global radiative forcing of the PFCs (*Mühle et al.*, 2010; *Oram et al.*, 2012). C_6F_{14} contributes the most among the higher molecular weight PFCs to the global radiative forcing, and has a similar forcing as that of C_3F_8 (*Mühle et al.*, 2010); the other PFCs measured in this study contribute approximately equally to global radiative forcing. In total the dry air mole fractions of the high molecular weight PFCs in 2011 contribute to a globally averaged radiative forcing of $0.35\,\mathrm{mW\,m^{-2}}$, which is 6 % of the total anthropogenic radiative forcing from PFCs (*Montzka et al.*, 2011). Although, this is still relatively small compared to the total radiative forcing of $2434\,\mathrm{mW\,m^{-2}}$ in 2008 for all species regulated under the Kyoto Protocol (*Montzka et al.*, 2011).

5.2 Global Emissions

5.2.1 Reference Run

The reference run modeled mole fractions using the bottom-up emission estimates from EDGARv4.2 are lower than the atmospheric observations for the high molecular weight PFCs (see Figures 5-7 through 5-11). In particular, the reference run produces modeled mole fractions that are 20 times lower and over a 1000 times lower than the observations for C_4F_{10} and C_5F_{12}, respectively (see Figure 5-7 and Figure 5-8). For C_5F_{12}, this is due to its global annual emissions from EDGARv4.2 peaking at less than $0.1\,\mathrm{tons\,yr^{-1}}$, with its only emission source being usage as a refrigerant in the Romania (see Figure 3-2). In contrast, the reference modeled mole fractions for

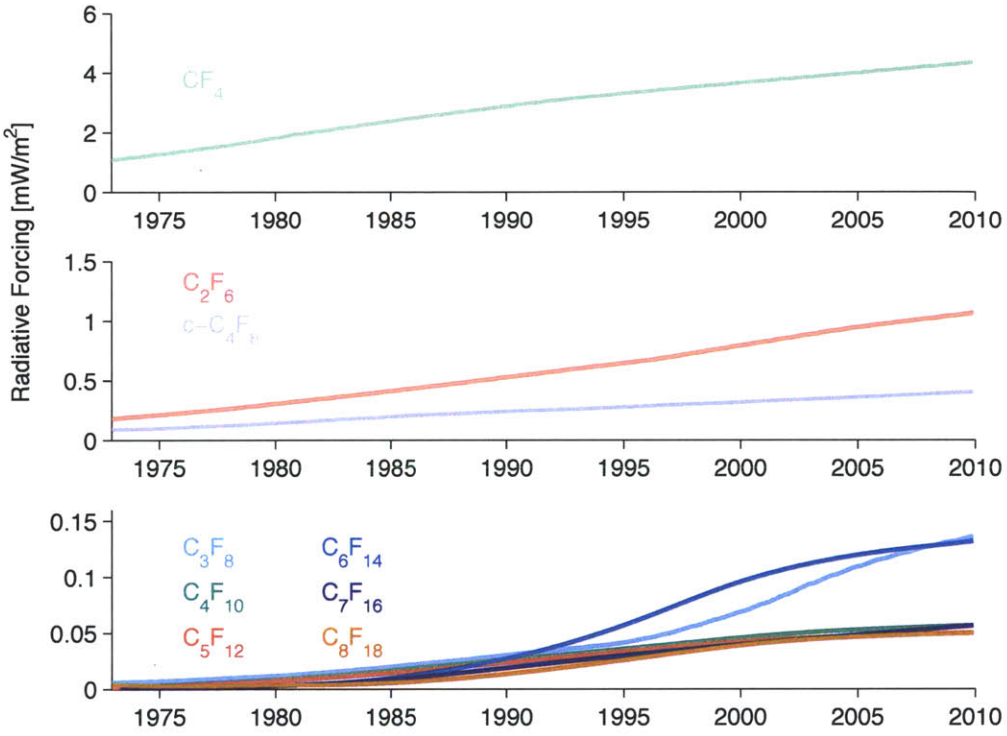

Figure 5-6: The globally averaged radiative forcing for each PFC from 1973 to 2010. The CF_4, C_2F_6, C_3F_8 atmospheric observations are from *Mühle et al.* (2010). The c-C_4F_8 observations are from Jens Mühle (*SIO, personal communication, 2012*). The C_4F_{10}, C_5F_{12}, C_6F_{14}, C_7F_{16} and C_8F_{18} atmospheric histories are based on the globally averaged smoothing spline fits to the observations.

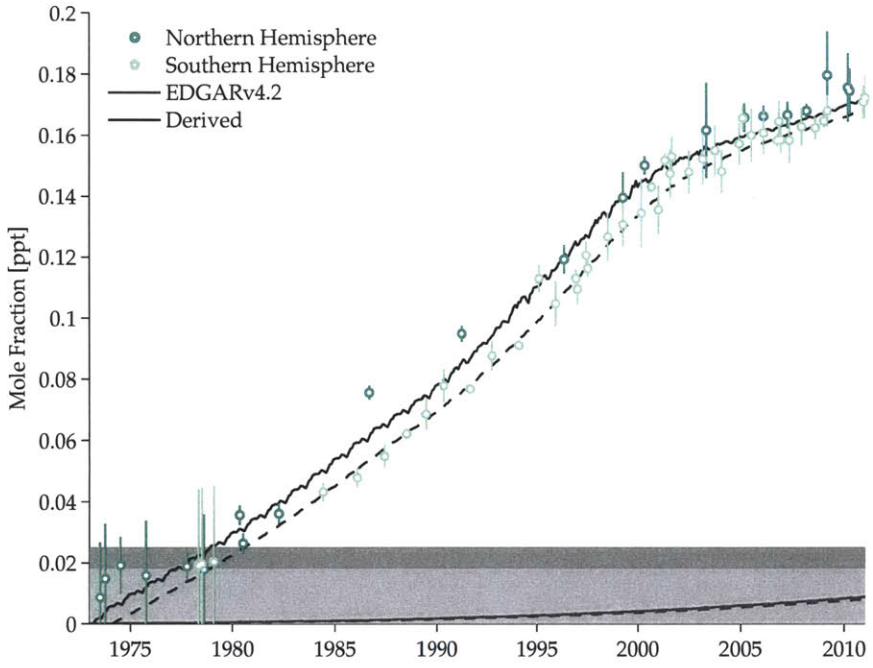

Figure 5-7: MOZARTv4.5 model output at the observation grid cells (Northern Hemisphere - solid line and Southern Hemisphere - dashed line) for the reference run using emissions based on EDGARv4.2 (grey lines) and the final derived emissions (black lines). The open circles are the atmospheric observations (Northern Hemisphere - dark color and Southern Hemisphere - light color), with the vertical lines being the associated observational uncertainty. The detection limits for the instruments are shown as the grey shading, with dark grey for the SIO instrument and the light grey for the CSIRO instrument.

C_6F_{14} are similar to the observations (see Figure 5-9), although the reference run is somewhat lower in the mid 1990s, suggesting an underestimation of emissions in EDGARv4.2 during this period. For C_7F_{16} and C_8F_{18}, the model reference run is about 50 % lower than atmospheric observations (see Figures 5-10 and 5-11).

5.2.2 Derived Global Emission Estimates

Using the inverse method outlined in Section 3.2, we provide new global emission estimates constrained by our atmospheric observations and an independent estimate of the annual growth rate in emissions. The derived emissions and their associated

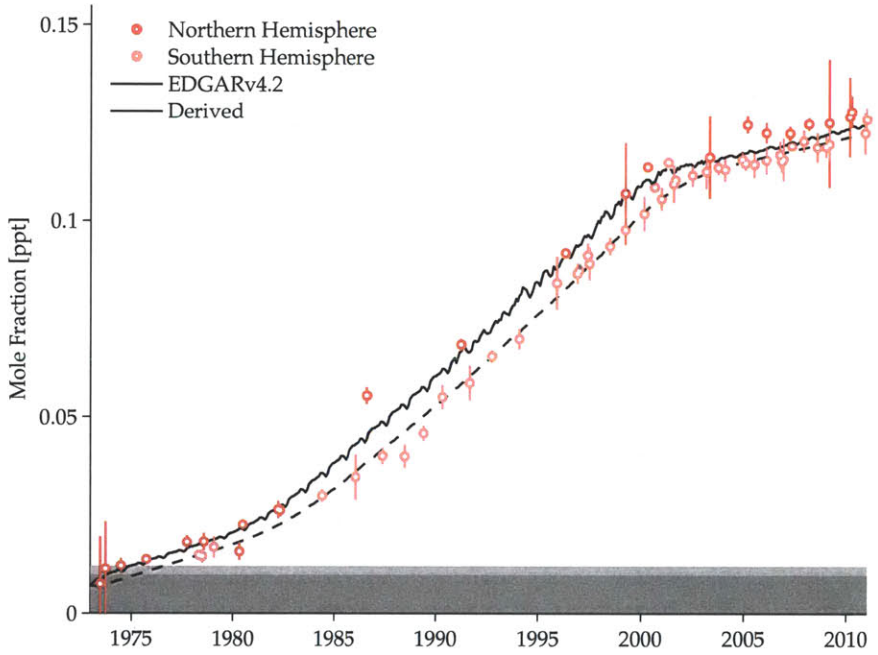

Figure 5-8: Same as Figure 5-7 but for C_5F_{12}. Note: The reference run using the EDGARv4.2 emissions is too small to be seen on this scale.

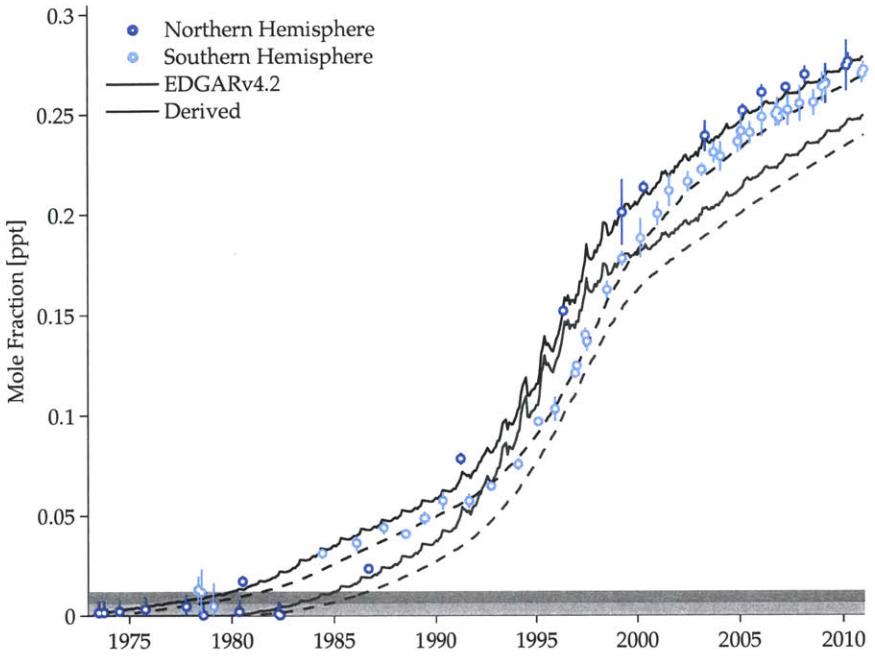

Figure 5-9: Same as Figure 5-7 but for C_6F_{14}.

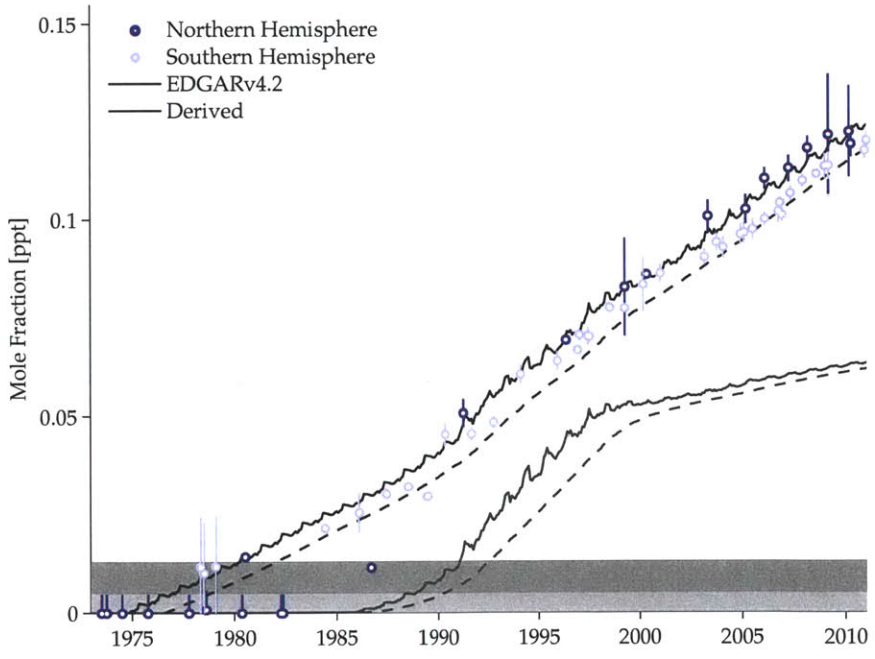

Figure 5-10: Same as Figure 5-7 but for C_7F_{16}.

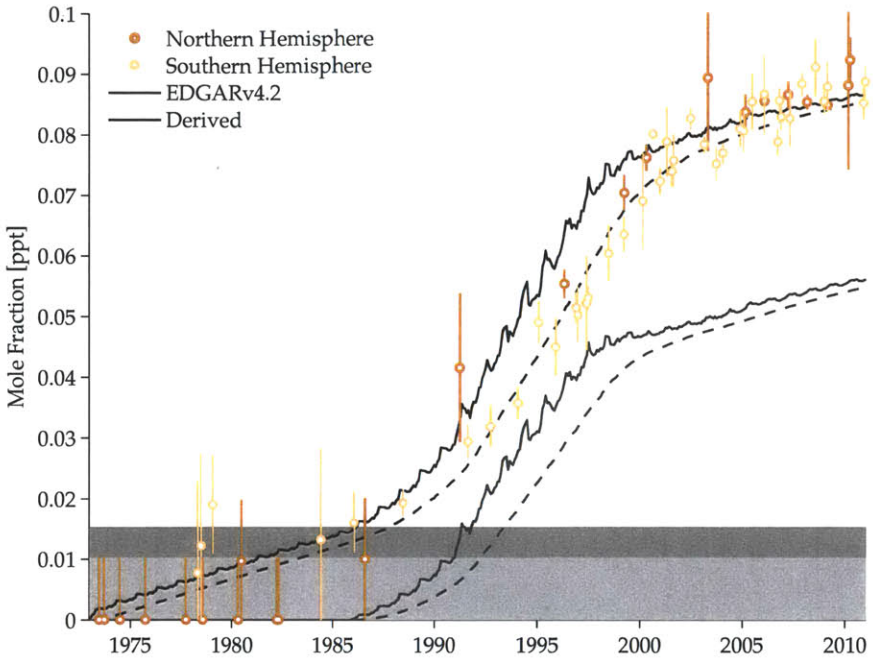

Figure 5-11: Same as Figure 5-7 but for C_8F_{18}.

uncertainties are presented in Figures 5-12 through 5-16 and in numerical form in Table 5.6. The derived emissions for C_4F_{10} and C_5F_{12} are relatively constant over the time period with average emission rates and 1-σ uncertainties of 196±33 tons yr^{-1} and 171±42 tons yr^{-1}, respectively. The largest decline in emissions for C_4F_{10} and C_5F_{12} was from 1999 to 2005; since 2005 the emission rates have remained relatively constant.

The C_6F_{14} increase in emission rates, starting in the 1990s, has a later onset than that of C_4F_{10} and C_5F_{12}, and has a similar emission profile as that of C_3F_8, as shown in *Mühle et al.* (2010). Of the PFCs studied here, C_6F_{14} has the largest emissions with a 1980 to 2010 average emission rate and 1-σ uncertainty of 510±62 tons yr^{-1}. The derived emissions for C_7F_{16} and C_8F_{18} are both higher than the bottom-up estimates of C_7F_{16} in EDGARv4.2. Interestingly while the other high molecular weight PFC emissions have decreased in the past 10 to 20 years, the derived emissions for C_7F_{16} have remained relatively constant for the last ten years, with an average emission

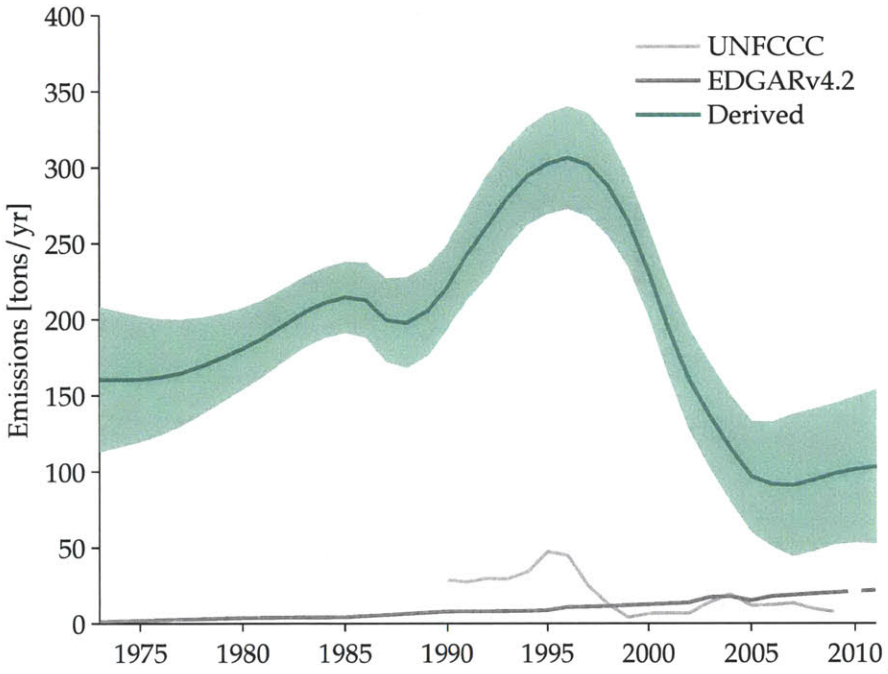

Figure 5-12: The global annual emissions for C_4F_{10} derived in this study are shown as the solid color line, and the associated 1-σ uncertainty in the emissions is represented as the light color shading. The available bottom-up emissions data are also shown from EDGARv4.2 (solid dark grey line) and UNFCCC (solid light grey line). The interpolated data used in the reference run from EDGARv4.2 from 2009 to 2011 are shown as the dashed grey line.

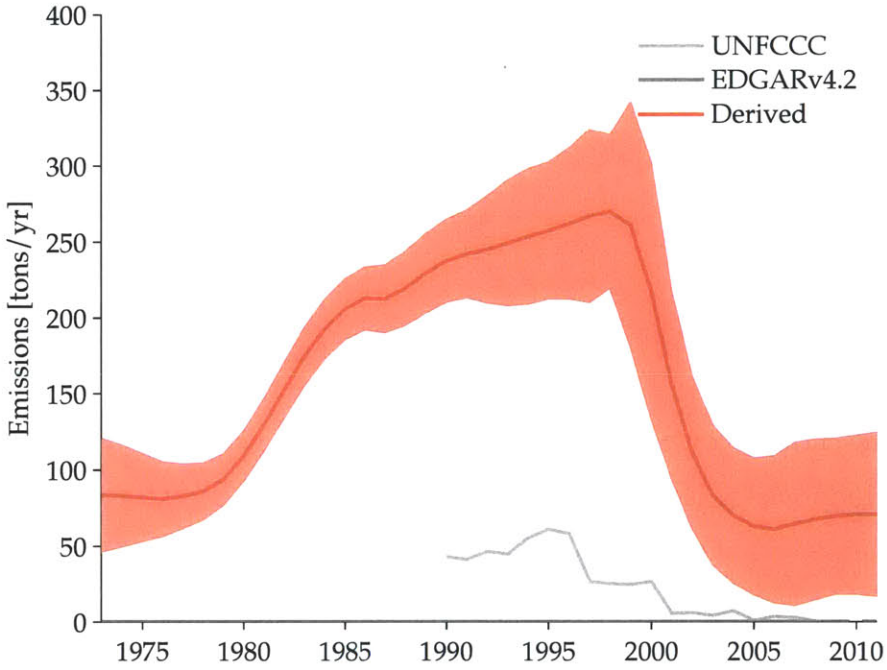

Figure 5-13: Same as Figure 5-12 but for C_5F_{12}. Note: The EDGARv4.2 emissions are too small to be seen on this scale.

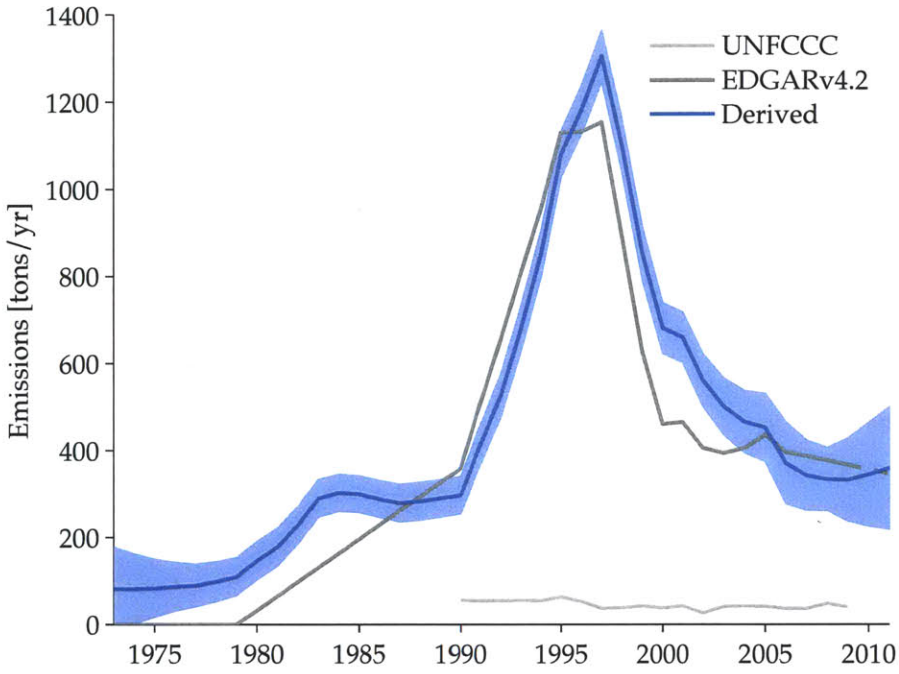

Figure 5-14: Same as Figure 5-12 but for C_6F_{14}.

rate over the entire study period of 251 ± 37 tons yr^{-1}. The average emission rate from 1980 to 2010 for C_8F_{18} is 195 ± 34 tons yr^{-1}.

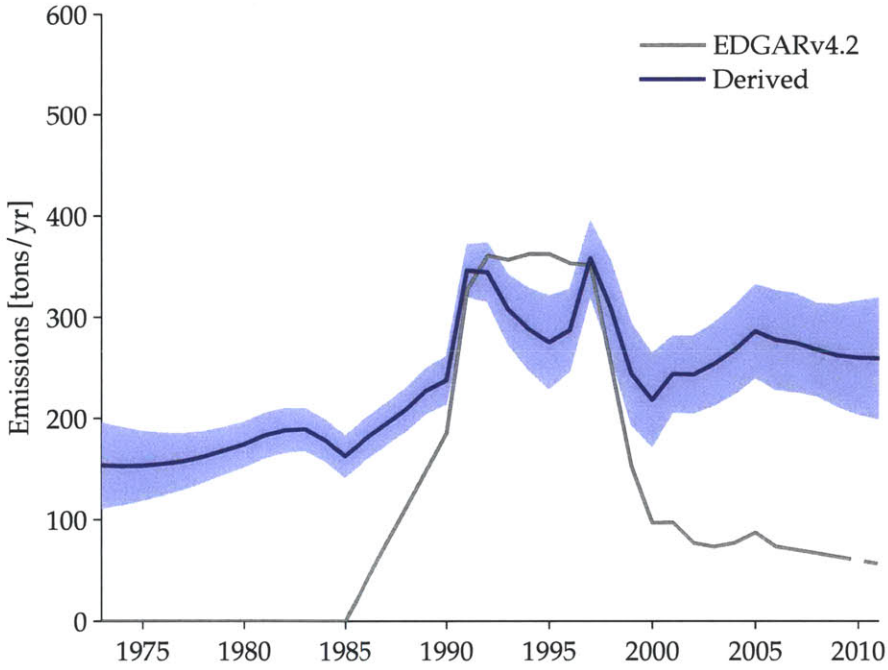

Figure 5-15: Same as Figure 5-12 but for C_7F_{16}.

Table 5.5: Northern and Southern Hemisphere and Global Average Annual Mean Mole Fractions and Growth Rates and Associated Uncertainties 1980-2011 for C_8F_{18}*

	Northern Hemisphere		Southern Hemisphere		Global Average	
	Mole Fraction	Growth Rate	Mole Fraction	Growth Rate	Mole Fraction	Growth Rate
Year	[ppt**]	[ppq yr^{-1}***]	[ppt]	[ppq yr^{-1}]	[ppt]	[ppq yr^{-1}]
1980	0.001 ± 0.004	0.4 ± 1.3	0.011 ± 0.009	0.5 ± 2.9	0.006 ± 0.006	0.5 ± 2.1
1981	0.001 ± 0.004	0.4 ± 1.4	0.012 ± 0.007	0.4 ± 2.7	0.007 ± 0.006	0.4 ± 2.1
1982	0.002 ± 0.004	0.3 ± 1.5	0.012 ± 0.007	0.4 ± 2.4	0.007 ± 0.006	0.3 ± 1.9
1983	0.002 ± 0.004	0.3 ± 1.5	0.012 ± 0.007	0.4 ± 2.0	0.007 ± 0.006	0.3 ± 1.7
1984	0.002 ± 0.005	0.7 ± 1.5	0.013 ± 0.008	0.5 ± 1.5	0.008 ± 0.007	0.6 ± 1.5
1985	0.003 ± 0.005	1.3 ± 1.7	0.013 ± 0.009	0.7 ± 0.9	0.008 ± 0.007	1.0 ± 1.3
1986	0.005 ± 0.006	1.9 ± 1.7	0.014 ± 0.009	0.9 ± 0.7	0.010 ± 0.008	1.4 ± 1.2
1987	0.007 ± 0.007	2.5 ± 1.5	0.015 ± 0.009	1.3 ± 0.9	0.011 ± 0.008	1.9 ± 1.2
1988	0.010 ± 0.008	3.1 ± 1.1	0.017 ± 0.008	1.6 ± 1.1	0.013 ± 0.008	2.3 ± 1.1
1989	0.013 ± 0.008	3.6 ± 0.7	0.019 ± 0.007	2.0 ± 1.2	0.016 ± 0.008	2.8 ± 1.0
1990	0.017 ± 0.008	4.1 ± 0.5	0.021 ± 0.006	2.3 ± 1.2	0.019 ± 0.007	3.2 ± 0.8
1991	0.021 ± 0.008	4.5 ± 0.5	0.023 ± 0.005	2.7 ± 1.2	0.022 ± 0.007	3.6 ± 0.8
1992	0.026 ± 0.008	4.8 ± 0.7	0.026 ± 0.004	3.0 ± 1.1	0.026 ± 0.006	3.9 ± 0.9
1993	0.031 ± 0.007	5.0 ± 0.9	0.029 ± 0.003	3.4 ± 0.9	0.030 ± 0.005	4.2 ± 0.9
1994	0.036 ± 0.007	5.1 ± 1.0	0.033 ± 0.002	3.8 ± 0.8	0.034 ± 0.004	4.4 ± 0.9
1995	0.041 ± 0.006	5.2 ± 1.0	0.037 ± 0.002	4.1 ± 0.6	0.039 ± 0.004	4.6 ± 0.8
1996	0.046 ± 0.005	5.1 ± 1.0	0.041 ± 0.002	4.4 ± 0.5	0.044 ± 0.003	4.8 ± 0.8
1997	0.051 ± 0.004	5.0 ± 1.0	0.045 ± 0.002	4.6 ± 0.4	0.048 ± 0.003	4.8 ± 0.7
1998	0.056 ± 0.003	4.8 ± 0.8	0.050 ± 0.002	4.8 ± 0.4	0.053 ± 0.002	4.8 ± 0.6
1999	0.061 ± 0.002	4.5 ± 0.7	0.055 ± 0.002	4.9 ± 0.4	0.058 ± 0.002	4.7 ± 0.6
2000	0.065 ± 0.002	4.2 ± 0.6	0.060 ± 0.002	4.9 ± 0.4	0.063 ± 0.002	4.5 ± 0.5
2001	0.069 ± 0.001	3.7 ± 0.5	0.065 ± 0.002	4.6 ± 0.4	0.067 ± 0.002	4.2 ± 0.4
2002	0.073 ± 0.001	3.2 ± 0.4	0.069 ± 0.002	4.2 ± 0.4	0.071 ± 0.002	3.7 ± 0.4
2003	0.076 ± 0.001	2.8 ± 0.4	0.073 ± 0.002	3.5 ± 0.4	0.074 ± 0.001	3.1 ± 0.4
2004	0.078 ± 0.001	2.3 ± 0.5	0.076 ± 0.001	2.9 ± 0.4	0.077 ± 0.001	2.6 ± 0.4
2005	0.081 ± 0.001	2.0 ± 0.6	0.079 ± 0.001	2.4 ± 0.4	0.080 ± 0.001	2.2 ± 0.5
2006	0.082 ± 0.002	1.6 ± 0.8	0.081 ± 0.001	2.0 ± 0.3	0.082 ± 0.002	1.8 ± 0.6
2007	0.084 ± 0.002	1.4 ± 1.0	0.083 ± 0.001	1.7 ± 0.3	0.083 ± 0.002	1.5 ± 0.7
2008	0.085 ± 0.003	1.2 ± 1.2	0.085 ± 0.001	1.4 ± 0.3	0.085 ± 0.002	1.3 ± 0.8
2009	0.086 ± 0.004	1.0 ± 1.2	0.086 ± 0.001	1.2 ± 0.4	0.086 ± 0.003	1.1 ± 0.8
2010	0.087 ± 0.006	1.0 ± 1.1	0.087 ± 0.001	1.0 ± 0.4	0.087 ± 0.003	1.0 ± 0.7
2011	0.088 ± 0.007	1.0 ± 0.7	0.088 ± 0.001	0.9 ± 0.4	0.088 ± 0.004	0.9 ± 0.6

*Annual hemispheric mean mole fractions and growth rates are estimated from the smoothing cubic spline fits.
**ppt = parts-per-trillion dry air mole fraction.
***ppq = parts-per-quadrillion dry air mole fraction.

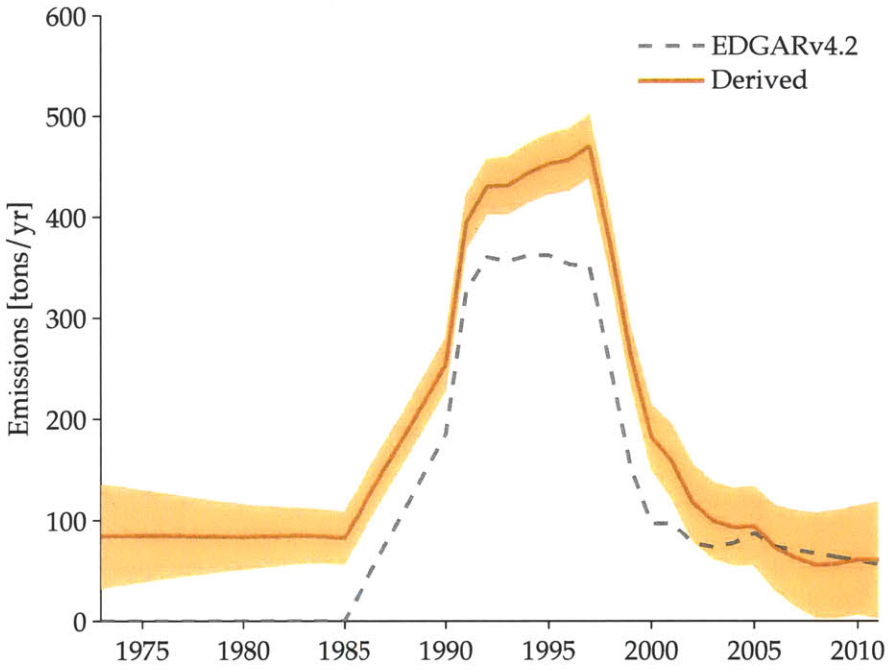

Figure 5-16: Same as Figure 5-12 but for C_8F_{18}. The C_8F_{18} reference emissions are also shown as a dashed line, as no bottom-up estimates are available and the emissions of C_7F_{16} from EDGARv4.2 were used as a proxy.

5.2.3 Final Modeled Mole Fractions

MOZARTv4.5 was run using the emissions derived in this study, shown in Figures 5-12 through 5-16, and produced modeled mole fractions that were much closer to the observations (as expected from the inversion) (see Figures 5-7 through 5-11). Figure 5-17 shows the residuals of the final runs (take as the observed mole fractions minus the final modeled mole fractions) using the derived emissions. Most of the residuals are within their estimated observational error and no significant trends are found in the residuals, confirming that the derived emissions represent an improved estimate from the priors. The largest residuals are seen in the late 1970s and early 1980s for C_6F_{14}, C_7F_{16} and C_8F_{18}. This is possibly due to nonlinearities in the analysis of the the early archived air samples, which have unexpected higher mole fractions in the

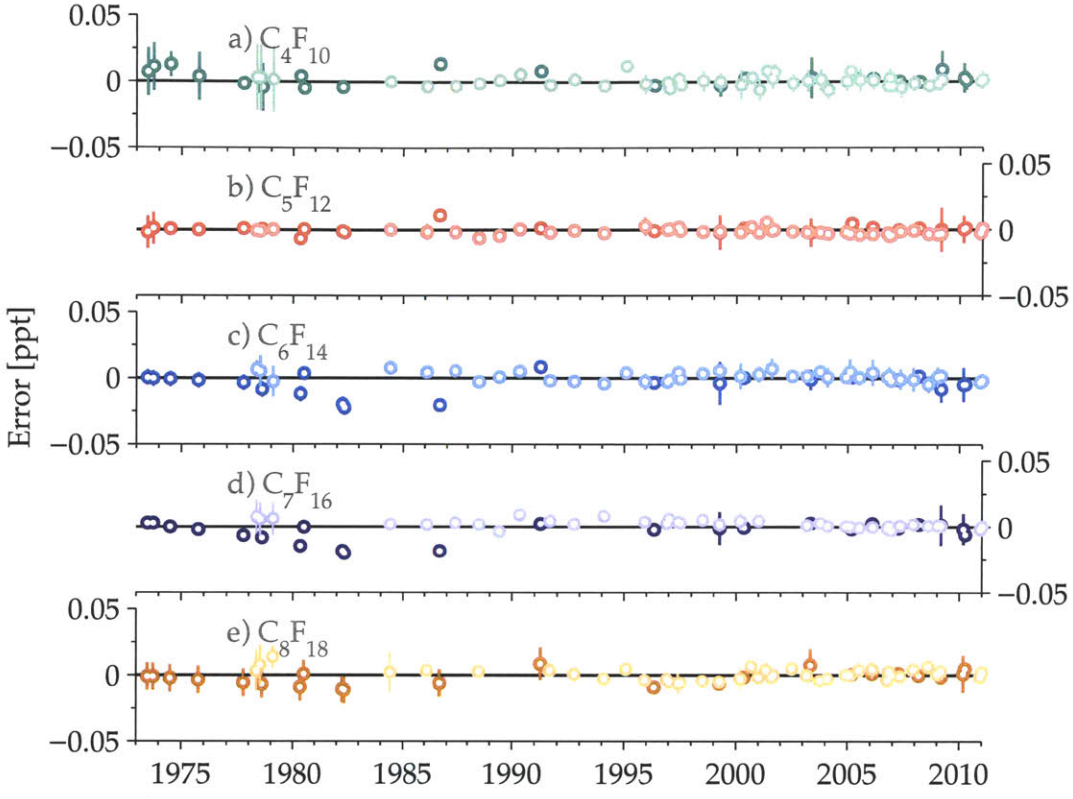

Figure 5-17: The mole fraction residuals (Northern Hemisphere - dark and Southern Hemisphere - light), taken as the observations minus the final modeled mole fractions, for a) C_4F_{10}, b) C_5F_{12}, c) C_6F_{14}, d) C_7F_{16} and e) C_8F_{18}. The vertical lines represent the uncertainty associated with each observation. A zero line is also plotted for reference.

SH than NH samples, and/or the fact that the NH samples were filled with different techniques than the SH samples and not filled for the explicit purpose of being an air archive.

5.2.4 Comparison with Bottom-Up Inventories

EDGARv4.2

The EDGARv4.2 emissions are approximately 20 and 1000 times lower than the derived emissions for C_4F_{10} and C_5F_{12}, respectively. Furthermore, the EDGARv4.2 temporal profiles for C_4F_{10} and C_5F_{12} emissions are drastically different than those derived from the observations, with emissions in EDGARv4.2 being relatively lower in

the 1980s and then increasing with time. EDGARv4.2 estimates that all of the emissions for C_5F_{12} are from refrigeration usage in Romania and are less than 0.1 tons yr^{-1} (see Figure 3-2). These EDGARv4.2 estimates for C_5F_{12} are from the UNFCCC reported inventories; although these reported inventories for C_5F_{12} include more countries than just Romania and are larger in total than those estimated in EDGARv4.2. In contrast, the derived emissions for C_6F_{14} agree fairly well with EDGARv4.2. The derived emissions for C_7F_{16} and C_8F_{18} are both higher than those of C_7F_{16} in EDGARv4.2.

Figure 5-18 shows the total PFC emissions, using their 100-year time horizon GWPs, in CO_2-equivalents for C_4F_{10}, C_5F_{12}, C_6F_{14} and C_7F_{16} for the EDGARv4.2 bottom-up emissions and the emissions derived in this study. In total, the radiative impact of the high molecular weight PFC emissions from EDGARv4.2 are underestimated by 20 to 50 % as compared to the top-down emissions derived in this study constrained by atmospheric observations.

Table 5.6: Annual Mean Global Emission Rates and Uncertainties for C_4F_{10}, C_5F_{12}, C_6F_{14}, C_7F_{16} and C_8F_{18}

Year	C_4F_{10} [tons yr^{-1}]	C_5F_{12} [tons yr^{-1}]	C_6F_{14} [tons yr^{-1}]	C_7F_{16} [tons yr^{-1}]	C_8F_{18} [tons yr^{-1}]
1980	181 ± 27	108 ± 16	147 ± 44	174 ± 22	83 ± 32
1981	188 ± 25	129 ± 17	179 ± 43	183 ± 22	83 ± 30
1982	197 ± 23	152 ± 18	229 ± 43	188 ± 22	83 ± 29
1983	205 ± 23	174 ± 19	290 ± 43	189 ± 21	84 ± 27
1984	211 ± 23	192 ± 20	303 ± 42	178 ± 20	83 ± 26
1985	215 ± 23	206 ± 20	300 ± 42	162 ± 20	81 ± 26
1986	213 ± 24	213 ± 21	289 ± 42	179 ± 20	116 ± 25
1987	200 ± 27	212 ± 22	279 ± 43	193 ± 21	150 ± 25
1988	198 ± 29	219 ± 24	284 ± 43	208 ± 21	183 ± 25
1989	206 ± 29	229 ± 26	290 ± 43	227 ± 22	218 ± 25
1990	222 ± 27	238 ± 27	298 ± 43	238 ± 24	253 ± 26
1991	243 ± 30	242 ± 29	414 ± 45	346 ± 26	395 ± 26
1992	262 ± 33	245 ± 35	526 ± 49	345 ± 29	431 ± 27
1993	280 ± 32	249 ± 41	678 ± 52	308 ± 34	432 ± 28
1994	295 ± 32	254 ± 45	851 ± 53	288 ± 41	444 ± 29
1995	303 ± 33	258 ± 45	1080 ± 53	275 ± 46	453 ± 30
1996	307 ± 33	262 ± 50	1182 ± 55	287 ± 41	457 ± 30
1997	302 ± 34	267 ± 57	1305 ± 59	359 ± 37	471 ± 31
1998	288 ± 32	270 ± 50	1100 ± 61	309 ± 47	374 ± 29
1999	265 ± 29	261 ± 81	852 ± 61	244 ± 50	263 ± 28
2000	232 ± 28	218 ± 85	681 ± 58	218 ± 46	182 ± 32
2001	194 ± 30	155 ± 62	659 ± 58	244 ± 38	158 ± 37
2002	161 ± 33	110 ± 50	561 ± 60	243 ± 38	117 ± 38
2003	137 ± 34	83 ± 46	501 ± 65	254 ± 41	99 ± 38
2004	115 ± 35	69 ± 44	466 ± 71	268 ± 44	92 ± 38
2005	97 ± 36	62 ± 45	452 ± 78	286 ± 46	93 ± 39
2006	92 ± 41	60 ± 48	371 ± 94	278 ± 49	72 ± 42
2007	91 ± 47	64 ± 53	343 ± 80	274 ± 49	62 ± 47
2008	95 ± 47	67 ± 53	334 ± 72	268 ± 46	55 ± 52
2009	99 ± 46	69 ± 51	333 ± 95	262 ± 51	56 ± 53
2010	102 ± 48	70 ± 52	345 ± 118	260 ± 56	60 ± 53

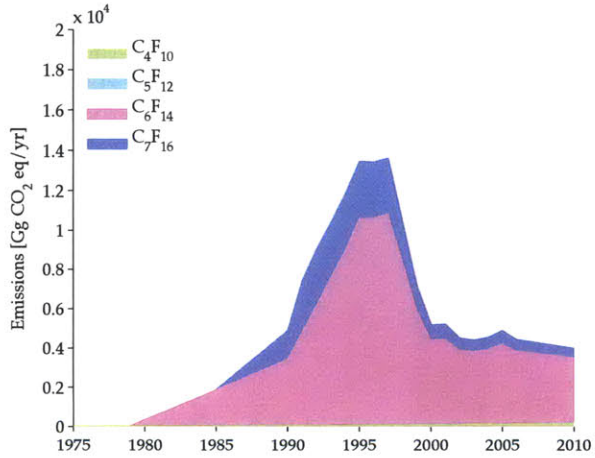

(a) EDGARv4.2

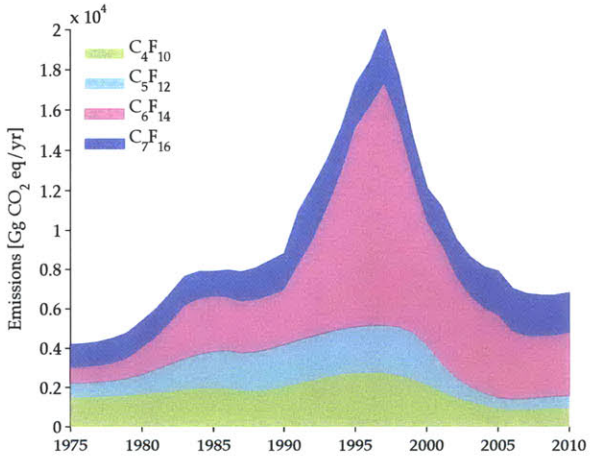

(b) Derived

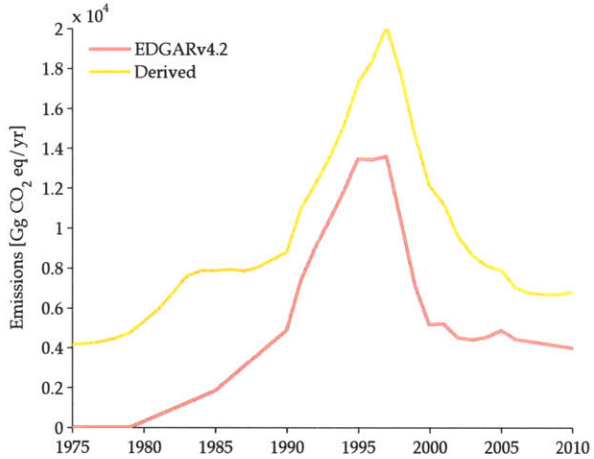

(c) Total EDGARv4.2 and Derived

Figure 5-18: High molecular weight PFC emissions (C_4F_{10}, C_5F_{12}, C_6F_{14} and C_7F_{16}) in CO_2-equivalents for a) EDGARv4.2, b) the derived emissions in this study and c) the totals for the two data sets.

UNFCCC

Overall the UNFCCC reported inventories are five to ten times lower than the emissions reported in this study based on the observations for C_4F_{10}, C_5F_{12} and C_6F_{14}. In general, the UNFCCC emission inventories should be considered as lower bounds on global emissions, as they do not include some major national greenhouse gas emitters. As mentioned in Chapter 3, the countries with the largest emissions reported to the UNFCCC is Belgium followed by France. We see that the reported inventories to the UNFCCC for CF_4 and C_2F_6 are much more reasonable; suggesting that the discrepancies in the industry reports to the UNFCCC could be from the semiconductor industry.

Figure 5-19 shows the semiconductor chip sales from the *Semiconductor Industry Association* (2012). For the past 10 years the majority of chip sales have been in Asia and Japan. Japan is the only Asian country that reports inventories to the UNFCCC and is 1.2 % of the total inventories, as compared to ~20 % of the total semiconductor sales (*Semiconductor Industry Association*, 2012). The majority of countries that report individual PFC emissions to the UNFCCC are in Europe. As seen in Figure 5-19, Europe accounts for 10 to 20 % of the total semiconductor chip sales. Thus, the fact that there are many emitting countries that are not reporting offers a possible explanation for the significantly lower UNFCCC inventories as compared to our derived top-down global estimates. Additionally, some Annex 1 countries, such as Japan, report an aggregated total of a mixture of PFC emissions in CO_2-equivalents and do not report all individual PFC emissions. Both C_7F_{16} and C_8F_{18} are not reported to the UNFCCC; however based on our results, their emissions are larger than those of C_4F_{10} and C_5F_{12} and should be considered in future inventories.

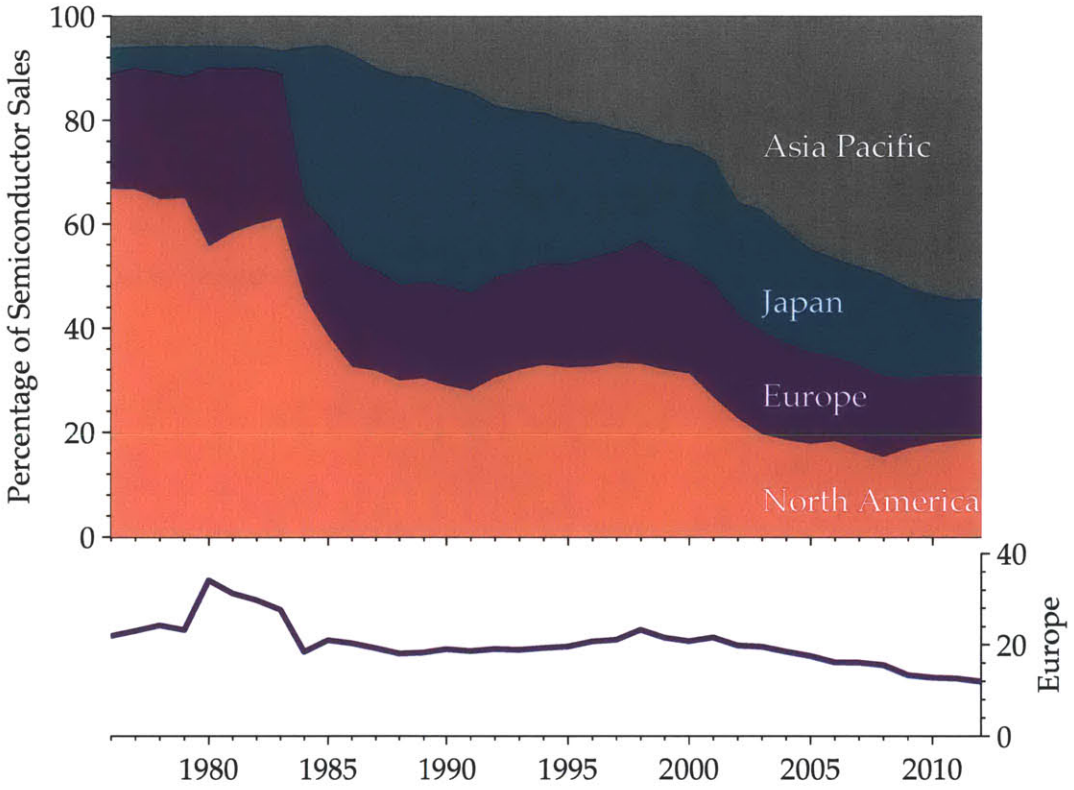

Figure 5-19: Percentage of semiconductor industry sales by region from 1976 to 2011 (*Semiconductor Industry Association*, 2012). The bottom panel shows the relative percentage of sales from Europe as compared to the global total.

5.3 Comparison with *Laube et al. (2012)*

5.3.1 Observations

Recently *Laube et al.* (2012) also published atmospheric observations for C_4F_{10}, C_5F_{12}, C_6F_{14} and C_7F_{16}. For some species, their results agree fairly well with those presented here. The most notable differences are for C_5F_{12}, where *Laube et al.* (2012) report a 2010 global average dry air mole fraction that is 14 % higher than that presented here, and for C_7F_{16}, where *Laube et al.* (2012) report a 2010 dry air mole fraction that is 7 % lower than the estimate from measurements in this study. These differences can most likely be attributed to differences in calibration scales. In particular, the calibration scale estimated by *Laube et al.* (2012) for C_7F_{16} was prepared using an 85 % n-isomer of C_7F_{16}, and this may be a contributing factor to the differences between the two studies.

5.3.2 Emissions

Our derived emissions for C_4F_{10} agree fairly well with those presented by *Laube et al.* (2012). *Laube et al.* (2012) estimate lower emission rates from 1994 to 2001 than ours for C_6F_{14}. The C_6F_{14} observations from *Laube et al.* (2012) agree well with those presented in this thesis in the early 1980s and 1990s; however after this time period the observations and estimated emissions by *Laube et al.* (2012) are lower than those in this study. This is most likely due to a calibration scale difference, with that of *Laube et al.* (2012) leading to lower total dry air mole fractions than ours and possible nonlinearities in the early archive measurements. Furthermore as expected from the mole fractions differences noted above, we see discrepancies in the emission estimates for C_5F_{12} and C_7F_{16}. We see a general overestimation of C_5F_{12} emissions and an underestimation of C_7F_{16} emissions by *Laube et al.* (2012) compared with those estimated in this study. This is most likely due to the calibration scale differences. *Laube et al.* (2012) did not present atmospheric measurements or emission estimates for C_8F_{18}. Furthermore as no bottom-up estimates are available either, the C_8F_{18}

emissions derived in this study are the first reported estimates.

5.4 Radiative Impact of PFC Emissions

Using the 100-year time horizon GWPs, we provide an update to the total annual global PFC emissions in CO_2-equivalents (see Figure 5-20). CF_4, C_2F_6 and c-C_4F_8 contribute the most to the CO_2-equivalent emissions and hence the radiative forcing of the PFCs (*Mühle et al.*, 2010; *Oram et al.*, 2012). However, we find that the high molecular weight PFCs contribute significantly to the total PFC budget, with the C_6F_{14} equivalent emissions being comparable to those of C_3F_8 (*Mühle et al.*, 2010). Previous estimates of the CO_2 equivalent emissions (and hence radiative forcing) of PFCs in 2009 only included CF_4, C_2F_6, C_3F_8 and c-C_4F_8, and were 111 600 Gg CO_2-eq (*Mühle et al.*, 2010; *Oram et al.*, 2012); inclusion of the higher molecular weight PFCs considered here increases this number by 6 % to 118 700 Gg CO_2-eq.

The emissions of the high molecular weight PFCs, C_4F_{10}, C_5F_{12}, C_6F_{14}, C_7F_{16} and C_8F_{18}, from 1973 to 2010 have contributed to a cumulative total forcing of 400 000 Gg of CO_2-equivalents, which is comparable to the total reported HFC emissions in 2009 by Annex 1 countries to the UNFCCC (*United National Framework Convention on Climate Change Secretariat*, 2011). The high molecular weight PFC 2010 emission rates alone are comparable to the release of 7300 Gg of CO_2. The largest relative contribution by the high molecular weight PFCs to the global PFC CO_2-eq emission budget occured in 1997, when they contributed 15.4 % of the total equivalent emissions (see Figure 5-20). Since 1997, the relative contribution to the global CO_2-eq emissions of the high molecular weight PFCs has decreased, most likely due to their replacement with low GWP alternatives (*Office of Air and Radiation and Office of Atmospheric Programs, Climate Change Division*, 2006).

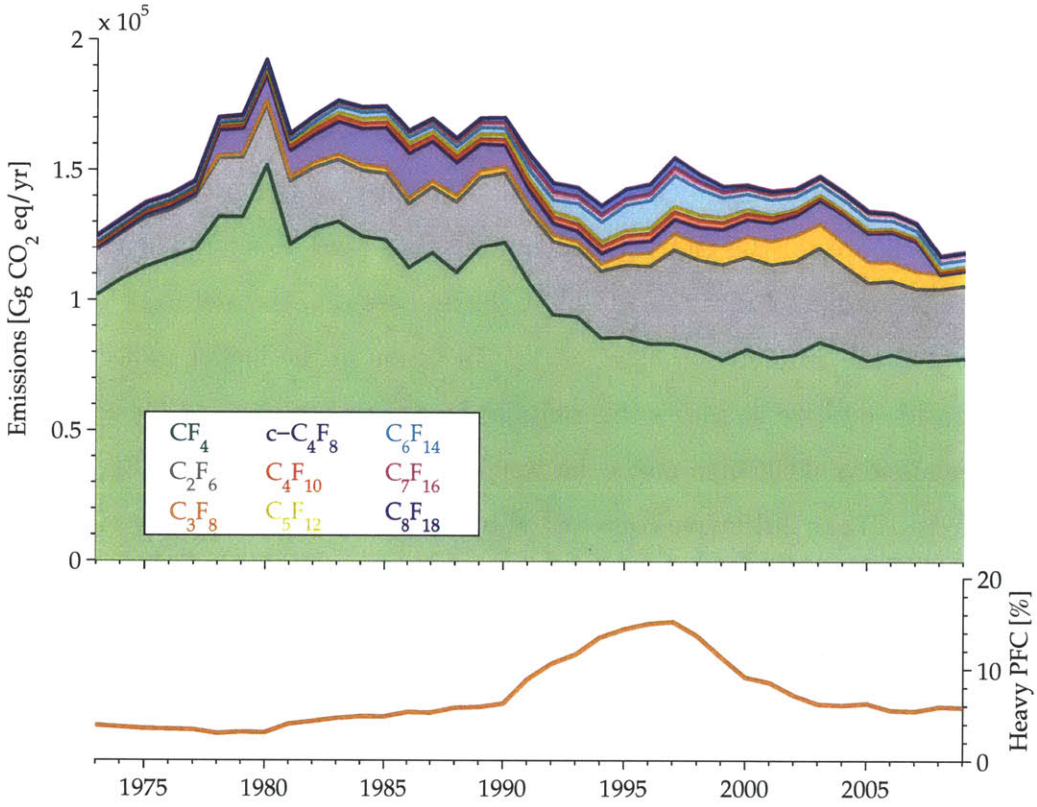

Figure 5-20: Global annual PFC emissions in CO_2-equivalents, using 100-year time horizon GWPs, from 1973 to 2009. The CF_4, C_2F_6 and C_3F_8 emissions are from *Mühle et al.* (2010) and the c-C_4F_8 emissions are from *Oram et al.* (2012). The bottom panel shows the relative percentage the high molecular weight PFCs studied here contribute to the new global total of PFC emissions in CO_2-equivalents.

Chapter 6

Conclusions

Atmospheric histories have been presented for the high molecular weight PFCs: C_4F_{10}, C_5F_{12}, C_6F_{14}, C_7F_{16} and C_8F_{18}. Their atmospheric histories are based on new measurements of a collection of NH archived air samples and a subset of the CGAA (SH) air samples. The archived air sample measurements were made with the cryogenic preconcentration GC-MS Medusa systems and were calibrated against a new calibration scale for these PFCs. The new calibration scales were determined by preparation of four primary gravimetric standards via the internal additions method; an additional primary standard was prepared by external additions and agreed well with the internal additions standards. In order to characterize any nonlinearities in the system, a set of diluted air samples were prepared and measured on both Medusas. The Medusas were found to be nearly linear after blank corrections. This linearity characterization is particularly critical for the older archive samples, which have the lowest dry air mole fractions.

C_6F_{14} was the most abundant of the PFCs studied here with a 2011 globally averaged dry air mole fraction of 0.27 ppt. C_4F_{10} and C_5F_{12} exhibited similar atmospheric histories, suggesting the possibility of them having similar emission sources, and have a 2011 globally averaged dry air mole fraction of 0.17 and 0.12 ppt, respectively. The 2011 globally averaged dry air mole fractions for C_7F_{16} and C_8F_{18} are 0.12 and 0.09 ppt, respectively. The contribution of all of the high molecular weight PFCs studied here to global radiative forcing is $0.35\,\mathrm{mW\,m^{-2}}$. While this is rela-

tively small compared to the total radiative forcing of 2434 mW m^{-2} in 2008 for all species regulated under the Kyoto Protocol, the high molecular weight PFC dry air mole fractions in 2011 contribute up to 6 % of the total anthropogenic PFC radiative forcing (*Montzka et al.*, 2011; *Mühle et al.*, 2010; *Oram et al.*, 2012).

Cubic-smoothing splines were fit to the atmospheric observations, and from these fits, long-term annual growth trends were estimated for each hemisphere. C_4F_{10} and C_5F_{12} had relatively constant growth from 1980 to 2000 and then declined to 2.2 and 1.4 ppq yr^{-1}, respectively, in 2011. The growth rates in atmospheric mole fractions of C_6F_{14}, C_7F_{16} and C_8F_{18} exhibited later onsets and more dramatic rates as compared to those of C_4F_{10} and C_5F_{12}. The 2011 growth rates for C_6F_{14}, C_7F_{16} and C_8F_{18} are 5.0, 3.4 and 0.9 ppq yr^{-1}, respectively. Similarly to C_4F_{10} and C_5F_{12}, the growth rates of C_6F_{14} and C_8F_{18} have declined since 2000. This slow down in growth suggests that recent emissions are decreasing as alternative compounds, with most likely lower GWPs, are used (*Office of Air and Radiation and Office of Atmospheric Programs, Climate Change Division*, 2006).

Global emission estimates from 1973 to 2010 have also been presented for C_4F_{10}, C_5F_{12}, C_6F_{14}, C_7F_{16} and C_8F_{18}, which were constrained by the new atmospheric observations and an independent estimate of their annual growth rate in emissions. C_6F_{14} had the largest emissions of the PFCs studied here, with these emissions being comparable to those of C_3F_8 (*Mühle et al.*, 2010). Using our newly derived GWPs for C_7F_{16} and C_8F_{18}, new estimates of the total radiative impact of all PFC emissions are on average about 7 % higher than previously reported from 1973 to 2009, concluding a previous underestimation of the total radiative forcing from PFC emissions. The high molecular weight PFCs contributed most significantly, up to 16 %, to the global PFC emissions in the 1990s. The high molecular weight PFCs have contributed to a total of 400 000 Gg of CO_2-equivalents to the atmosphere from 1973 to 2010.

Comparison with bottom-up inventories shows a significant underestimation by EDGARv4.2 for C_4F_{10} and C_5F_{12}, further illustrating the benefit of top-down emission estimates based on atmospheric observations for verifying bottom-up emission estimates. Additionally, the reported inventories to the UNFCCC by Annex 1 coun-

tries that have ratified the Kyoto Protocol are generally five to ten times lower than our derived emission rates for C_4F_{10}, C_5F_{12} and C_6F_{14}. However because our derived emissions are global, this discrepancy with the UNFCCC reported inventories cannot be attributed to individual countries. Furthermore, the country with the largest reported emissions to the UNFCCC for C_4F_{10}, C_5F_{12} and C_6F_{14} is Belgium; this may be attributable to different countries reporting a mixture of PFC emissions in CO_2-equivalents, as opposed to the individual PFC emissions. The emission inventories reported to the UNFCCC for CF_4 and C_2F_6 are more realistic, when compared to the top-down estimates, but we still see large discrepancies for C_3F_8. This suggests that this underreporting to the UNFCCC for C_3F_8 and the high molecular weight PFCs can possibly be attributed to the semiconductor industry, while the aluminum industry emission estimates, that dominate the CF_4 and C_2F_6 emissions, reported to the UNFCCC are more reasonable.

These large discrepancies between the top-down and bottom-up emission estimates call attention to the need for more transparent and accurate reporting of emissions. This is further supported by some of the inconsistencies, highlighted in this study, between the two available bottom-up inventories, EDGARv4.2 and UNFCCC; the most notable inconsistency being that the EDGARv4.2 emission estimates for C_5F_{12} only include those reported by Romania to the UNFCCC, while additional countries that also report C_5F_{12} emissions to the UNFCCC are not included in EDGARv4.2. A second discrepancy between the two bottom-up estimates is that EDGARv4.2 suggests that 50 to 90 % of emissions of C_6F_{14} are from Japan, while the report to the UNFCCC shows Japan's emissions being less than 2 % of the total inventories. This may be due to Japan reporting an aggregated total of emissions from a mixture of PFCs. Interestingly, the reported UNFCCC inventories show similar temporal trends as our derived top-down emissions, suggesting the UNFCCC methodology may be a better platform for emissions reporting.

Comparison with recently published work by *Laube et al.* (2012) shows similar atmospheric histories and emission estimates for C_4F_{10} as those presented in this work. One thing to note is that their emissions were not constrained by an inverse method,

and were instead determined qualitatively. Compared to the emissions reported in this thesis, *Laube et al.* (2012) estimated lower emission rates in the late 1990s for C_6F_{14}, most likely due to a calibration scale difference and nonlinearities in the analysis of early archived samples. There are more notable differences in the atmospheric observations and emission estimates for C_5F_{12} and C_7F_{16}, due to differing calibration scales. *Laube et al.* (2012) did not measure C_8F_{18}; therefore we have presented here, the first atmospheric observations and emission estimates for C_8F_{18}.

While emissions have declined in the past 10 years for the high molecular weight PFCs, because of their long lifetimes, PFCs are considered to have an essentially permanent effect on the Earth's radiative budget. Therefore, continued monitoring of their atmospheric abundances is essential to detect the trends in emissions of these potent greenhouse gases. Additionally, future observations of these high molecular weight PFCs will be important in confirming that the semiconductor industries, which primarily focus on the use of low molecular weight PFCs, are indeed reducing their global PFC emissions (*Semiconductor Industry Association*, 2001; *World Semiconductor Council*, 2005).

Appendix A

Atmospheric Observations

Appendix A shows the Northern and Southern Hemispheric archived air sample measurements for C_4F_{10} through C_8F_{18} (see Tables A.1 through A.5). Included is the sample fill date, location, mean dry air mole fractions, standard deviation of the repeat measurements and the number of measurements (n).

Table A.1: Northern and Southern Hemispheric Archived Air Measurements of C_4F_{10}

Fill Date	Location*		Mole Fraction [ppt**]	S.D. [ppt]	n
29 Jun 1973	NH	LJ	0.009	0.001	3
9 Oct 1973	NH	LJ	0.015	0.001	4
9 Oct 1973	NH	LJ	0.015	0.005	5
21 Jun 1974	NH	LJ	0.019	0.009	7
1 Oct 1975	NH	LJ	0.016	0.001	3
4 Oct 1977	NH	LJ	0.019	0.001	3
4 Oct 1977	NH	LJ	0.019	0.002	3
10 Aug 1978	NH	LJ	0.018	0.002	3
15 Apr 1980	NH	CM	0.026	0.003	4
6 May 1980	NH	LJ	0.036	0.003	4
23 Mar 1982	NH	LJ	0.036	0.003	8
7 May 1982	NH	LJ	0.056	0.001	5
10 Sep 1986	NH	HF	0.076	0.002	4
29 Mar 1991	NH	LJ	0.095	0.002	3
18 Apr 1996	NH	LJ	0.119	0.004	2
1 Apr 1999	NH	LJ	0.137	0.008	8
1 Apr 1999	NH	LJ	0.141	0.006	10
1 Apr 1999	NH	LJ	0.139	0.001	3
28 Apr 2000	NH	TH	0.150	0.002	3
20 Apr 2003	NH	TH	0.159	0.004	7
20 Apr 2003	NH	TH	0.162	0.007	5
14 Mar 2005	NH	TH	0.166	0.004	8
6 Feb 2006	NH	TH	0.166	0.003	7
20 Mar 2007	NH	TH	0.166	0.004	9
12 Mar 2008	NH	TH	0.168	0.001	5
2 Mar 2009	NH	TH	0.175	0.006	8
4 Mar 2009	NH	TH	0.180	0.003	2
17 Mar 2010	NH	TH	0.177	0.005	9
17 Mar 2010	NH	TH	0.176	0.004	11
17 Mar 2010	NH	TH	0.176	0.005	13
18 Mar 2010	NH	TH	0.174	0.007	9
25 Jun 2011	NH	TH	0.181	0.008	7
26 Sep 2011	NH	LJ	0.180	0.008	7

Fill Date	Location	Mole Fraction [ppt]	S.D. [ppt]	n
26 Apr 1978	SH	0.019	0.000	1
7 Jul 1978	SH	0.020	0.001	3
6 Feb 1979	SH	0.020	0.001	3
23 May 1984	SH	0.043	0.003	4
6 Feb 1986	SH	0.048	0.003	4
28 May 1987	SH	0.055	0.004	6
21 Jun 1988	SH	0.062	0.002	3
19 May 1989	SH	0.069	0.005	8
26 Apr 1990	SH	0.078	0.005	3
29 Aug 1991	SH	0.077	0.001	3
23 Sep 1992	SH	0.088	0.005	5
11 Feb 1994	SH	0.091	0.001	3
8 Feb 1995	SH	0.113	0.005	2
23 Nov 1995	SH	0.112	0.004	3
4 Dec 1995	SH	0.105	0.005	5
20 Nov 1996	SH	0.113	0.003	4
7 Jan 1997	SH	0.110	0.005	5
30 May 1997	SH	0.121	0.004	4
15 Jul 1997	SH	0.116	0.003	7
25 Jun 1998	SH	0.127	0.008	5
13 Apr 1999	SH	0.131	0.007	5
1 Mar 2000	SH	0.134	0.005	6
14 Mar 2000	SH	0.134	0.005	5
26 Aug 2000	SH	0.143	0.002	3
15 Jan 2001	SH	0.135	0.008	4
27 Apr 2001	SH	0.152	0.002	4
19 Jul 2001	SH	0.147	0.008	5
4 Sep 2001	SH	0.153	0.006	3
20 Jun 2002	SH	0.148	0.007	6
17 Feb 2003	SH	0.152	0.008	5
3 Oct 2003	SH	0.155	0.008	5
22 Jan 2004	SH	0.148	0.007	6
1 Dec 2004	SH	0.157	0.007	18
10 Feb 2005	SH	0.165	0.004	5
28 Jun 2005	SH	0.160	0.009	18
10 Feb 2006	SH	0.161	0.007	15
4 Oct 2006	SH	0.158	0.002	6
19 Oct 2006	SH	0.164	0.007	6
11 Dec 2006	SH	0.158	0.004	4
8 May 2007	SH	0.158	0.008	5
22 Nov 2007	SH	0.163	0.006	5
12 Aug 2008	SH	0.162	0.004	6
16 Dec 2008	SH	0.165	0.002	5
6 Mar 2009	SH	0.168	0.005	8
10 Dec 2010	SH	0.171	0.005	23
16 Dec 2010	SH	0.172	0.007	82

*Northern Hemisphere locations are: LJ = La Jolla, California; CM = Cape Meares, Oregon; HF = Harvard Forest, Massachusetts; TH = Trinidad Head, California. All Southern Hemisphere locations are Cape Grim, Tasmania.
*ppt = parts-per-trillion dry air mole fraction.

Table A.2: Northern and Southern Hemispheric Archived Air Measurements of C_5F_{12}

Fill Date	Location*		Mole Fraction [ppt**]	S.D. [ppt]	n
29 Jun 1973	NH	LJ	0.008	0.003	2
9 Oct 1973	NH	LJ	0.011	0.001	4
9 Oct 1973	NH	LJ	0.012	0.002	4
21 Jun 1974	NH	LJ	0.012	0.002	4
1 Oct 1975	NH	LJ	0.014	0.001	3
4 Oct 1977	NH	LJ	0.019	0.001	3
4 Oct 1977	NH	LJ	0.018	0.001	3
10 Aug 1978	NH	LJ	0.018	0.002	4
15 Apr 1980	NH	CM	0.023	0.001	2
6 May 1980	NH	LJ	0.016	0.002	4
23 Mar 1982	NH	LJ	0.027	0.002	8
7 May 1982	NH	LJ	0.026	0.002	5
10 Sep 1986	NH	HF	0.055	0.002	4
29 Mar 1991	NH	LJ	0.068	0.001	3
18 Apr 1996	NH	LJ	0.092	0.001	2
1 Apr 1999	NH	LJ	0.104	0.003	8
1 Apr 1999	NH	LJ	0.106	0.004	12
1 Apr 1999	NH	LJ	0.107	0.002	3
28 Apr 2000	NH	TH	0.113	0.001	3
20 Apr 2003	NH	TH	0.117	0.001	7
20 Apr 2003	NH	TH	0.115	0.005	5
14 Mar 2005	NH	TH	0.124	0.002	8
6 Feb 2006	NH	TH	0.122	0.002	7
20 Mar 2007	NH	TH	0.122	0.002	9
12 Mar 2008	NH	TH	0.124	0.001	5
2 Mar 2009	NH	TH	0.124	0.002	8
4 Mar 2009	NH	TH	0.127	0.006	2
17 Mar 2010	NH	TH	0.128	0.002	9
17 Mar 2010	NH	TH	0.127	0.002	11
17 Mar 2010	NH	TH	0.126	0.004	12
18 Mar 2010	NH	TH	0.128	0.004	9
25 Jun 2011	NH	TH	0.130	0.007	7
26 Sep 2011	NH	LJ	0.127	0.006	7

Fill Date	Location	Mole Fraction [ppt]	S.D. [ppt]	n
26 Apr 1978	SH	0.015	0.001	3
7 Jul 1978	SH	0.015	0.002	3
6 Feb 1979	SH	0.017	0.000	3
23 May 1984	SH	0.030	0.001	4
6 Feb 1986	SH	0.035	0.002	4
28 May 1987	SH	0.040	0.002	6
21 Jun 1988	SH	0.040	0.003	3
19 May 1989	SH	0.046	0.002	8
26 Apr 1990	SH	0.055	0.003	3
29 Aug 1991	SH	0.059	0.004	3
23 Sep 1992	SH	0.065	0.002	5
11 Feb 1994	SH	0.070	0.003	3
8 Feb 1995	SH	0.089	0.003	2
23 Nov 1995	SH	0.083	0.004	3
4 Dec 1995	SH	0.084	0.004	5
20 Nov 1996	SH	0.086	0.003	4
7 Jan 1997	SH	0.087	0.001	5
30 May 1997	SH	0.091	0.003	4
15 Jul 1997	SH	0.089	0.004	7
25 Jun 1998	SH	0.093	0.002	5
13 Apr 1999	SH	0.097	0.000	5
1 Mar 2000	SH	0.105	0.004	6
14 Mar 2000	SH	0.101	0.002	5
26 Aug 2000	SH	0.108	0.001	3
15 Jan 2001	SH	0.105	0.003	4
27 Apr 2001	SH	0.115	0.001	4
19 Jul 2001	SH	0.109	0.005	5
4 Sep 2001	SH	0.110	0.001	3
20 Jun 2002	SH	0.111	0.003	6
17 Feb 2003	SH	0.112	0.004	5
3 Oct 2003	SH	0.113	0.002	5
22 Jan 2004	SH	0.113	0.003	6
1 Dec 2004	SH	0.115	0.002	18
10 Feb 2005	SH	0.114	0.002	5
28 Jun 2005	SH	0.114	0.003	18
10 Feb 2006	SH	0.115	0.004	15
4 Oct 2006	SH	0.117	0.003	7
19 Oct 2006	SH	0.115	0.003	6
11 Dec 2006	SH	0.115	0.005	4
8 May 2007	SH	0.119	0.001	5
22 Nov 2007	SH	0.120	0.003	5
12 Aug 2008	SH	0.118	0.004	6
16 Dec 2008	SH	0.119	0.003	5
6 Mar 2009	SH	0.119	0.004	8
10 Dec 2010	SH	0.122	0.005	25
16 Dec 2010	SH	0.126	0.003	79

*Northern Hemisphere locations are: LJ = La Jolla, California; CM = Cape Meares, Oregon; HF = Harvard Forest, Massachusetts; TH = Trinidad Head, California. All Southern Hemisphere locations are Cape Grim, Tasmania.
*ppt = parts-per-trillion dry air mole fraction.

Table A.3: Northern and Southern Hemispheric Archived Air Measurements of C_6F_{14}

Fill Date	Location*		Mole Fraction [ppt**]	S.D. [ppt]	n
29 Jun 1973	NH	LJ	0.001	0.002	3
9 Oct 1973	NH	LJ	0.000	0.001	4
9 Oct 1973	NH	LJ	0.001	0.003	5
21 Jun 1974	NH	LJ	0.002	0.003	7
1 Oct 1975	NH	LJ	0.003	0.003	3
4 Oct 1977	NH	LJ	0.007	0.002	3
4 Oct 1977	NH	LJ	0.004	0.004	3
10 Aug 1978	NH	LJ	0.000	0.000	4
10 Aug 1978	NH	LJ	0.000	0.000	3
15 Apr 1980	NH	CM	0.017	0.003	3
6 May 1980	NH	LJ	0.002	0.002	4
23 Mar 1982	NH	LJ	0.001	0.001	8
7 May 1982	NH	LJ	0.000	0.000	5
10 Sep 1986	NH	HF	0.023	0.001	4
29 Mar 1991	NH	LJ	0.078	0.003	3
18 Apr 1996	NH	LJ	0.152	0.002	2
1 Apr 1999	NH	LJ	0.194	0.004	8
1 Apr 1999	NH	LJ	0.198	0.005	12
1 Apr 1999	NH	LJ	0.204	0.003	3
28 Apr 2000	NH	TH	0.213	0.003	3
20 Apr 2003	NH	TH	0.244	0.004	7
20 Apr 2003	NH	TH	0.239	0.003	5
14 Mar 2005	NH	TH	0.252	0.003	8
6 Feb 2006	NH	TH	0.261	0.004	6
20 Mar 2007	NH	TH	0.263	0.001	8
12 Mar 2008	NH	TH	0.270	0.004	5
2 Mar 2009	NH	TH	0.270	0.004	8
4 Mar 2009	NH	TH	0.264	0.002	2
17 Mar 2010	NH	TH	0.274	0.004	9
17 Mar 2010	NH	TH	0.276	0.003	11
17 Mar 2010	NH	TH	0.274	0.005	11
18 Mar 2010	NH	TH	0.276	0.004	9
25 Jun 2011	NH	TH	0.278	0.005	7
26 Sep 2011	NH	LJ	0.295	0.000	1

Fill Date	Location	Mole Fraction [ppt]	S.D. [ppt]	n
26 Apr 1978	SH	0.013	0.001	2
7 Jul 1978	SH	0.011	0.001	3
6 Feb 1979	SH	0.005	0.008	3
23 May 1984	SH	0.031	0.003	4
6 Feb 1986	SH	0.036	0.004	4
28 May 1987	SH	0.044	0.003	6
21 Jun 1988	SH	0.041	0.002	3
19 May 1989	SH	0.048	0.003	8
26 Apr 1990	SH	0.057	0.004	3
29 Aug 1991	SH	0.057	0.004	3
23 Sep 1992	SH	0.064	0.003	5
11 Feb 1994	SH	0.075	0.003	3
8 Feb 1995	SH	0.097	0.002	2
23 Nov 1995	SH	0.101	0.003	3
4 Dec 1995	SH	0.103	0.004	5
20 Nov 1996	SH	0.121	0.001	4
7 Jan 1997	SH	0.125	0.002	5
30 May 1997	SH	0.140	0.003	4
15 Jul 1997	SH	0.137	0.005	7
25 Jun 1998	SH	0.162	0.004	5
13 Apr 1999	SH	0.178	0.004	5
1 Mar 2000	SH	0.191	0.008	6
14 Mar 2000	SH	0.188	0.005	5
15 Jan 2001	SH	0.200	0.006	4
19 Jul 2001	SH	0.212	0.008	5
20 Jun 2002	SH	0.216	0.005	6
17 Feb 2003	SH	0.222	0.003	5
3 Oct 2003	SH	0.231	0.005	5
22 Jan 2004	SH	0.229	0.007	6
1 Dec 2004	SH	0.236	0.005	18
10 Feb 2005	SH	0.241	0.010	5
28 Jun 2005	SH	0.240	0.006	18
10 Feb 2006	SH	0.248	0.010	15
4 Oct 2006	SH	0.250	0.006	6
19 Oct 2006	SH	0.251	0.007	6
11 Dec 2006	SH	0.248	0.004	4
8 May 2007	SH	0.252	0.008	5
22 Nov 2007	SH	0.255	0.009	5
12 Aug 2008	SH	0.256	0.006	6
16 Dec 2008	SH	0.263	0.007	5
6 Mar 2009	SH	0.265	0.005	8
10 Dec 2010	SH	0.270	0.005	24
16 Dec 2010	SH	0.272	0.004	69

*Northern Hemisphere locations are: LJ = La Jolla, California; CM = Cape Meares, Oregon; HF = Harvard Forest, Massachusetts; TH = Trinidad Head, California. All Southern Hemisphere locations are Cape Grim, Tasmania.
*ppt = parts-per-trillion dry air mole fraction.

Table A.4: Northern and Southern Hemispheric Archived Air Measurements of C_7F_{16}

Fill Date	Location*		Mole Fraction [ppt**]	S.D. [ppt]	n
29 Jun 1973	NH	LJ	0.000	0.000	3
9 Oct 1973	NH	LJ	0.000	0.000	4
9 Oct 1973	NH	LJ	0.000	0.000	5
21 Jun 1974	NH	LJ	0.000	0.000	7
1 Oct 1975	NH	LJ	0.000	0.000	3
4 Oct 1977	NH	LJ	0.004	0.005	3
4 Oct 1977	NH	LJ	0.000	0.000	3
10 Aug 1978	NH	LJ	0.000	0.000	4
10 Aug 1978	NH	LJ	0.001	0.002	3
15 Apr 1980	NH	CM	0.014	0.001	4
6 May 1980	NH	LJ	0.000	0.000	4
23 Mar 1982	NH	LJ	0.000	0.000	8
7 May 1982	NH	LJ	0.000	0.000	5
10 Sep 1986	NH	HF	0.012	0.000	3
29 Mar 1991	NH	LJ	0.051	0.004	3
18 Apr 1996	NH	LJ	0.069	0.000	2
1 Apr 1999	NH	LJ	0.083	0.002	8
1 Apr 1999	NH	LJ	0.084	0.002	11
1 Apr 1999	NH	LJ	0.079	0.003	3
28 Apr 2000	NH	TH	0.086	0.001	3
20 Apr 2003	NH	TH	0.094	0.003	7
20 Apr 2003	NH	TH	0.101	0.002	5
14 Mar 2005	NH	TH	0.103	0.004	7
6 Feb 2006	NH	TH	0.110	0.003	7
20 Mar 2007	NH	TH	0.113	0.003	9
12 Mar 2008	NH	TH	0.118	0.003	5
2 Mar 2009	NH	TH	0.120	0.004	8
4 Mar 2009	NH	TH	0.123	0.004	2
17 Mar 2010	NH	TH	0.122	0.005	9
17 Mar 2010	NH	TH	0.123	0.007	11
17 Mar 2010	NH	TH	0.122	0.005	13
18 Mar 2010	NH	TH	0.119	0.003	8
25 Jun 2011	NH	TH	0.124	0.008	7
26 Sep 2011	NH	LJ	0.133	0.000	1

Fill Date	Location	Mole Fraction [ppt]	S.D. [ppt]	n
26 Apr 1978	SH	0.012	0.001	3
7 Jul 1978	SH	0.010	0.000	3
6 Feb 1979	SH	0.012	0.001	3
23 May 1984	SH	0.022	0.001	4
6 Feb 1986	SH	0.025	0.002	4
28 May 1987	SH	0.030	0.002	6
21 Jun 1988	SH	0.032	0.001	3
19 May 1989	SH	0.030	0.001	8
26 Apr 1990	SH	0.045	0.003	3
29 Aug 1991	SH	0.045	0.002	3
23 Sep 1992	SH	0.048	0.002	5
11 Feb 1994	SH	0.061	0.002	3
8 Feb 1995	SH	0.069	0.000	2
23 Nov 1995	SH	0.057	0.002	3
4 Dec 1995	SH	0.064	0.002	5
20 Nov 1996	SH	0.067	0.001	4
7 Jan 1997	SH	0.071	0.002	5
30 May 1997	SH	0.070	0.002	4
15 Jul 1997	SH	0.070	0.002	7
25 Jun 1998	SH	0.078	0.001	5
13 Apr 1999	SH	0.077	0.001	5
1 Mar 2000	SH	0.081	0.003	6
14 Mar 2000	SH	0.083	0.003	5
15 Jan 2001	SH	0.086	0.002	4
17 Feb 2003	SH	0.090	0.002	5
3 Oct 2003	SH	0.094	0.002	5
22 Jan 2004	SH	0.093	0.003	6
1 Dec 2004	SH	0.096	0.003	18
10 Feb 2005	SH	0.097	0.003	5
28 Jun 2005	SH	0.098	0.003	18
10 Feb 2006	SH	0.100	0.002	15
4 Oct 2006	SH	0.102	0.003	7
19 Oct 2006	SH	0.104	0.001	6
11 Dec 2006	SH	0.101	0.002	4
8 May 2007	SH	0.107	0.002	5
22 Nov 2007	SH	0.110	0.002	5
12 Aug 2008	SH	0.112	0.001	6
16 Dec 2008	SH	0.114	0.003	5
6 Mar 2009	SH	0.114	0.004	8
10 Dec 2010	SH	0.118	0.002	24
16 Dec 2010	SH	0.120	0.002	79

*Northern Hemisphere locations are: LJ = La Jolla, California; CM = Cape Meares, Oregon; HF = Harvard Forest, Massachusetts; TH = Trinidad Head, California. All Southern Hemisphere locations are Cape Grim, Tasmania.
*ppt = parts-per-trillion dry air mole fraction.

Table A.5: Northern and Southern Hemispheric Archived Air Measurements of C_8F_{18}

Fill Date	Location*		Mole Fraction [ppt**]	S.D. [ppt]	n
29 Jun 1973	NH	LJ	0.000	0.000	3
9 Oct 1973	NH	LJ	0.000	0.000	4
9 Oct 1973	NH	LJ	0.000	0.000	5
21 Jun 1974	NH	LJ	0.000	0.000	7
1 Oct 1975	NH	LJ	0.000	0.000	3
4 Oct 1977	NH	LJ	0.000	0.000	3
10 Aug 1978	NH	LJ	0.000	0.000	4
10 Aug 1978	NH	LJ	0.000	0.000	3
15 Apr 1980	NH	CM	0.010	0.002	3
6 May 1980	NH	LJ	0.000	0.000	4
23 Mar 1982	NH	LJ	0.000	0.000	8
7 May 1982	NH	LJ	0.000	0.000	5
10 Sep 1986	NH	HF	0.010	0.002	4
29 Mar 1991	NH	LJ	0.042	0.012	3
18 Apr 1996	NH	LJ	0.056	0.002	2
1 Apr 1999	NH	LJ	0.071	0.003	8
1 Apr 1999	NH	LJ	0.071	0.002	11
1 Apr 1999	NH	LJ	0.070	0.000	3
28 Apr 2000	NH	TH	0.076	0.002	3
20 Apr 2003	NH	TH	0.081	0.002	7
20 Apr 2003	NH	TH	0.091	0.005	5
14 Mar 2005	NH	TH	0.084	0.003	8
6 Feb 2006	NH	TH	0.085	0.002	7
20 Mar 2007	NH	TH	0.086	0.002	9
12 Mar 2008	NH	TH	0.085	0.001	5
2 Mar 2009	NH	TH	0.088	0.002	8
4 Mar 2009	NH	TH	0.085	0.000	2
17 Mar 2010	NH	TH	0.086	0.002	9
17 Mar 2010	NH	TH	0.090	0.004	11
17 Mar 2010	NH	TH	0.088	0.006	12
18 Mar 2010	NH	TH	0.092	0.004	9
25 Jun 2011	NH	TH	0.090	0.002	7
26 Sep 2011	NH	LJ	0.091	0.003	6

Fill Date	Location	Mole Fraction [ppt]	S.D. [ppt]	n
26 Apr 1978	SH	0.008	0.002	3
7 Jul 1978	SH	0.012	0.004	3
6 Feb 1979	SH	0.019	0.008	3
23 May 1984	SH	0.013	0.002	4
6 Feb 1986	SH	0.016	0.004	4
21 Jun 1988	SH	0.019	0.002	3
29 Aug 1991	SH	0.030	0.003	3
23 Sep 1992	SH	0.032	0.004	5
11 Feb 1994	SH	0.036	0.003	3
8 Feb 1995	SH	0.049	0.004	2
23 Nov 1995	SH	0.040	0.001	3
4 Dec 1995	SH	0.045	0.003	5
20 Nov 1996	SH	0.052	0.003	4
7 Jan 1997	SH	0.050	0.005	5
30 May 1997	SH	0.052	0.008	4
15 Jul 1997	SH	0.053	0.002	7
25 Jun 1998	SH	0.061	0.005	5
13 Apr 1999	SH	0.064	0.003	5
1 Mar 2000	SH	0.075	0.003	6
14 Mar 2000	SH	0.069	0.004	5
26 Aug 2000	SH	0.080	0.001	3
15 Jan 2001	SH	0.072	0.002	4
27 Apr 2001	SH	0.079	0.006	4
19 Jul 2001	SH	0.074	0.003	5
4 Sep 2001	SH	0.076	0.004	3
20 Jun 2002	SH	0.083	0.002	6
17 Feb 2003	SH	0.078	0.001	5
3 Oct 2003	SH	0.075	0.003	5
22 Jan 2004	SH	0.077	0.002	6
1 Dec 2004	SH	0.081	0.003	18
10 Feb 2005	SH	0.081	0.003	5
28 Jun 2005	SH	0.085	0.005	18
10 Feb 2006	SH	0.087	0.007	15
4 Oct 2006	SH	0.079	0.002	5
19 Oct 2006	SH	0.086	0.002	6
11 Dec 2006	SH	0.083	0.002	4
8 May 2007	SH	0.083	0.005	5
22 Nov 2007	SH	0.088	0.002	5
12 Aug 2008	SH	0.091	0.005	6
16 Dec 2008	SH	0.085	0.002	5
6 Mar 2009	SH	0.088	0.004	7
10 Dec 2010	SH	0.085	0.003	23
16 Dec 2010	SH	0.089	0.003	84

*Northern Hemisphere locations are: LJ = La Jolla, California; CM = Cape Meares, Oregon; HF = Harvard Forest, Massachusetts; TH = Trinidad Head, California. All Southern Hemisphere locations are Cape Grim, Tasmania.
*ppt = parts-per-trillion dry air mole fraction.

Bibliography

3M Electronics Markets Materials Division, Performance Fluid PF-5060, 3M, St. Paul, M.N., 2003.

Air and Radiation Global Programs Division, Substitutes in non-aerosol solvent cleaning under SNAP as of September 28, 2006, in *US EPA Report*, United States Environmental Protection Agency, Washington, D.C., 2006.

Arnold, T., J. Mühle, P. K. Salameh, C. M. Harth, D. J. Ivy, and R. F. Weiss, Automated measurement of nitrogen trifluoride in ambient air, *Anal. Chem.*, *84*(11), 4798–4804, 2012, doi:10.1021/ac300373e.

Bravo, I., A. Aranda, M. D. Hurley, G. Marston, D. R. Nutt, K. P. Shine, K. Smith, and T. J. Wallington, Infrared absorption spectra, radiative efficiencies, and global warming potentials of perfluorocarbons: Comparison between experiment and theory, *J. Geophys. Res.*, *115*(D24317), 1–12, 2010, doi:10.1029/2010JD014771.

Chen, Y.-H., and R. G. Prinn, Estimation of atmospheric methane emissions between 1996 and 2001 using a three-dimensional global chemical transport model, *J. Geophys. Res.*, *111*(D10307), 1–25, 2006, doi:10.1029/2005JD006058.

Deeds, D. A., M. K. Vollmer, J. T. Kulongoski, B. R. Miller, J. Mühle, C. M. Harth, J. A. Izbicki, D. R. Hilton, and R. F. Weiss, Evidence for crustal degassing of CF_4 and SF_6 in Mojave Desert groundwaters, *Geochim. Cosmochi. Ac.*, *72*(4), 999–1013, 2008, doi:10.1016/j.gca.2007.11.027.

Ellison, S. L. R., and M. Thompson, Standard additions: myth and reality, *The Analyst*, *133*, 992–997, 2008, doi:10.1039/b717660k.

Emmons, L. K., S. Walters, P. G. Hess, J.-F. Lamarque, G. G. Pfister, D. Fillmore, C. Granier, A. Guenther, D. Kinnison, T. Laepple, J. Orlando, X. Tie, G. Tyndall, C. Wiedinmyer, S. L. Baughcum, and S. Kloster, Description and evaluation of the Model for Ozone and Related chemical Tracers, version 4 (MOZART-4), *Geosci. Model Dev.*, *3*, 43–67, 2010, doi:10.5194/gmd-3-43-2010.

Enting, I. G., C. M. Trudinger, and D. M. Etheridge, Propagating data uncertainty through smoothing spline fits, *Tellus B*, *58*, 305–309, 2006, doi:10.1111/j.1600-0889.2006.00193.x.

European Commission, Joint Research Centre (JRC)/Netherlands Environmental Assessment Agency (PBL), Emission Database for Global Atmospheric Research (EDGAR), *Release 4.0*, 2009, http://edgar.jrc.ec.europa.eu; last access: 15 December 2011.

Forster, P., V. Ramaswamy, P. Artaxo, T. Berntsen, R. Betts, D. W. Fahey, J. Haywood, J. Lean, D. C. Lowe, G. Myhre, J. Nganga, R. Prinn, G. Raga, M. Schulz, and R. Van Dorland, Changes in atmospheric constituents and in radiative forcing, in *Climate Change 2007: The Physical Science Basis. Contribution of Working Group 1 to the Fourth Assessment Report of the Intergovernmental Panel on Climate Change*, edited by S. Solomon *et al.*, Cambridge Univ. Press, Cambridge, United Kingdom and New York, N.Y., USA., 2007.

Forte Jr., R., A. McCulloch, and P. Midgley, Emissions of substitutes for ozone-depleting substances, in *Good Practice Guidance and Uncertainty Management in National Greenhouse Gas Inventories*, pp. 257–270, IPCC National Greenhouse Gas Inventories Programme, Kanagawa, Japan, 2000.

Francey, R. J., L. P. Steele, D. A. Spencer, R. L. Langenfelds, R. M. Law, P. B. Krummel, P. J. Fraser, D. M. Etheridge, N. Derek, S. A. Coram, L. N. Cooper, C. E. Allison, L. Porter, and S. Baly, The CSIRO (Australia) measurement of greenhouse gases in the global atmosphere, in *Baseline Atmospheric Program Australia 1999-2000*, edited by N. W. Tindale *et al.*, pp. 42–53, Bur. of Meteorol., Melbourne, Victoria, Australia, 2003.

Harnisch, J., R. Borchers, P. Fabian, and M. Maiss, Tropospheric trends for CF_4 and C_2F_6 since 1982 derived from SF_6 dated stratospheric air, *Geophys. Res. Lett.*, *23*(10), 1099–1102, 1996*a*, doi:10.1029/96GL01198.

Harnisch, J., R. Borchers, P. Fabian, H. W. Gäggeler, and U. Schotterer, Effect of natural tetrafluoromethane, *Nature*, *384*, 32, 1996*b*, doi:10.1038/384032a0.

Harvey, R., Estimates of U.S. emissions of high-Global Warming Potential gases and the costs of reductions, U.S. Environmental Protection Agency, Washington, D.C., 2000.

International Aluminium Institute, Results of the 2010 Anode Effect Survey: Report on the Aluminum Industry's Global Perfluorocarbon Gases Emissions Reduction Programme, International Aluminium Institute, London, United Kingdom, 2011.

Ivy, D. J., M. Rigby, M. Baasandorj, J. B. Burkholder, and R. G. Prinn, Global emission estimates and radiative impact of C_4F_{10}, C_5F_{12}, C_6F_{14}, C_7F_{16} and C_8F_{18}, *Atmos. Chem. Phys. Discuss.*, *12*, 12987–13014, 2012, doi:10.5194/acpd-12-12987-2012.

Kalnay, E., M. Kanamitsu, R. Kistler, W. Collins, D. Deaven, L. Gandin, M. Iredell, S. Saha, G. White, J. Woollen, Y. Zhu, M. Chelliah, W. Ebisuzaki, W. Higgins, J. Janowiak, K. C. Mo, C. Ropelewski, J. Wang, A. Leetmaa, R. Reynolds,

R. Jenne, and D. Joseph, The NCEP/NCAR 40-year reanalysis project, *Bull. Amer. Meteor. Soc.*, *77*(3), 437–471, 1996, doi:10.1175/1520-0477(1996)077.

Kopylov, S. N., The influence of oxidation of HFC's and FC's on their fire extinguishing and explosion preventing characteristics, *Halon Alternatives Technical Working Conference*, 342–349, 2002.

Krummel, P. B., R. L. Langenfelds, P. J. Fraser, L. P. Steele, and L. W. Porter, Archiving of Cape Grim air, in *Baseline Atmospheric Program (Australia) 2005-2006*, edited by J. M. Cainey *et al.*, pp. 55–57, Bur. of Meteorol., Melbourne, Victoria, Australia, 2007.

Langenfelds, R. L., P. J. Fraser, R. J. Francey, L. P. Steele, L. W. Porter, and C. E. Allison, The Cape Grim air archive: The first seventeen years, 1978-1995, in *Baseline Atmospheric Program (Australia) 1994-1995*, edited by R. J. Francey *et al.*, pp. 53–70, Bur. of Meteorol., Melbourne, Victoria, Australia, 1996.

Laube, J. C., C. Hogan, M. J. Newland, F. S. Mani, P. J. Fraser, C. A. M. Brenninkmeijer, P. Martinerie, D. E. Oram, T. Röckmann, J. Schwander, E. Witrant, G. P. Mills, C. E. Reeves, and W. T. Sturges, Distributions, long term trends and emissions of four perfluorocarbons in the remote parts of the atmosphere and firn air, *Atmos. Chem. Phys.*, *12*, 4081–4090, 2012, doi:10.5194/acp-12-4081-2012.

Miller, B. R., R. F. Weiss, P. K. Salameh, T. Tanhua, B. R. Greally, J. Mühle, and P. G. Simmonds, Medusa: A sample preconcentration and GC/MS detector system for in situ measurements of atmospheric trace halocarbons, hydrocarbons, and sulfur compounds, *Anal. Chem.*, *80*(5), 1536–1545, 2008, doi:10.1021/ac702084k.

Montzka, S. A., S. Reimann, A. Engel, K. Krüger, S. O'Doherty, and W. T. Sturges, Ozone-depleting substances (ODSs) and related chemicals, in *Scientific Assessment of Ozone Depletion: 2010*, number 52 in Global Ozone Research and Monitoring Project, edited by C. A. Ennis, pp. 1–108, World Meteorol. Org., Geneva, Switzerland, 2011.

Mühle, J., A. L. Ganesan, B. R. Miller, P. K. Salameh, C. M. Harth, B. R. Greally, M. Rigby, L. W. Porter, L. P. Steele, C. M. Trudinger, P. B. Krummel, S. O'Doherty, P. J. Fraser, P. G. Simmonds, R. G. Prinn, and R. F. Weiss, Perfluorocarbons in the global atmosphere: tetrafluoromethane, hexafluoroethane, and octafluoropropane, *Atmos. Chem. Phys.*, *10*, 5145–5164, 2010, doi:10.5194/acp-10-5145-2010.

NIST Mass Spec Data Center, Stein, S. E., Director, Mass spectra, in *NIST Chemistry WebBook, NIST Standard Reference Database*, number 69, edited by P. J. Linstrom and W. G. Mallard, National Institute of Standards and Technology, Gaithersburg, Maryland, Gaithersburg, M.D., USA, http://webbook.nist.gov; last access: 9 October 2009.

Office of Air and Radiation and Office of Atmospheric Programs, Climate Change Division, Uses and Emissions of Liquid PFC Heat Transfer Fluids from the Electronics Sector, in *US EPA Report 430-R-06-901*, pp. 1–37, Washington, D.C., 2006.

Oram, D. E., F. S. Mani, J. C. Laube, M. J. Newland, C. E. Reeves, W. T. Sturges, S. A. Penkett, C. A. M. Brenninkmeijer, T. Röckmann, and P. J. Fraser, Long-term tropospheric trend of octafluorocyclobutane (c-C_4F_8 or PFC-318), *Atmos. Chem. Phys.*, *12*, 261–269, 2012, doi:10.5194/acp-12-261-2012.

Pinnock, S., M. D. Hurley, K. P. Shine, T. J. Wallington, and T. J. Smyth, Radiative forcing of climate by hydrochlorofluorocarbons and hydrofluorocarbons, *J. Geophys. Res.*, *100*(D11), 23227–23238, 1995, doi:10.1029/95JD02323.

Prinn, R. G., R. F. Weiss, P. J. Fraser, P. G. Simmonds, D. M. Cunnold, F. N. Alyea, S. O'Doherty, P. Salameh, B. R. Miller, J. Huang, R. H. J. Wang, D. E. Hartley, C. Harth, L. P. Steele, G. Sturrock, P. M. Midgley, and A. McCulloch, A history of chemically and radiatively important gases in air deduced from ALE/GAGE/AGAGE, *J. Geophys. Res.*, *105*(D14), 17751–17792, 2000.

Ravishankara, A. R., S. Solomon, A. A. Turnipseed, and R. F. Warren, Atmospheric lifetimes of long-lived halogenated species, *Science*, *259*(5092), 194–199, 1993, doi:10.1126/science.259.5092.194.

Rigby, M., J. Mühle, B. R. Miller, R. G. Prinn, P. B. Krummel, L. P. Steele, P. J. Fraser, P. K. Salameh, C. M. Harth, R. F. Weiss, B. R. Greally, S. O'Doherty, P. G. Simmonds, M. K. Vollmer, S. Reimann, J. Kim, K.-R. Kim, H. J. Wang, J. G. J. Olivier, E. J. Dlugokencky, G. S. Dutton, B. D. Hall, and J. W. Elkins, History of atmospheric SF_6 from 1973 to 2008, *Atmos. Chem. Phys.*, *10*, 10305–10320, 2010, doi:10.5194/acp-10-10305-2010.

Rigby, M., A. L. Ganesan, and R. G. Prinn, Deriving emissions time series from spare atmospheric mole fractions, *J. Geophys. Res.*, *116*(D08306), 1–7, 2011, doi:10.1029/2010JD015401.

Roehl, C. M., D. Boglu, C. Brühl, and G. K. Moortgat, Infrared band intensities and global warming potentials of CF_4, C_2F_6, C_3F_8, C_4F_{10}, C_5F_{12}, and C_6F_{14}, *Geophys. Res. Lett.*, *22*(7), 815–818, 1995, doi:10.1029/95GL00488.

Saikawa, E., C. A. Schlosser, and R. G. Prinn, Process Modeling of Global Soil Nitrous Oxide Emissions, Report No. 206, MIT Joint Program on the Science and Policy of Global Change, Cambridge, M.A., 2011.

Saito, T., Y. Yokouchi, A. Stohl, S. Taguchi, and H. Mukai, Large emissions of perfluorocarbons in East Asia deduced from continuous atmospheric measurements, *Environ. Sci. Technol.*, *44*(11), 4089–4095, 2010, doi:10.1021/es1001488.

Schwaab, K., F. Dettling, D. Bernhardt, C. Elsner, R. Sartorius, K. Reimann, R. Remus, and W. Plehn, Fluorinated Greenhouse Gases, in *Products and Processes: An*

Evaluation of Technical Measures to Reduce Greenhouse Gas Emissions, German Federal Environmental Agency, Dessau, Germany, 2004.

Semiconductor Industry Association, Semiconductor Industry Association Announces PFC Reduction and Climate Partnership with US EPA, *Press release*, Semiconductor Industry Association, 2001.

Semiconductor Industry Association, STATS: Global billings report history (3- month moving average) 1976 - April 2012, 2012.

Shine, K. P., L. K. Gohar, M. D. Hurley, G. Marston, D. Martin, P. G. Simmonds, T. J. Wallington, and M. Watkins, Perfluorodecalin: global warming potential and first detection in the atmosphere, *Atmos. Environ.*, *39*(9), 1759–1763, 2005, doi:10.1016/j.atmosenv.2005.01.001.

Tsai, W., Environmental hazards and health risk of common liquid perfluoro-n-alkanes, potent greenhouse gases, *Environ. Int.*, *35*(2), 418–424, 2009, doi:10.1016/j.envint.2008.08.009.

Tuma, P., and L. Tousignant, Reducing emissions of PFC heat transfer fluids, presented at SEMI Technical Symposium, 2001, 3M Specialty Materials.

UNEP Technology and Economic Assessment Panel, The implications to the Montreal Protocol of the inclusion of HFCs and PFCs in the Kyoto Protocol, in *Report of the TEAP HFC and PFC Task Force*, pp. 1–86, United Nations Environment Programme, 1999.

United National Framework Convention on Climate Change Secretariat, National greenhouse gas inventory data for the period 1990-2009, United Nations Office at Geneva, Geneva, Switzerland, 2011.

World Semiconductor Council, Semiconductor Manufacturers Reduce PFC Emissions, *Press release*, World Semiconductor Council, 2005.